

ABSTRACT

Title of Dissertation: CERAMIC MATERIALS DEVELOPMENT
FOR INTERMEDIATE TEMPERATURE
SOLID OXIDE FUEL CELL (IT-SOFC)

Ke-Ji Pan
Ph.D of Chemical Engineering
2016

Thesis Directed By: Professor Eric D. Wachsman
Department of Chemical and Biomolecular
Engineering

Solid oxide fuel cell (SOFC) is an electrochemical device that converts chemical energy into electric power with high efficiency. Traditional SOFC has its disadvantages, such as redox cycling instability and carbon deposition while using hydrocarbon fuels. It is because traditional SOFC uses Ni-cermet as anode. In order to solve these problems, ceramic anode is a good candidate to replace Ni. However, the conductivity of most ceramic anode materials are much lower than Ni metal, and it introduces high ohmic resistance. How to increase the conductivity is a hot topic in this research field.

Based on our proposed mechanism, several types of ceramic materials have been developed. Vanadium doped perovskite, $\text{Sr}_{1-x/2}\text{V}_x\text{Ti}_{1-x}\text{O}_3$ (SVT) and $\text{Sr}_{0.2}\text{Na}_{0.8}\text{Nb}_{1-x}$

$x\text{V}_x\text{O}_3$ (SNNV), achieved the conductivity as high as $300 \text{ S}\cdot\text{cm}^{-1}$ in hydrogen, without any high temperature reduction. GDC electrolyte supported cell was fabricated with $\text{Sr}_{0.2}\text{Na}_{0.8}\text{Nb}_{0.9}\text{V}_{0.1}\text{O}_3$ and the performance was measured in hydrogen and methane respectively. Due to vanadium's intrinsic problems, the anode supported cell is not easy. Fe doped double perovskite $\text{Sr}_2\text{CoMoO}_6$ (SFCM) was also developed. By carefully doping Fe, the conductivity was improved over one magnitude, without any vigorous reducing conditions. SFCM anode supported cell was successfully fabricated with GDC as the electrolyte. By impregnating Ni-GDC nano particles into the anode, the cell can be operated at lower temperatures while having higher performance than the traditional Ni-cermet cells. Meanwhile, this SFCM anode supported SOFC has long term stability in the reformat containing methane.

During the anode development, cathode improvement caused by a thin Co-GDC layer was observed. By adding this Co-GDC layer between the electrolyte and the cathode, the interfacial resistance decreases due to fast oxygen ion transport. This mechanism was confirmed via isotope exchange. This Co-GDC layer works with multiple kinds of cathodes and the modified cell's performance is 3 times as the traditional Ni-GDC cell. With this new method, lowering the SOFC operation temperature is feasible.

CERAMIC MATERIALS DEVELOPMENT FOR INTERMEDIATE
TEMPERATURE SOLID OXIDE FUEL CELL (IT-SOFC)

by

Ke-Ji Pan

Thesis submitted to the Faculty of the Graduate School of the
University of Maryland, College Park, in partial fulfillment
of the requirements for the degree of
Doctor of Philosophy
2016

Advisory Committee:

Professor Eric D. Wachsman, Chair
Professor Michael Zachariah
Associate Professor Chunsheng Wang
Assistant Professor Dongxia Liu
Professor Bryan Eichhorn

© Copyright by
Ke-Ji Pan
2016

Acknowledgements

First of all, I thank my advisor Dr. Eric Wachsman for the guidance and supporting me on this research. I also thank him for helping me with my publications, patent application, and academic conference attendance. I thank Dr. Hee Sung Yoon, who is former research scientist, for helping me with SOFC fabrication techniques and solving engineering issues. I thank Bryan Blackburn for the collaboration on the ARPA-E project.

In addition, I thank my colleague Mohammed Hussain Abdul Jabbar. We spent a lot of time working together on the ceramic anode project. Then, I thank everyone in the SOFC group for the suggestions and assistance from you on my research. I thank my friend Dong Ding and Yunhui Gong. We discussed technical issues about this project and I did get useful information.

At last, I thank all my family members. Without their support in my life, I cannot accomplish these projects or even have success. After my graduation, I will spend more time with them, especially my wife and my kid.

Table of Contents

Acknowledgements.....	ii
Table of Contents.....	iii
List of Tables.....	v
List of Figures.....	vi
List of Abbreviations.....	x
Chapter 1: Introduction of Solid Oxide Fuel Cell.....	1
1.1 Introduction to Different Types of Fuel Cell.....	1
1.2 Structure of SOFC.....	3
1.3 Microstructure and Polarization Resistance.....	4
1.4 Problems with Current Ni-Cermet Anode.....	8
Chapter 2: Principles of Designing Conductive Ceramics.....	12
2.1 General Conduction Mechanism.....	12
2.2 Electron Hopping Mechanism.....	14
2.3 Current Ceramic Anode materials.....	16
2.4 Ceramic Anode Requirements.....	20
2.5 Methods of Designing New Ceramic Anode.....	21
Chapter 3: Vanadium doped SrTiO ₃	25
3.1 Introduction.....	25
3.2 Experiments.....	26
3.2.1 Material Synthesis.....	26
3.2.2 Phase Purity Determination.....	27
3.2.3 Electronic Conductivity Measurement.....	27
3.3 Material Properties Discussion.....	27
3.4 Conclusion.....	34
Chapter 4: Strontium and Vanadium co-doped NaNbO ₃	36
4.1 Introduction.....	36
4.2 Experiments.....	37
4.2.1 Material Synthesis.....	37
4.2.2 Phase Purity Determination.....	38
4.2.3 Compatibility Test with Electrolytes.....	38
4.2.4 Conductivity Measurements.....	39
4.2.5 Electrolyte Supported Cell Fabrication.....	39
4.3 Material Properties and Discussion.....	40
4.4 Performance of Electrolyte Supported Cell.....	48
4.5 Conclusion.....	53
Chapter 5: Modified Molybdenum Double Perovskite.....	55
5.1 Introduction.....	55
5.2 Experiments.....	57
5.2.1 Material Synthesis.....	57
5.2.2 Phase Purity Examination.....	58
5.2.3 Conductivity Measurement.....	58
5.2.4 Chemical Compatibility with the Electrolyte.....	59
5.3 Material Properties and Discussion.....	59
5.3.1 Phase Purity Discussion.....	59

5.3.2 Conductivity Discussion	63
5.4 Electrolyte Supported Cell Fabrication and Performance	65
5.4.1 Electrolyte Cell Fabrication	65
5.4.2 Electrolyte Cell Performance and Infiltration Effects	66
5.5 Anode Supported Cell Fabrication and Performance	70
5.5.1 Introduction to Anode Supported Cells	70
5.5.2 Anode Supported Cell Fabrication.....	72
5.5.3 Anode Supported Cell Performance	73
5.5.4 SFCM Cell with Normal Electronic Blocking Layers	76
5.5.5 SFCM Cell with Co-GDC Electronic Blocking Layers.....	85
5.6 Conclusion	96
Chapter 6: Improving Cathode Performance By Adding Cathode Functional layer..	99
6.1 Introduction.....	99
6.2 Experiments	102
6.2.1 Cathode Functional Layer (CFL) Preparation	102
6.2.2 Determination of Oxygen Surface Exchange Coefficient	102
6.2.3 Impedance Analysis of Symmetrical Cell.....	103
6.2.4 Cell Performance Analysis	103
6.3 Results and Discussion	104
6.3.1 Mechanism of Interfacial Resistance Decrease	104
6.3.2 Cathodes Improvement By CFL	107
6.3.3 Cell Performance Improvement by CFL.....	112
6.4 Conclusion	115
Chapter 7: Mixed Protonic Electronic Conductors.....	117
7.1 Introduction.....	117
7.2 Conduction Mechanism	119
7.3 Experiments	121
7.4 Results and Discussion	122
7.4 Conclusion	124
Chapter 8: Summary and Future Work.....	126
References.....	134
Bibliography	147
Publications.....	148

List of Tables

Table 2.1 Standard Reduction Potentials of B-site cations in perovskite	22
Table 3.1 Linear Shrinkage and Relative Densities of SVT30 under Different Sintering Temperatures	33

List of Figures

Figure 1.1 Four Types of Fuel Cells	2
Figure 1.2 Fuel Cell Configuration with Anode Function layer	4
Figure 1.3 Microstructures of Ni-YSZ.....	5
Figure 1.4 Impedance of Ni/Co-YSZ/YSZ/Ni/Co-YSZ Symmetrical cell	7
Figure 1.5 R_{ct} of Different Ni-YSZ function Layer Thickness	8
Figure 1.6 Redox Cycling of Ni-YSZ Cell	9
Figure 1.7 Carbon deposits at anode side after staying humidified methane for 100 Hours. Carbon deposited at the anode side	10
Figure 2.1 Theoretical Brouwer Diagram	12
Figure 2.2 Structure of Perovskite $SrTiO_3$	15
Figure 2.3 Conductivity of LST ⁷¹	18
Figure 2.4 Double Perovskite Sr_2FeMoO_6	19
Figure 3.1 SVT20-40 X-Ray patterns after calcined at 1000°C for 4h. All compositions have strontium vanadate impurities	29
Figure 3.2 B site cation surrounded by bigger oxygen anions. The lower limit of B site cation ionic radii r_B can be calculated from r_o	29
Figure 3.3 SVT20-40 X-Ray Patterns after Sintered at 1350°C for 4h. The secondary phase intensity decreases.	30
Figure 3.4 SEM images of SVT30 with different sintering temperatures	30
Figure 3.5 EDS Analysis of SVT30 Surface after Sintered at 1350°C	32
Figure 3.6 Conductivity of SVT with Different Vanadium doping level. 35% V doped sample has the highest conductivity and all compositions are metallic conductors.	34
Figure 4.1 XRD Patterns of SNNV10, SNNV20 and SNNV30 after firing at 1300°C for 4h. All compositions have perovskite phases with minor impurities at low angles with high vanadium doped sample	41
Figure 4.2 XRD patterns of reduced SNNV10, SNNV20 and SNNV30. SNNV10 and SNNV20 are still single phases. SNNV30 has impurities formed during reduction (* unknown impurities).....	42
Figure 4.3 Examples of different strontium doped SNNV samples. 20% strontium can stabilize the perovskite phase. 10% strontium doped sample totally decomposes after reduction	43
Figure 4.4 Conductivities of SNNV10, SNNV20 and SNNV30 after reduction in 10% H_2 / 90% N_2 . More vanadium dopant level, higher conductivity.	45
Figure 4.5 High temperature treated (1300°C) nano 8YSZ and SNNV30 mixture. They react with each other and form unknown materials	46
Figure 4.6 High temperature treated (1300°C) nano GDC and SNNV30 mixture. No reaction between the two compounds	46
Figure 4.7 SNNV-GDC composites' conductivities at different temperatures. It has the opposite trend compared with SNNV single material. SNNV10- GDC has the highest conductivity	48
Figure 4.8 220 μm GDC supported cell with SNNV-GDC anode and LSCF- GDC cathode. 10 wt% GDC infiltrated into SNNV-GDC anode. Cell was	

tested at 650°C in H ₂ and CH ₄ . CH ₄ performance is much lower than H ₂ performance. In dry conditions the cell works better.	49
Figure 4.9 Impedance comparison between SNNV-GDC cells in dry and humidified hydrogen at 650°C. An ohmic resistance increase was observed while switching to humidified fuel.	50
Figure 4.10 220 μm GDC supported cell with SNNV-GDC anode and LSCF-GDC cathode. 10 wt% Ni-GDC infiltrated into SNNV-GDC anode. Cell was tested in dry H ₂ and dry CH ₄	51
Figure 4.11 SEM images of cell structure. (A) Overall cell structure with thick GDC electrolyte, LSCF-GDC cathode and SNNV10-GDC anode. (B) Interface between cathode and anode. Cathode thickness is around 20μm. (C) Anode microstructure (D) well distributed Ni-GDC nano particles.....	52
Figure 4.12 EDS analysis of the interface between GDC electrolyte and SNNV10-GDC anode. No sodium and niobium diffusion but there is vanadium migrate from the anode to the electrolyte	53
Figure 5.1 Ordered Sr ₂ CoMoO ₆ and cation X doped Sr ₂ CoMoO ₆ with a disordered structure. The electron transport route is shortened by doping.	56
Figure 5.2 SFCM X-Ray patterns after calcination at 1100°C. All Compositions show perovskite phase without impurities.....	60
Figure 5.3 X-Ray Pattern comparison among SFCM with and without matched Co/Mo. When cobalt content is lower than molybdenum SrMoO ₄ impurity comes out.	62
Figure 5.4 X-Ray Patterns of Calcined SrFe _{0.2} Co _{0.4} Mo _{0.4} O ₃ Powder and reduced SrFe _{0.2} Co _{0.4} Mo _{0.4} O ₃ Dense sample. Before and after reduction, no impurity phase forms	63
Figure 5.5 Conductivity of SFCMs at 650°C in 10% H ₂ / 90% N ₂ Hydrogen. Conductivity of SrCo _{0.5} Mo _{0.5} O ₃ obtained from literature ⁷³	64
Figure 5.6 300μm GDC dense electrolyte supported cells with SFCM244 anode and LSCF-GDC cathode. Comparison among the cells without any infiltration, with GDC infiltration, with Ni-GDC (1:7) infiltration	68
Figure 5.7 Button cell performance at 650°C in wet H ₂ and in wet CH ₄ . Cell(1) Ni:GDC =1:7, Cell(2) Ni:GDC =1:2, Cell(1) Ni:GDC =2:3, Cell(1) Ni:GDC =1:1. All cells have the loading around 10 wt%.	70
Figure 5.8 Anode support cell configuration	73
Figure 5.9 Cell Performance of SFCM cell in hydrogen from 650°C to 500°C.	74
Figure 5.10 OCV drops with time in SFCM cell at 650°C	76
Figure 5.11 SFCM cells with ESB electronic blocking layer and LSM-ESB cathode	77
Figure 5.12 SEM and EDS mapping for SFCM anode supported GDC-ESB bilayer cell. ESB can block Co diffusion.....	78
Figure 5.13 Cell performance with different thickness of GDC and ESB at 650°C in hydrogen. Increasing thickness of ESB has higher improvement than increasing thickness of GDC.....	80
Figure 5.14 Performance of cells with GDC-LSGM bilayer in H ₂ at 650°C. Both OCV and cell performance are improved	81

Figure 5.15 OCV degradation of single layer GDC cell, GDC-ESB bilayer cell and GDC-LSGM bilayer cell. All cells have degradation with different rates. GDC-LSGM has the best stability among the three. Anode side is exposed to hydrogen at 650°C.	83
Figure 5.16 Conductivity of different electrolytes. ESB shows a nonlinear relationship of conductivity and temperature right below 600°C	84
Figure 5.17 Configuration of SFCM-GDC cell with 5 μ m Co-GDC electronic blocking layer. SSC-GDC is the cathode.....	87
Figure 5.18 Performance of SFCM anode supported cell with Co-GDC electronic blocking layer. The performance is high at low temperatures. ..	88
Figure 5.19 SEM images A) Cross section of SFCM anode /GDC electrolyte /CFL/SSC-GDC cathode B-C) Porous microstructure of SFCM anode and D) Ni-GDC infiltrated SFCM.	90
Figure 5.20 Impedance plots of the cells between 550°C and 450°C in hydrogen. All measurements were done at OCV conditions.	91
Figure 5.21 Ohmic, polarization, and total resistance of the cells between 550°C and 450°C in hydrogen. All measurements were done at OCV conditions.	92
Figure 5.22 Long term stability of SFCM cell at 450°C in H ₂ . The cell is working under a constant current of 0.2A/cm ²	94
Figure 5.23 SEM images of SFCM cell after long term test in hydrogen. Ni agglomeration is observed.	95
Figure 5.24 SFCM anode supported cell in 81% H ₂ , 16%CH ₄ and 3% water mixture. The cell ran at 450°C at a constant current density of 0.2A/cm ² . The cell is stable after 150 hours.	96
Figure 6.1 Schemes of symmetrical cells. The left one is the baseline sample and the right one is the sample with Co-GDC CFL.....	103
Figure 6.2 Oxygen isotope exchange curves of Co-GDC and standard GDC. Co-GDC started to exchange surface oxygen as low as 300°C.	105
Figure 6.3 Oxygen surface exchange coefficients of Co-GDC and GDC. Within whole temperature range, Co-GDC has faster oxygen exchange.	105
Figure 6.4 Scheme of the interface between SSC-GDC cathode and GDC electrolyte. By adding Co-GDC CFL the mass transport is improved and the bonding strength is enhanced.....	106
Figure 6.5 Polarization resistance of SSC-GDC on Co-GDC CFL. Temperature ranges from 450°C to 600°C	108
Figure 6.6 Polarization resistance of LSC-GDC on Co-GDC CFL. Temperature ranges from 450°C to 600°C	108
Figure 6.7 Polarization resistance of LSCF-GDC on Co-GDC CFL. Temperature ranges from 450°C to 600°C.....	109
Figure 6.8 Polarization resistance of SSC-GDC cathode on Co-GDC CFL at 500°C. When the CFL contains 5% Co, the improvement is the highest. When CFL contains 2% or 10% Co, the performances are similar.	110
Figure 6.9 Polarization resistance of LSC-GDC cathode on Co-GDC CFL at 500°C. When CFL contains 2% Co, the performance is the best.	111
Figure 6.10 Polarization resistance of LSCF-GDC cathode on Co-GDC CFL at 500°C. Compared with SSC and LSC. CFL has less effect on LSCF, mainly	

because LSCF should be fired at higher temperature, and the surface Co on CFL evaporates.	111
Figure 6.11 SEM Images of Ni-GDC cells with 2% Co-GDC CFL. (A) Thick 14 μ m 2% Co-GDC prepared by blade coating. (B) Thin 2% Co-GDC prepared by drop coating. The estimated thickness is less than 1 μ m, and the layer cannot be differentiated from SSC-GDC cathode.	112
Figure 6.12 Performance of standard Ni-GDC cell. 20 μ m GDC electrolyte and SSC-GDC cathode are used in the cell configuration. The cell was tested in humidified hydrogen between 500 $^{\circ}$ C to 650 $^{\circ}$ C.	114
Figure 6.13 Performance of Ni-GDC cell with 7 μ m CFL. 20 μ m GDC electrolyte and SSC-GDC cathode are used in the cell configuration. The cell was tested in humidified hydrogen between 500 $^{\circ}$ C to 650 $^{\circ}$ C.	114
Figure 6.14 Performance of Ni-GDC cell with very thin CFL (<1 μ m) . 20 μ m GDC electrolyte and SSC-GDC cathode are used in the cell configuration. The cell was tested in humidified hydrogen between 500 $^{\circ}$ C to 650 $^{\circ}$ C.	115
Figure 7.1 Hydrogen permeation membrane and oxygen permeation membrane	118
Figure 7.2 proton conduction in an ABO ₃ perovskite material. Protons are hopping among the oxygen sites ¹⁹²	120
Figure 7.3 XRD patterns of sintered bodies of BZYN, BLZYN and BEZYN. All compositions show single phases after sintering	123
Figure 7.4 Conductivity of BZYN, BLZYN, and BEZYN. With A site dopant, the conductivity decreases due to lower protonic conductivity. BEZYN has much higher conductivity than BLZYN	124
Figure 8.1 20% Fe doped Sr ₂ NiMoO ₆ . The sample was sintered at 1300 $^{\circ}$ C and reduced at 650 $^{\circ}$ C. The phase is stable before and after reduction.	129
Figure 8.2 Conductivity comparison between SFCM and SFNM. All samples were reduced at 650 $^{\circ}$ C in 10% H ₂ / 90% N ₂	130
Figure 8.3 PPDs of SFCM cell and SFNM cell. All cells were tested at 650 $^{\circ}$ C.	131
Figure 8.4 XRD patterns of LSCM before and after reduction. Before reduction there is SrMoO ₄ impurity at all sintering temperatures, while it is gone after reduction.	132
Figure 8.5 Conductivity of LSCM after sintering at 1350 $^{\circ}$ C and 1450 $^{\circ}$ C. Both samples were reduced at 650 $^{\circ}$ C in 10% H ₂ / 90% N ₂	132

List of Abbreviations

SOFC: Solid Oxide Fuel Cell

PEMFC: Proton Exchange Membrane Fuel Cell

MCFC: Molten Carbonate Fuel Cell

YSZ: Yttrium Stabilized Zirconia

GDC: Gadolinium Doped Ceria

ESB: Erbium Stabilized Bismuth

LSGM: $\text{La}_{0.8}\text{Sr}_{0.2}\text{Ga}_{0.8}\text{Mg}_{0.2}\text{O}$

LSCF: $\text{La}_{0.6}\text{Sr}_{0.4}\text{Co}_{0.2}\text{Fe}_{0.8}\text{O}_{3-\delta}$

LSM: $\text{La}_{0.6}\text{Sr}_{0.4}\text{MnO}_{3-\delta}$

LSC: $\text{La}_{0.6}\text{Sr}_{0.4}\text{CoO}_{3-\delta}$

SSC: $\text{Sm}_{0.5}\text{Sr}_{0.5}\text{CoO}_{3-\delta}$

BSCF: $\text{Ba}_{0.5}\text{Sr}_{0.5}\text{Co}_{0.8}\text{Fe}_{0.2}\text{O}_{3-\delta}$

BPSCF: $\text{PrBa}_{0.5}\text{Sr}_{0.5}\text{Co}_{2-x}\text{Fe}_x\text{O}_{5+\delta}$

YST: Yttrium doped SrTiO_3

LST: Lanthanum doped SrTiO_3

SNT: Niobium doped SrTiO_3

SVT: Vanadium doped SrTiO_3

SNNV: Strontium & Vanadium co-doped NaNbO_3

SFCM: $\text{SrFe}_{1-2x}\text{Co}_x\text{Mo}_x\text{O}_3$

SFNM: $\text{SrFe}_{1-2x}\text{Ni}_x\text{Mo}_x\text{O}_3$

LSCM: $\text{La}_{0.6}\text{Sr}_{0.4}\text{Cr}_{0.9}\text{Mo}_{0.1}\text{O}_{3-\delta}$

PMMA: Poly(methyl methacrylate)

XRD: X-Ray Diffraction

SEM: Scanning Electron Microscope

TPB: Triple Phase Boundary

ASR: Area Specific Resistance

OCV: Open Circuit Potential

PPD: Peak Power Density

AFL: Anode Functional Layer

CFL: Cathode Functional Layer

PLD: Pulsed Laser Deposition

Chapter 1: Introduction of Solid Oxide Fuel Cell

1.1 Introduction to Different Types of Fuel Cell

A fuel cell is a device that directly converts chemical energy to electricity and heat. Compared to the combustion engine and electric generator, which also utilize fuels to produce energy, fuel cells are highly efficient, have less pollution to the environment, and without any noise. Other renewable energies such as solar and wind, are not sustainable, as they are only functional when there is sunshine or wind. Even though they can be coupled with energy storage device like batteries, it cannot solve all problems due to battery capacity, lifetime issues and add-on cost in equipment and maintenance. Based on these reasons, fuel cells are now a hot topic in the new energy research field as it can be a continuous power supply as long as there is fuel.

There are several types of fuel cells: Proton exchange membrane fuel cell (PEM fuel cell), alkali fuel cell, molten carbonate fuel cell and solid oxide fuel cell. All of these fuel cells consist of an electrolyte to conduct ions, an anode to oxidize fuels and a cathode to accept the oxidizer. PEM fuel cells and alkaline fuel cells have ionic conductive polymer membrane and can be operated at low temperature ($< 100^{\circ}\text{C}$), but there is difficulty in the water management. Additionally, PEM fuel cells require noble metals as the catalyst which increases the manufacturing cost and alkaline fuel cells suffer from low power density. Molten carbonate fuel cells (MCFCs) and solid oxide fuel cells (SOFCs) have to be operated at high temperature (above 600°C), but high temperature operation doesn't require the use of a noble metal as a catalyst and the

efficiency is higher than both PEM and alkaline fuel cells. In the figure below, it is shown that MCFCs need both oxygen and carbon dioxide as oxidizers, which limits its application. So SOFCs are a better choice among these types of fuel cells. SOFCs can directly use air as the oxidizer with high power output and efficiency. Usually, whatever type it is, fuel cells utilize hydrogen gas as the fuel but it is relatively expensive. Researchers are focusing on utilizing other fuels like natural gas, diesel, and other hydrocarbons, as well as lowering the operation temperature. These are key hurdles for fuel cells that prevent them from becoming a widely used technology today.

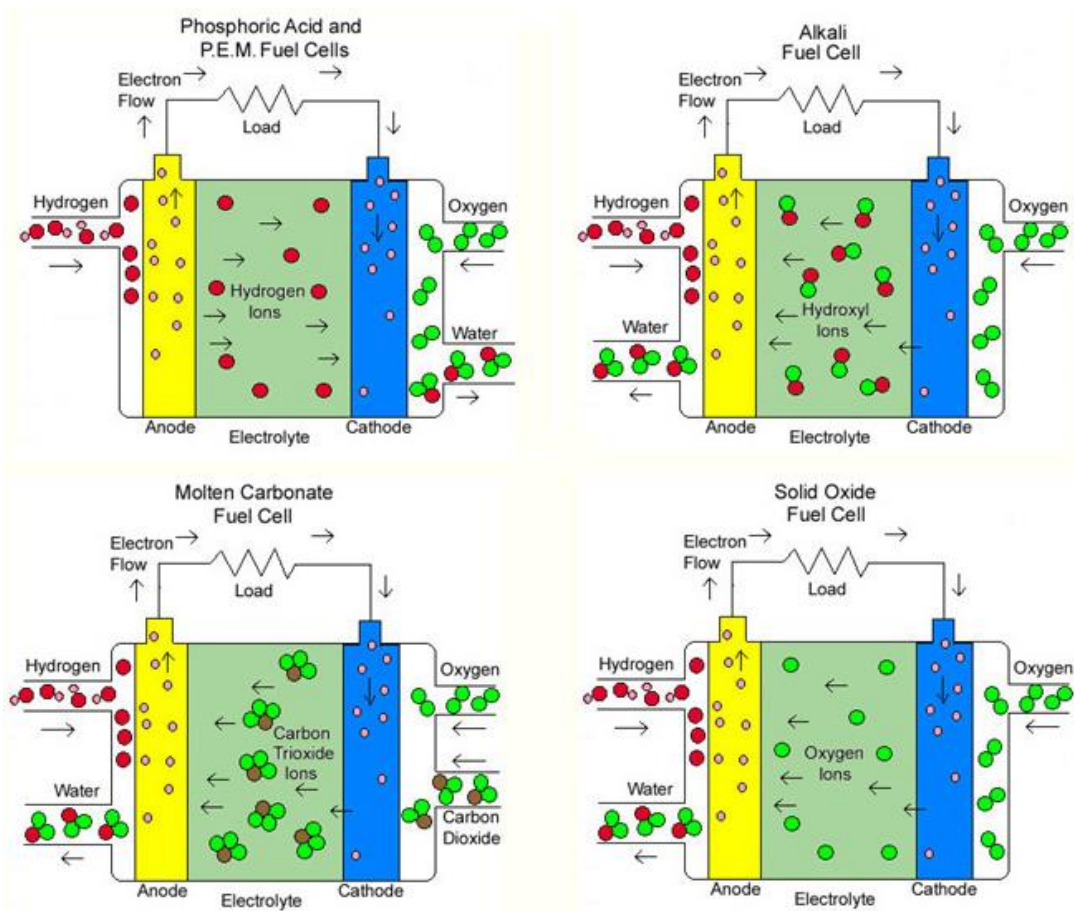


Figure 1.1 Four Types of Fuel Cells

1.2 Structure of SOFC

The SOFC structure usually has three layers: ionic conductive electrolyte between the electronic-ionic mixed conductive anode and cathode. A suitable electrolyte should be high in ionic conductivity but has low electronic conductivity and the electrolyte must be stable in both oxidizing and reducing atmospheres at high temperatures. Typically, the ionic conductivity criteria of the electrolyte is above $0.01 \text{ S}\cdot\text{cm}^{-1}$ at operating conditions, otherwise there is too much resistance. Some well known electrolytes, such as yttrium stabilized zirconia (YSZ), gadolinium doped ceria (GDC) and lanthanum strontium magnesium gallate (LSGM) have to be operated above 700°C , 550°C and 700°C respectively.^{1,2} Considering the operation temperature, conductivity and material cost, GDC is now a good candidate for future research.

When optimizing the electrodes, many aspects have to be considered: stability, electronic conductivity, ionic conductivity, catalytic activity, chemical & mechanical compatibility with the electrolyte. Among these issues, conductivity and catalytic activity are most important. The electrolyte's conductivity is lower than the electrodes', so the electrolyte must be relatively thin to minimize the resistance. To maintain the mechanical strength, thick electrode supported SOFCs are now well established. This thick supporting electrode must have very high electronic conductivity. Usually, a suitable electrode has conductivity higher than $10 \text{ S}\cdot\text{cm}^{-1}$ under fuel cell operation conditions. Between the anode and cathode, the cathode side has higher activation energy, which means higher polarization resistance, thus an anode supported cell is the best configuration. The example of anode supported cell is shown above.³

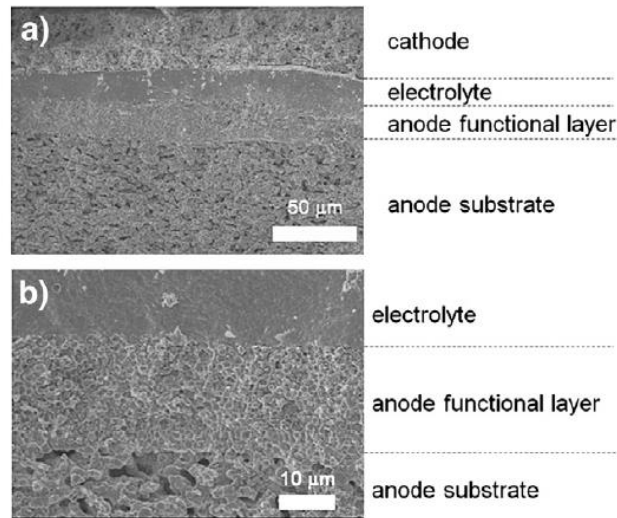


Figure 1.2 Fuel Cell Configuration with Anode Function layer

Because most of the reaction takes place at the triple phase boundary (TPB), extending the length of TPB can greatly increase the active sites. Therefore, an anode functional layer (AFL) with higher surface area but matched ionic-electronic conductivity is introduced between the anode and electrolyte. The details will be discussed in 1.3

1.3 Microstructure and Polarization Resistance

The performance of the fuel cell depends on many things. Besides the intrinsic properties of the electrode and electrolytes, the microstructures also have a big effect on SOFC. In this section, there is one important term “Triple Phase Boundary” –TPB. As we know, a good electrode should have good ionic conductivity, electronic conductivity, catalytic activity, stability, etc. Even though we could carefully design a good material, it is difficult to meet all the criteria to be a state-of-art master piece. Most of the time, it is not easy to find a material that has both high ionic conductivity

and electronic conductivity. To solve this problem, the simplest way is to make a composite, a mixed network of electronic and ionic conductors, for example, Ni-YSZ and Ni-GDC. There is a scheme shown below. ⁴

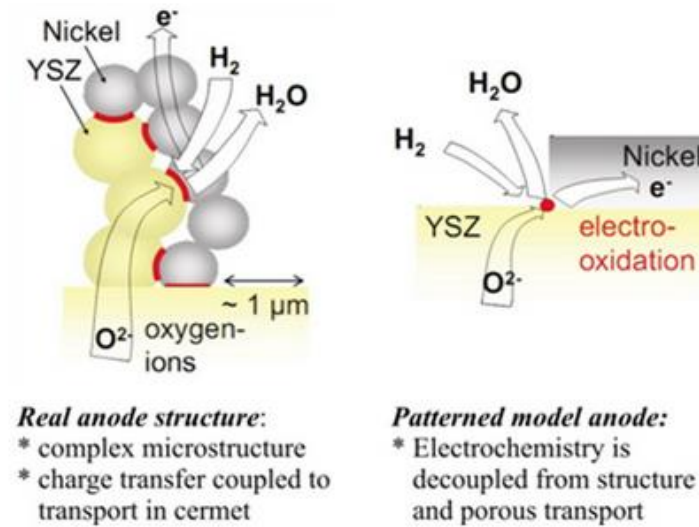


Figure 1.3 Microstructures of Ni-YSZ

In this case, nickel conducts electrons and YSZ conducts oxygen ions. The red lines in the figure shows the boundaries of Ni phase, YSZ phase, and gas phase, which is the TPB mentioned before. The reaction, $O_0^X \rightarrow V_0^{oo} + 2e' + 1/2O_2$, only takes place at the boundaries. Therefore, microstructure plays a key role. As TPB is the active site for the reaction, extending the length of the triple phase boundary should be considered in the fabrication process. This is why anode function layer is added between anode support layer and electrolyte. Anode function layer (AFL) is a thin layer less than 20 μm with fine pores and small grains size. It has a long TPB and the electronic and ionic conductivity are calculated and matched with each other. With adding this layer, the fuel cell performance can be improved. ⁵⁻¹⁰

The total resistance of anode can be concluded in 4 parts as follows,

$$R_{\text{Anode}} = R_{\text{Gas Diffusion}} (R_g) + R_{\text{Surface Adsorption/Diffusion}} (R_{\text{AD}}) + R_{\text{Charge Transfer}} (R_{\text{CT}}) + R_{\text{Ohmic}}$$

$R_{\text{Gas Diffusion}}$ and R_{Ohmic} are functions of:

- Microstructure (porosity & phase fraction, tortuosity, connectivity)
- Conductance (solid phase conductivity or gas phase diffusivity)

$R_{\text{Surface Adsorption/Diffusion}}$ are functions of:

- Microstructure (surface area/volume)
- Kinetics (surface coverage, surface diffusivity)

$R_{\text{Charge Transfer}}$ is a function of:

- Microstructure (LTPB, surface area/volume)
- Kinetics (Oxygen reduction rate)

Usually R_{AD} is hard to separate from R_{CT} in the impedance measurement and we consider R_{CT} is the total polarization resistance in general. To quantify the resistance of each part, a symmetric cell setup is applied. Symmetric cell is an electrolyte supported cell with both sides painted with analyzing electrodes. The cell is tested under designed operation conditions and the impedance is measured. Typically, we can obtain two arcs in the Nyquist plot, just like what is shown in Figure 1.4¹¹. From zero to the first intersect is the ohmic part which includes electrolyte and electrode ohmic resistance. The first arc represents the charge transfer, which is related to the catalytic activity. In this figure, Ni-YSZ has smaller polarization resistance than Co-YSZ because Ni is a better catalyst for hydrogen. The second arc is the concentration polarization, in other

words, it means R_g . The concentration polarization is related with gas diffusion in the electrodes, determined by porosity, pore morphology, and gas flow rate.

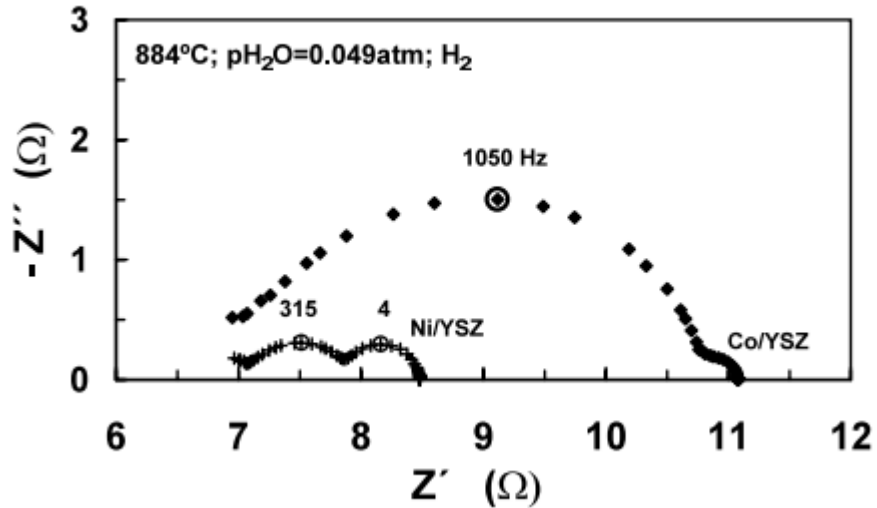


Figure 1.4 Impedance of Ni/Co-YSZ/YSZ/Ni/Co-YSZ Symmetrical cell

TPB can be extended by increasing the porosity and decreasing the particle size. Additionally, a thicker anode function layer also contains more triple phase boundaries. With increasing length of TPB, R_{CT} is decreases. However, large AFL thickness hampers the gas diffusion, resulting to large concentration polarization, which is represented by the second impedance arc in the plot above. These competing factors result in a tradeoff. With thick AFL and small pore size, R_{CT} decreases but R_g increases. To find the best configuration is the most important work in the AFL fabrication. Sang Hoon Hyun¹², Anil V. Virkar¹³ (Figure 1.5 shown below), K. Chen⁷, among others have analyzed the Area Specific Resistance (ASR) of AFLs with different thickness. In Ni-YSZ or Ni-GDC cells, the effective thickness of the AFL is much lower than that of the anode support. To obtain enough mechanical strength, anode support or anode substrate is above 300 μm , but the AFL is ideally around 50 μm and if carefully tailoring

the ionic conductivity, 10-20 μm is enough. Beyond that level, R_{CT} reaches to a plateau. After that, as can be imagined, increasing thickness, increases R_g and the total performance decreases.

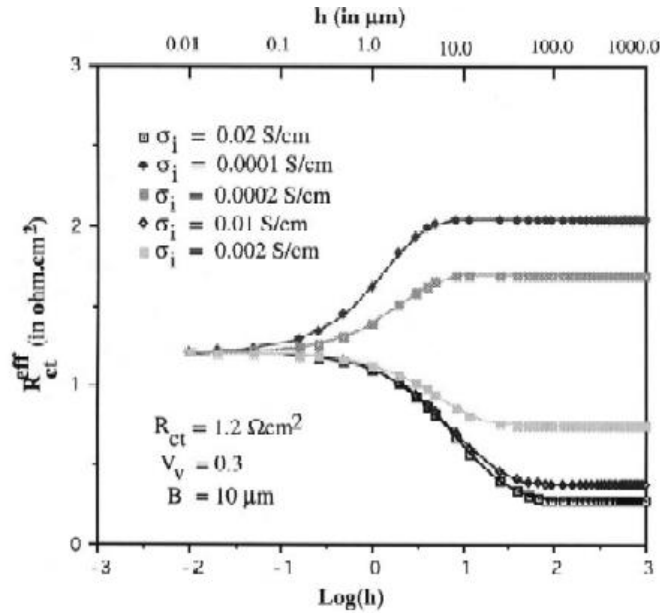


Figure 1.5 R_{ct} of Different Ni-YSZ function Layer Thickness

Another aspect to consider is that small pore size also increases the TPB but makes gas diffusion difficult. K.T. Lee etc.¹⁴ fabricated Ni-GDC AFL with different initial NiO loading, which means different porosity. He demonstrated that the AFL porosity really affects the ASR and 60% NiO shows the best performance.

1.4 Problems with Current Ni-Cermet Anode

For traditional SOFC anode materials, porous Ni-YSZ and Ni-GDC composites are often fabricated to achieve both high ionic conductivity and electronic conductivity. However, even though nickel is highly electronically conductive and catalytically active, there are problems with it such as volume change during thermal cycling, carbon

deposition while using hydrocarbon fuels¹⁵⁻¹⁹ and low sulfur tolerance.^{20,21} Here is the pictures that can explain the redox instability with details, showing in the figure below¹⁰

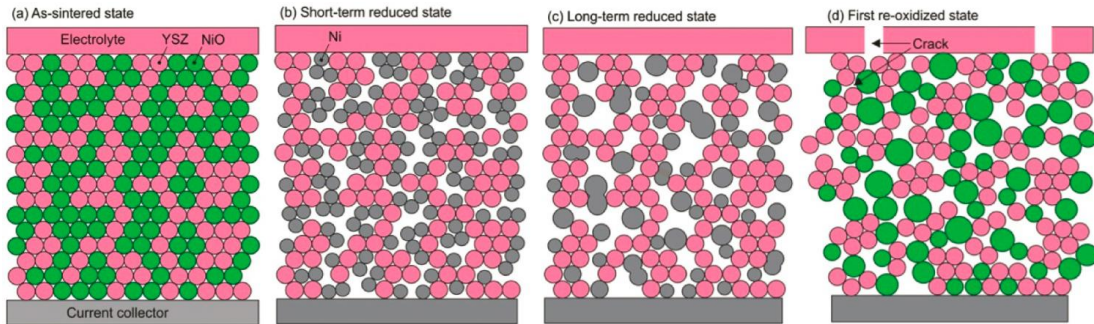


Figure 1.6 Redox Cycling of Ni-YSZ Cell

After sintering the Ni-YSZ cell, we can get the dense NiO-YSZ dense composite supported SOFC. When the cell is exposed in reducing atmosphere at high temperatures, which is the fuel cell operation condition, NiO gets reduced to Ni metal. This process goes with volume shrinkage of NiO phase due to different molecular weight and density between NiO and Ni. The volume change gives around 25% porosity which is good for SOFC, because the porosity allows the fuel to diffuse into the cell and react at the triple phase boundaries. Ni here is the electronic conductor and catalyst for hydrogen oxidation reaction. However, during long term operation, Ni gets coarsened, agglomerated and deformed. The Ni network starts to lose connection, decreasing the electronic conductivity and the overall catalytic activity is lowered with smaller surface area. At this point, the cell performance is deteriorated. However, the worst scenario is that if the fuel supply is cut off or the temperature drops accidentally, Ni get oxidized again to form NiO. The volume expansion introduces a lot of internal stress and the cell dies from cracking electrolyte, showing in the figure above.

Hydrogen is relatively expensive, so everyone is trying to find alternative fuels with low cost. SOFC has the capability to use hydrocarbons. The oxygen ion moves from cathode side to anode side, and in principle it can oxidize variety types of fuels. Thus, SOFC is fuel flexible. But when the hydrocarbons are directly used as fuel, like methane, it causes problems in Ni-Cermet SOFCs. Our lab prepared a Ni-GDC cermet supported cell, using 20 μm GDC as electrolyte and 20 μm $\text{La}_{0.6}\text{Sr}_{0.4}\text{Co}_{0.2}\text{Fe}_{0.8}\text{O}_3$ (LSCF)-GDC as cathode. The cell ran in humidified methane at 650°C for 100 hours. After that the cell sealant was opened and carbon deposition at the anode side was observed (Figure 1.7)

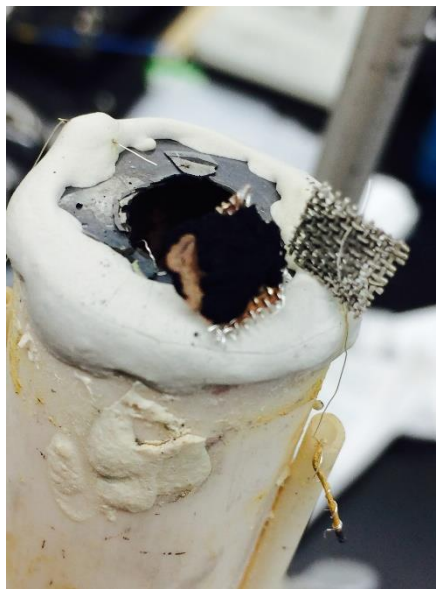


Figure 1.7 Carbon deposits at anode side after staying humidified methane for 100 Hours. Carbon deposited at the anode side

Carbon covers the anode, decreasing the reaction active sites and block the gas diffusion pass way. The cell performance drops and dies finally. Ni can not only catalyze hydrocarbon oxidation reaction, it also breaks the C-H bond and forms carbon.

Considering these issues, conductive ceramics is accepted as an exciting alternative to nickel in the world, in that it is more redox stable and doesn't catalyze carbon formation reaction. Nevertheless, the conductivities of ceramics are much lower than nickel, which are deleterious to the performance of SOFCs. Our idea is to find a new electronically conductive ceramic material which meets both the conductivity and stability requirements.

Chapter 2: Principles of Designing Conductive Ceramics

2.1 General Conduction Mechanism

Common ceramics are insulators, so some effort should be done to improve the conductivity and shift material from insulator to conductors, finally achieving $10 \text{ S}\cdot\text{cm}^{-1}$, which is the requirement of SOFC anode.

Typical conductive ceramic materials are semi-conductors. When doped with an aliovalent element, there are free electrons (n type) or free electronic holes (p type) in the lattice, and these electrons and electronic holes are charge carriers which make the ceramic conductive.²² But the materials in SOFCs are different. They don't have free electrons or electronic holes. The charge carriers really depend on the oxygen partial pressure. When the oxygen partial pressure increases or decreases, the crystal lattice accepts or releases oxygen, which generates electrons or electron holes. The figure below is a theoretical brouwer diagram.²³

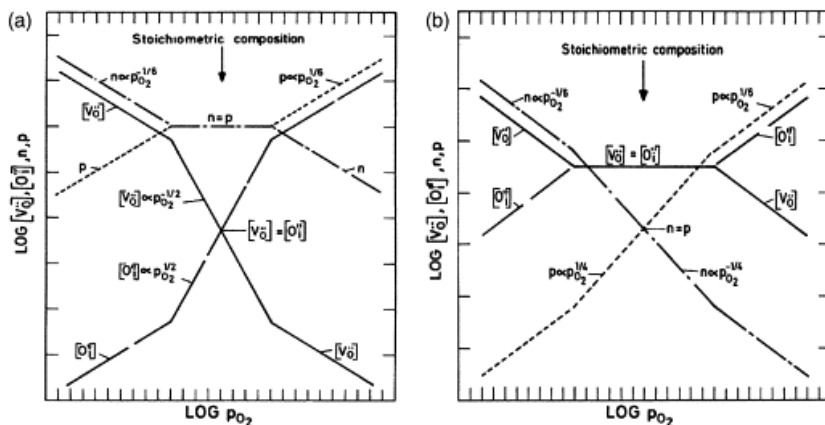
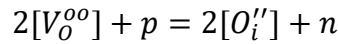
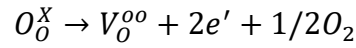
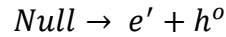


Figure 2.1 Theoretical Brouwer Diagram

The diagram is based on the defect chemical equilibrium



When oxygen partial pressure is high, p type conductivity is dominant according to the Brouwer diagram. Some materials can show high conductivity within this region, and they might be candidates for SOFC cathode. Examples are $La_xSr_{1-x}MnO_3$ (LSM) with different ratios of lanthanum to strontium, which have the conductivity between 100 S*cm^{-1} to 300 S*cm^{-1} ²⁴⁻²⁶ and $La_xSr_{1-x}Co_yFe_{1-y}O_3$ (LSCF) with the conductivity from 125 S*cm^{-1} up to 1000 S*cm^{-1} , depending on the temperature and atmosphere. ²⁷⁻³¹

In contrast to the cathode, anode materials are operated within low P_{O_2} region. In this region, electrons and oxygen vacancies are dominant charge carriers. If the material is electronically conductive, it is called an n-type conductor. The conductivity can be expressed as follows,

$$\sigma = e u n$$

σ = electronic conductivity

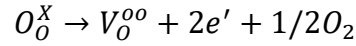
e = charge of single electron

u = mobility of electrons

n = concentration of charge carriers

In this relationship, the charge of an electron is constant ($1.6 \cdot 10^{-19} \text{ C}$). To increase the intrinsic conductivity, The electron concentration and mobility should be improved.

While a reducing atmosphere is present, the metal oxide starts to lose oxygen to form oxygen vacancies and electrons.



As we can imagine, the more oxygen it loses, the more free electrons will form, which means potentially high conductivity. But the stability of the material must also be considered. When the ceramic is gradually releasing oxygen, it means the original structure is gradually breaking down. At a certain level, the material decomposes irreversibly, which must be prevented in the SOFC, because it may cause cracking during operation. The intermediate temperature fuel cell operation condition is between 500°C and 700°C and the oxygen partial pressure is usually below 10^{-20} atm. It is quite a challenge to maintain stability for most metal oxides. Considering these factors, a perovskite type ceramic material is a good choice because it is relatively more stable than other structures and has a good potential to achieve high conductivities.

2.2 Electron Hopping Mechanism

In perovskite structure, the most prevalent conduction mechanism is electron hopping mechanism.³² A perovskite has the ABO_3 formula with large cation at the A site and small cation at the B site. The A site cation has the coordination number of 12 and the B site cation has the coordination number of 6, which forms oxygen surrounded B site octahedrals. This structure can tolerate oxygen vacancies and because of these densely packed B-site octahedrals. The stability and conductivity is higher than those of other structures. Here $SrTiO_3$ is used as an example for the further discussion (**Figure 2.2**)

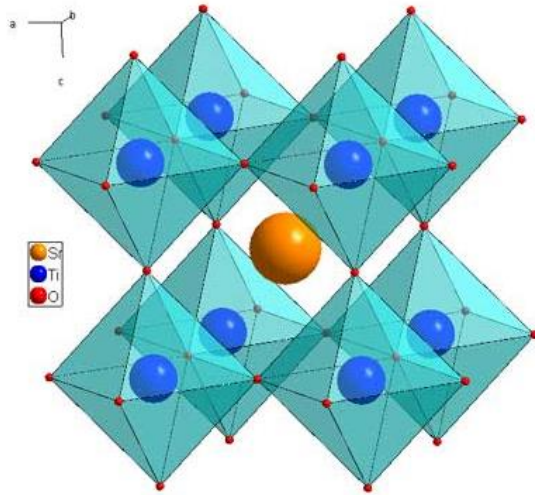
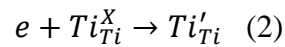
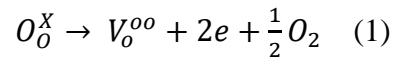
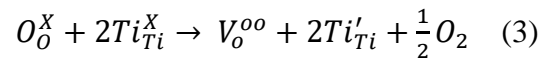


Figure 2.2 Structure of Perovskite SrTiO₃

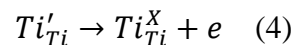
When this material is exposed to reducing atmosphere at high temperatures. The following reduction takes place.

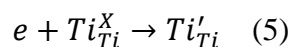


(1)+(2)



During reduction, the lattice oxygen is removed by hydrogen or hydrocarbons at anode side, leaving one oxygen vacancy and two localized electrons. In strontium titanate, titanium has multivalences (4+ state and 3+ state). The electron can be incorporated into the nearby Ti⁴⁺ and form Ti³⁺. So the overall reaction can be re-written as Eq (3). The lattice oxygen is removed and the valence of titanium shifts from 4+ state to 3+ state. And then, electrons hop from one Ti site to another Ti site, which is electron hopping mechanism.





Because electrons must combine with the cation, the B site should consist of multivalent cations that can change its valence state. The B site cation is “reduced” by charge carriers and the charge carriers hop among these B site cations to achieve conductivity. The more easily the valence changes (easily shift from high valence state to low valence state, and from low valence state to high valence state), the higher mobility it achieves. For a typical n-type conductor, which requires that the valence state can decrease during operation. Such candidate cations include: Ti^{4+} , Nb^{5+} , Mo^{6+} , W^{6+} , V^{5+} , Sn^{4+} , Eu^{3+} , etc. P-type conductors are the opposite. While oxygen partial pressure increases, oxygen incorporates into the lattice and generates electron holes. Electron holes combine with the B site cation to increase its valence state. In other words, the cation is oxidized. Similar to n-type conductors, electron holes hop among those B site cations during operation conditions. Examples are LSCF^{33,34} and LSM³⁵. In these cases, when an oxidizing atmosphere is present, Co^{2+} , Fe^{3+} and Mn^{3+} shift to Co^{3+} , Fe^{4+} and Mn^{4+} . With these valences shifting up and down, the materials could show high conductivities. P-type B site candidates are Fe^{3+} , Mn^{3+} , $Co^{2+/3+}$, Cr^{3+} etc.³⁶⁻

³⁸ By carefully tailoring the composition, it seems feasible to make a perovskite material to meet the requirements of conductivity and stability.

2.3 Current Ceramic Anode materials

There are some ceramic anode materials that can be alternative to nickel metal.³⁹⁻⁴² As mentioned before, most of these kinds of materials are perovskite which have the high conductivity and stability. One candidate is SrTiO₃ based materials. Some researchers

use niobium doped strontium titanate (SNT or STN) as an anode material for SOFCs. SNT has the electronic conductivity of $6.5 \text{ S}\cdot\text{cm}^{-1}$ after reduction at 930°C and shows good redox stability⁴³. However SNT has to be reduced or sintered in hydrogen at high temperatures, which makes it infeasible for intermediate or low temperature solid oxide fuel cells.⁴⁴⁻⁴⁷ In such fuel cells, most of the electrolyte is not stable under these severe reducing conditions. GDC is a typical electrolyte used in intermediate temperature fuel cells, but this ceria based electrolyte can show electronic conductivity in hydrogen at high temperatures.^{48,49} This is because of reduction of Ce^{4+} to Ce^{3+} . When the temperature is even lower (below 600°C), bismuth electrolyte is a good choice because it has high ionic conductivity.⁵⁰⁻⁵⁸ However, bismuth is very easy to get reduced to form metallic bismuth.⁵⁹⁻⁶² Besides the electrolyte, regular cathode materials are not stable in reducing conditions, like LSCF and LSM⁶³⁻⁶⁵. Either the conductivity decreases or the cathode material decomposes during reduction. Considering these, the overall fabrication process of a SOFC should be conducted in air instead of reducing atmospheres like N_2 or H_2 . Therefore, it comes with one requirement, the anode conductivity should show up in fuel cell operation conditions, below 650°C in H_2 .

Our lab reduced $\text{Sr}_{0.875}\text{Ti}_{0.75}\text{Nb}_{0.25}\text{O}_3$ (SNT25) under 10% H_2/N_2 at 650°C for over one day but only got the conductivity around $0.2 \text{ S}\cdot\text{cm}^{-1}$, which is too low for the anode. The mechanism is $\text{Nb}^{5+}/\text{Nb}^{4+}$ and $\text{Ti}^{4+}/\text{Ti}^{3+}$ B-site cation valence transition with electron hopping showing above. Due to relatively high reduction potential of Nb^{5+} and Ti^{4+} , this transition is not easy below 900°C especially for the $\text{Ti}^{4+}/\text{Ti}^{3+}$ transition, resulting few charge carriers and high hopping energy barrier. In an SOFC, the

electrolyte and cathode have to be sintered in air, which are not compatible with SNT owing to the reduction atmosphere sintering. Lanthanum or Yttrium doped SrTiO₃ (LST and YST) is similar to SNT. For example, in yttrium doped SrTiO₃^{66,67}, titanium works as a multivalent cation. Instead of doping at B site, LST and YST dope rare earth elements at the A site and partially shift the valence state of Titanium from 4+ to 3+ to form Ti⁴⁺/Ti³⁺ pairs. Ti⁴⁺ is quite stable, so such a valence shift should be conducted in hydrogen at high temperature (around 1000°C).^{66,68-70} After reduction, the conductivity is up to 1700S*cm⁻¹ (shown in Figure 2.3)⁷¹ but if the material is sintered in air there will be a lot of impurities which are difficult to eliminate. Although high conductivity can be achieved, the catalytic activity is pretty low, that requires infiltration of catalytic active materials such like Ni, Pd and Pt.

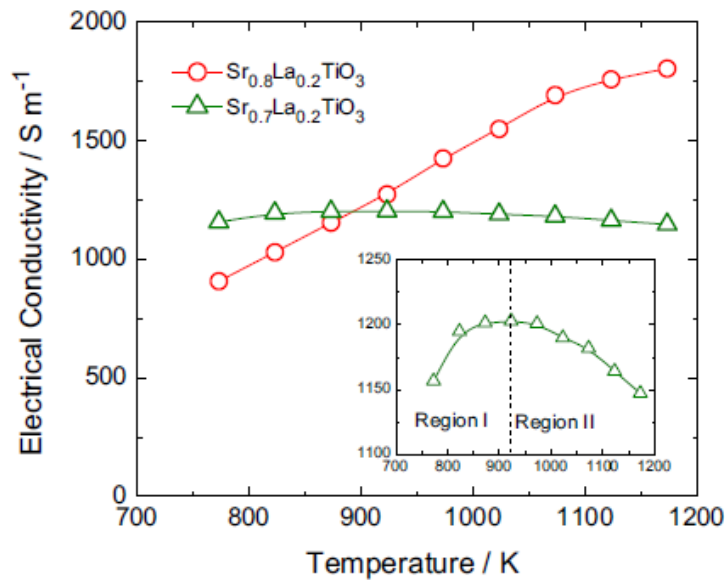


Figure 2.3 Conductivity of LST⁷¹

There is another type of material called double perovskite with the structure shown in Figure 2.4. It has a general formula of A₂BB'O₆ with alternative B-octahedral and B'-

octahedral. In this type of materials, molybdenum based double perovskite Sr_2MMoO_6 , and Ba_2MMoO_6 ($M = \text{Mg, Mn, Co, Ni, Fe}$) show n type conductivity under reducing conditions.⁷²⁻⁸¹ For $M=\text{Mg,Co,Ni,Mn}$, the conductivity is below $10 \text{ S}\cdot\text{cm}^{-1}$. Only when $M=\text{Fe}$, the conductivity is around $200 \text{ S}\cdot\text{cm}^{-1}$. However, in order to get single phase material, hydrogen sintering to high temperature reduction is necessary, or there is SrMoO_4 (BaMoO_4) impurity present. This impurity is an insulating phase which harms the electronic conduction and under fuel cell operation conditions, it undergoes a phase change. There is a big volume change in the phase transition. Such a process may also crack the structure, and the fuel cell performance is deteriorated.

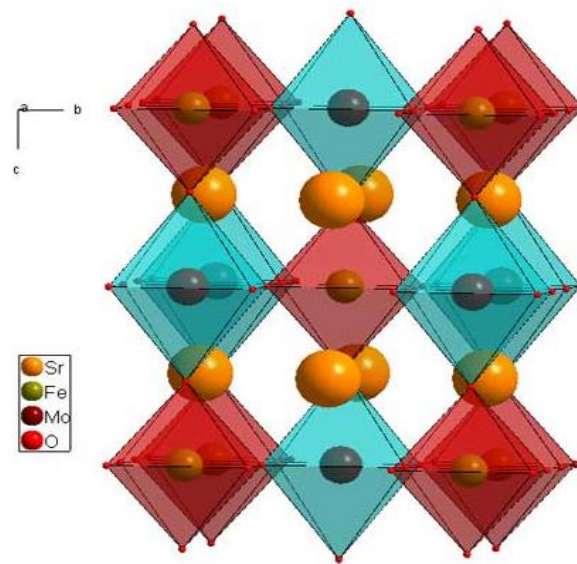


Figure 2.4 Double Perovskite $\text{Sr}_2\text{FeMoO}_6$

Besides these, there are still other types of materials like $\text{La}_{0.7}\text{Sr}_{0.3}\text{VO}_3$ ^{82,83} and $\text{Ba}(\text{Sr})\text{SnO}_3$ ⁸⁴. $\text{La}_{0.7}\text{Sr}_{0.3}\text{VO}_3$ reveals good conductivity ($\approx 100 \text{ S}\cdot\text{cm}^{-1}$) after reduction, but it also undergoes a phase change during redox cycling and the volume expands and shrinks a lot in this process. It has the same stability problem as Ni-Cermet. The barium stannate has a conductivity about $20 \text{ S}\cdot\text{cm}^{-1}$ under fuel cell operation condition based

on our experiment, but it gradually decomposed which makes it impossible to be a good anode.

2.4 Ceramic Anode Requirements

To be a good anode material, some criteria has to be fulfilled. Currently, GDC electrolyte is a promising candidate to replace YSZ, because GDC has higher ionic conductivity and can be operated at lower temperatures. Therefore, it is important that the anode can work well with GDC electrolyte.

The requirements for an ideal anode material for use with a GDC electrolyte are:

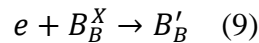
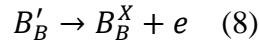
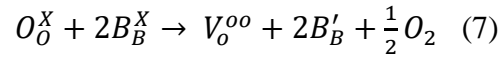
- 1) Anode should have the sintering temperature not higher than 1450°C. GDC has a sintering temperature around 1450°C in air, and if using Bi₂O₃^{85,86} or other transition metal oxide⁸⁷⁻⁸⁹, its sintering temperature can be lowered to 900°C.
- 2) Anode should be sintered in air and operated in hydrogen or methane, which means it has to be stable in both oxidizing and reducing atmospheres. Before and after reduction, the material should be single phase or at least with only very little impurities.
- 3) No tendency to react with GDC. Chemically and thermally stable with GDC.
- 4) Good conductivity. The anode material should have relatively high electronic conductivity to be anode support. To make AFL, we should find out the material which both have high electronic conductivity and ionic conductivity
- 5) Catalytic activity
- 6) Low cost and light weight.

2.5 Methods of Designing New Ceramic Anode

Now we know the conduction mechanism and requirements of anode materials. Then what shall we do to design a new material? For the ceramic anode materials, conductivity and stability are the most important. So new ways should be found to develop the material that is stable and also has high conductivity. Based on our experiment observations, perovskite has the best potential to achieve high conductivity because of it is a densely packed structure and electron hopping distance is short. At another aspect, this densely packed structure can increase the stability because the columbic force between cations and anions are strong.

In an n-type semiconductor, the conductivity equation can be written as follows, where the charge carriers are electrons. Here B is the B-site cation in perovskite structure.

$$\sigma_e = q_e \cdot C_e \cdot u_e \quad (6)$$



To improve the conductivity, either the concentration of electrons (C_e) or the electron mobility should be improved. In order to increase C_e , we should have a B-site cation that is easy to get reduced. If the mobility needs improvement, the valence state of B-site cation should be easy to shift. Therefore, certain criteria has to be set up to screen suitable B-site cation in perovskite.

Here standard reduction potential is used as the reference to select B-site cations. As we know, standard reduction potential can show the how easily the element can get reduced in standard conditions. Based on the value of the potential, we can also find out the easiness of the reversible reaction. Therefore, we can get information about whether a certain element is easy to reduce (related with C_e), and whether the valence is easy to change (related to mobility). Even though, the standard condition is different from the working condition of a fuel cell and the chemical environments are also different, we can still use it to predict material property and narrow down the material candidates. Examples are shown in Table 2.1⁹⁰

Example	Standard Reduction Potentials (SRP)	Results (Reduced at 650°C)
SrTiO ₃	$\text{TiO}_2 + 4\text{H}^+ + \text{e}^- \rightarrow \text{Ti}^{3+} + \text{H}_2\text{O} \quad -0.666\text{V}$	few charge carriers, insulator
BaPrO ₃	$\text{Pr}^{4+} + \text{e}^- \rightarrow \text{Pr}^{3+} \quad 3.2\text{V}$	low mobility, $0.1\text{S}\cdot\text{cm}^{-1}$
SrSnO ₃	$\text{Sn}^{4+} + 2\text{e}^- \rightarrow \text{Sn}^{2+} \quad 0.154\text{V}$ $\text{Sn}^{2+} + 2\text{e}^- \rightarrow \text{Sn} \quad -0.138\text{V}$	tend to decompose
NaNbO ₃	$\text{Nb}_2\text{O}_5 + 10\text{H}^+ + 4\text{e}^- \rightarrow 2\text{Nb}^{3+} + 5\text{H}_2\text{O} \quad -0.1\text{V}$	conductivity $2\text{S}\cdot\text{cm}^{-1}$

Table 2.1 Standard Reduction Potentials of B-site cations in perovskite

The first material is SrTiO₃, which is shown in the Chapter 2.2 as the example for explaining electron hopping mechanism. Ti⁴⁺ has the reduction potential of -0.666V. Usually negative reduction potential means the material is more difficult to reduce than

hydrogen. Therefore, when the SrTiO₃ is exposed in hydrogen, very minimal Ti goes to 3+ state, resulting few electrons. As we know, SrTiO₃ is an insulator. In BaPrO₃, Pr has two valence states of 4+ and 3+ , and the reduction potential is very positive. At this aspect, there should be high concentration of electrons. However, as a result of this highly positive reduction potential, the reversible reaction is too difficult to takes place. Pr³⁺ cannot get oxidized again and go back to Pr⁴⁺. When the electrons incorporates into Pr⁴⁺ and form Pr³⁺, they are trapped there. Thus, the mobility is low. For BaPrO₃, the conductivity is only around 0.1S*cm⁻¹ which is too low to be an anode support. The reason is the low mobility. SrSnO₃ seems to be a good candidate. The reduction potential is positive and not too high, but still it has some other problems. Sn⁴⁺ can get reduced to Sn²⁺, but Sn²⁺ can also be further reduced to Sn⁰. Sn⁰ is tin metal phase. Under reducing conditions, SrSnO₃ possibly decomposes and it may not be a good anode material. Until now, researchers are still developing the stannate materials and try to make it SOFC anode. ⁸⁴ At last, it is NaNbO₃. Nb⁵⁺ can be reduced to lower valence state with a reduction potential of -0.1V. It is not a small negative value and 0.1V promises high electron mobility. We tested this composition at 650°C in 10% H₂ /N₂, and the conductivity is around 2 S*cm⁻¹ that is higher than the other three materials.

As a result, using standard reduction potential can predict the perovskite material conductivity. By checking the value of the standard reduction potentials, we can foresee the limiting step for electronic conduction, whether it is the low electron concentration or the low electron mobility. NaNbO₃ has a relatively good conductivity, but it still does not reach the anode conductivity requirement, which is 10 S*cm⁻¹. Something

should be done to further improve the conductivity. The following chapters will introduce some new materials designed based on this method.

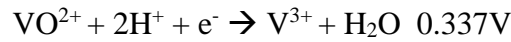
Chapter 3: Vanadium doped SrTiO₃

3.1 Introduction

As shown in the previous chapter, SrTiO₃ is an insulator, because Ti⁴⁺ has a very negative reduction potential. Ti⁴⁺ is difficult to reduce to Ti³⁺. In SrTiO₃ system, it lacks free electrons. Therefore some researchers doped lanthanide into Sr site and reduce the compositions at high temperature, examples are shown in Chapter 2. When temperature increases, a stronger reduction driving force is applied on the titanate and Ti⁴⁺ is easier to lower its valence state and give out free electrons. By doing this, Y doped SrTiO₃ can reach 100 S*cm⁻¹ when its reduction temperature is above 1000°C. However, it is very sensitive to the temperatures. T Kolodiaznyi et al. also annealed this sample in hydrogen at a lower temperature of 800°C for 1 week. The conductivity is below 0.1S*cm⁻¹.⁹¹ It means there is equilibrium ratio of Ti³⁺/Ti⁴⁺ and the concentration of Ti³⁺ is high in vigorous reduction conditions, but low in mediocre reduction conditions, especially below 800°C. For an IT-SOFC, the operation temperature is much lower than 800°C. So these titanates cannot be used as SOFC anode material because the conductivity is too low. At another aspect, we could not pretreat the cell in hydrogen above 800°C before letting it run below 650°C, because the electrolyte GDC isn't stable in this vigorous reduction conditions. Ce⁴⁺ is easier to reduce to Ce³⁺ and it introduces leakage current and lowers the cell performance.

The problem with SrTiO₃ is few free electrons. Our idea is to dope certain cations which is easier to reduce. As a result, electrons can be directly generated in fuel cell operation

conditions and this titanate may be suitable for IT-SOFC anode. Based on the reduction potential, a multivalent cation with positive reduction potential is necessary. Considering solubility, the cation can should also have a valence state and a ionic radii close to Ti^{4+} (60pm). As a result, Vanadium may be a good candidate to improve the conductivity of $SrTiO_3$. V^{5+} has a ionic radii of 54pm and the valence state is 5+, which is not far from Ti^{4+} . The reduction potential of V is shown below⁹⁰



V^{5+} has a very large positive reduction potential. Even in a mild reduction condition, V^{5+} can very easily go to V^{4+} and gives out electrons. Moreover, even V^{4+} has a positive reduction potential, so more electrons will be generated. At last, vanadium metal is not easy to form so there is little chance of decomposition. In this way, we can expect V doped $SrTiO_3$ should have high conductivity.

3.2 Experiments

3.2.1 Material Synthesis

$Sr_{1-x/2}V_xTi_{1-x}O_3$ (SVT) was synthesized by conventional solid state reaction. Vanadium dopant level x ranges from 20% to 40%. The samples are called SVT20, SVT25, SVT30, SVT35 and SVT40. There is Sr deficiency in this composition due to V has higher valence state than Ti. To compensate the oxygen excess of doping V at Ti site, A site deficiency is necessary. Stoichiometric amounts of $SrCO_3$ (Sigma Aldrich 99.9%), TiO_2 (Inframat Advanced Materials, Rutile, Nano Powder, 99%) and V_2O_5

(Alfa Aesar, 99.6% min) were mixed and ball milled in ethanol for 24h. The precursors were then dried in a 100 °C oven with constant air flow. The powders were calcined at 1000°C and then ball milled again in ethanol for another 24h and dried. Green bodies were pressed under 100MPa and sintered at 1350°C for 4h with a ramping rate of 3°C / hour.

3.2.2 Phase Purity Determination

To confirm phase purity, X-ray diffraction was performed on the calcined and sintered samples respectively, using a Bruker D8 Advance diffractometer with CuK α radiation. The degree ranges from 15° to 85° with a step 0.015°/s.

3.2.3 Electronic Conductivity Measurement

Electronic conductivity was measured with four probe DC method. Sintered pellets were cut into bar type samples approximately 20mm x 2mm x 2mm and reduced in 10% H₂ balanced with N₂ at 650°C for one day. Keithley 2400 was used as a current source and coupled with Keithley 2000 for voltage measurement.

3.3 Material Properties Discussion

Calcined and sintered SVT samples were taken X-Ray diffraction by Bruker D8 Advance diffractometer. After calcination, all compositions show single cubic perovskite phases but there are a lot of impurities no matter what the vanadium doping level is, shown in Figure 3.1. After indexing, the secondary phases are strontium

vanadate, mixed compositions with different Sr and V ratio, such as $\text{Sr}_3\text{V}_2\text{O}_8$, $\text{Sr}_2\text{V}_2\text{O}_7$, $\text{Sr}_4\text{V}_2\text{O}_9$ etc. With increasing vanadium amount, the intensity of strontium vanadate peaks become stronger. It seems the solubility of V in SrTiO_3 is low and V prefers to stay outside the perovskite phase. One reason that causes the low solubility may be the smaller ionic radii of V^{5+} (54pm) than Ti^{4+} . In Figure 3.2, we can see the arrangement of B site cation and oxygen anion. The ionic radii of oxygen is big, around 140pm in solid. If B site cation is big, oxygen anions stay far away from each other. If B site cation gets smaller, the oxygen anions move towards to each other and finally at certain point, they touch with each other. However, in some cases, B site cation is even smaller than this limit. Due to the steric hindrance, oxygen anions cannot move even closer. The strong columbic force start to repel them away and the structure is not stable. Therefore, if the dopant is way too small, the solubility is low. The limit of B site ionic radii can be calculated based on the equation below

$$2r_O = \sqrt{2} (r_O + r_B)$$

Oxygen ionic radii is 140pm in perovskite, so we can obtain the limit of B site cation radii is 59pm. According to this, even a 10% V doped sample has an average B site ionic radii of 59pm, which is right on the limit. When the V dopant level increases, the composition tends to form secondary phases. At another aspect, V has higher valence state than Ti. The chemical property difference can also affect the solubility.

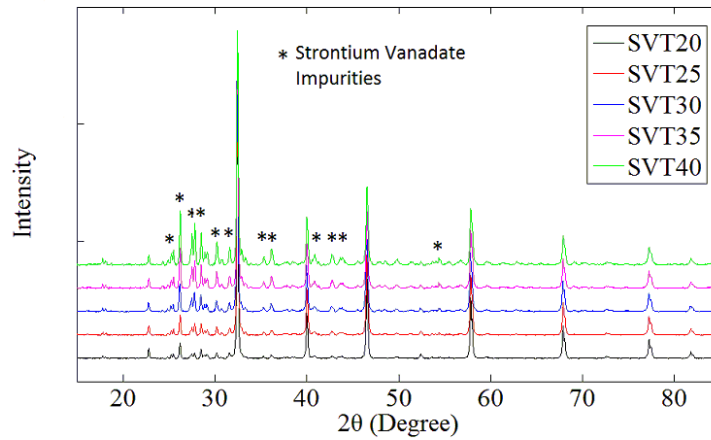


Figure 3.1 SVT20-40 X-Ray patterns after calcined at 1000°C for 4h. All compositions have strontium vanadate impurities

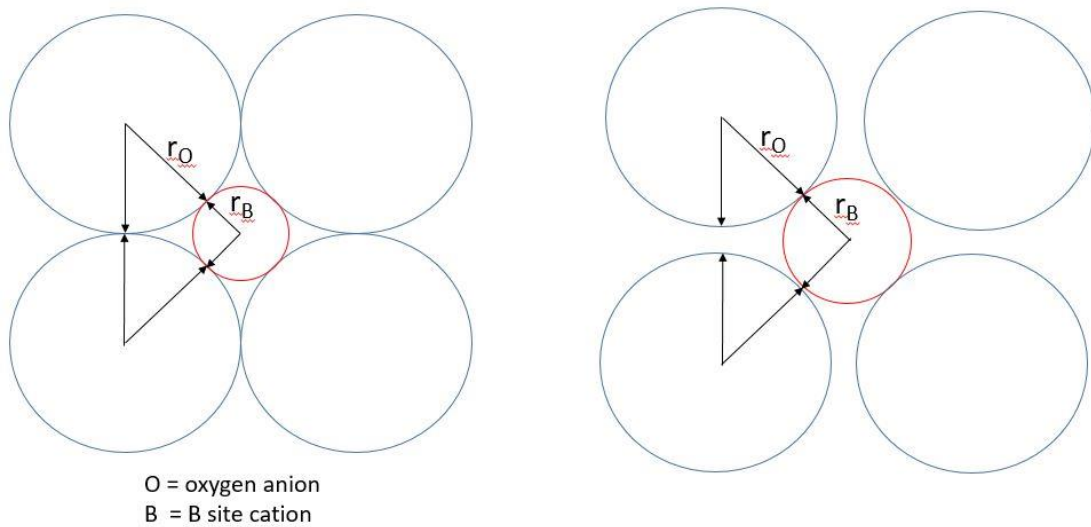


Figure 3.2 B site cation surrounded by bigger oxygen anions. The lower limit of B site cation ionic radii r_B can be calculated from r_o

Surprisingly, after sintered at 1350°C for another 4 hours, the strontium vanadate phase disappears. All compositions give cubic perovskite phase with minor impurities, as shown in Figure 3.3. It is very important to find out whether high temperature sintering

can increase the solubility. During materials synthesis, the right phase formation requires a certain temperature. Below that point, there are secondary phases.

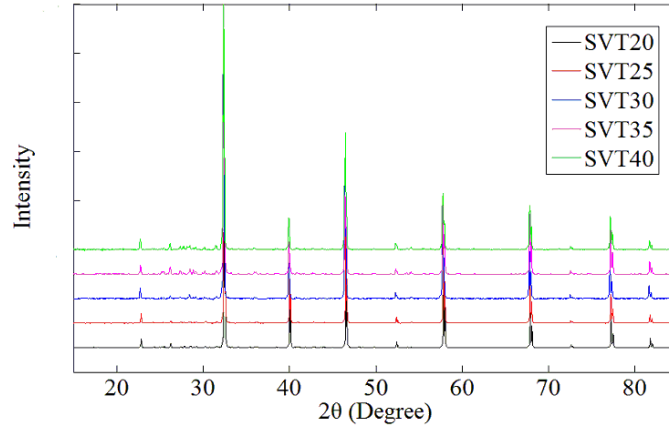


Figure 3.3 SVT20-40 X-Ray Patterns after Sintered at 1350°C for 4h. The secondary phase intensity decreases.

To confirm whether it is single phase after high temperature sintering, SVT30 was selected as an example to check the morphology via SEM and the elements distribution via EDS. The sintering temperature has been scanned from 1250°C to 1400°C. As shown in Figure 3.4

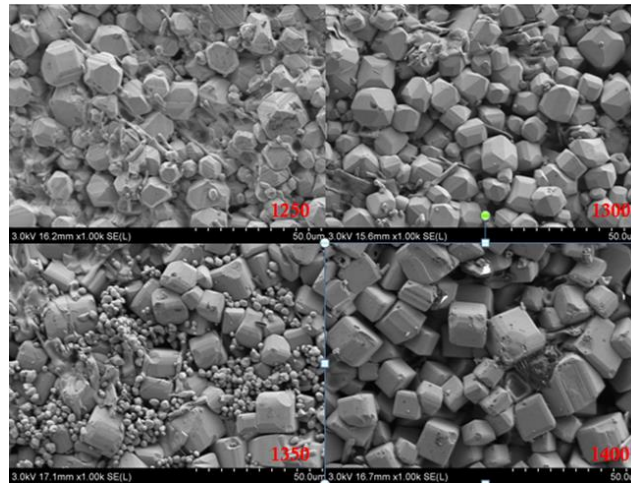


Figure 3.4 SEM images of SVT30 with different sintering temperatures

According to SEM images of SVT30 sintered from 1250°C to 1400°C, only the sample sintered at 1400°C has the single phase. While sintered at lower temperatures, there are secondary phases sitting in the grain boundaries. Even at 1250°C, big grains are observed. It is the main perovskite phase with an average grain size of 10µm and when the sintering temperature is increasing, the grain size doesn't change a lot. However, the morphology of the secondary phase appears quite differently at these sintering temperatures. At 1250°C, there are fibers filling in the gaps among the main grains. At 1300°C the secondary phase agglomerates and not evenly distributed. When the sintering temperature goes up to 1350°C, the secondary phase becomes ball shape and settles in the grain boundaries. We speculate the secondary phase composition changes, due to high temperature sintering. Most of V contained compounds have low melting point and it is easy to evaporate during sintering and change the stoichiometry. When the sintering temperature goes up to 1400°C, no secondary phase is observed, which confirms our speculation. At this point, all impurities go away, leaving big gaps among the main grains. These gaps have bad effect on conductivity, because they introduce high porosity, and the percolation of grains is bad. Conductivity decreases when the grain starts to lose connection.⁹²⁻⁹⁵ After sintering, the secondary phase is kind of glassy phase as X-ray doesn't give strong signals for these impurities.

It is also necessary to know the compositions of the main phase and the impurities. So EDS analysis is brought into the discussion. The bottom image is the element analysis for the main grain and the right hand side is for the impurities. The main phase is SrTiO₃ with V dopant. However, the dopant concentration is quite low, which is around 6%.

Based on previous calculation, the solubility limit is 10%. In the real case, the value is even smaller, probably because of different chemical properties between V and Ti, or there is V evaporation during high temperature sintering. For the impurities, the composition is abnormal. The oxygen amount is too low to form a regular metal oxide. Considering it is impossible to form Sr or V metal after sintering, we can only conclude EDS analysis is not accurate for oxygen detection in glassy phase. In spite of this, according to Sr to V ratio, we can still find out the glassy phase has a composition close to $\text{Sr}_3\text{V}_2\text{O}_8$.

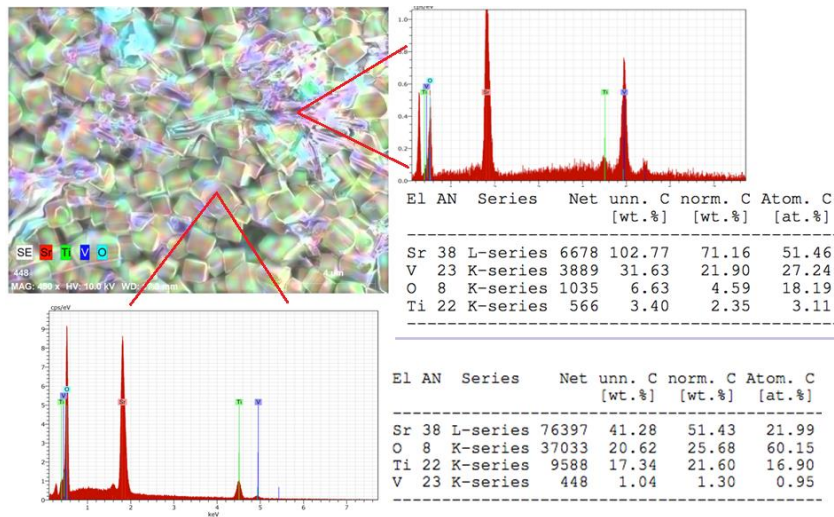


Figure 3.5 EDS Analysis of SVT30 Surface after Sintered at 1350°C

Linear shrinkages of SVT30 with different sintering temperatures also were also measured. From 1250°C to 1350°C, the linear shrinkage increases with sintering temperature increases. However, if it reaches 1400°C, the linear shrinkage dramatically drops to 18.3% (Table 3.1). When the sintering temperature is lower than 1350°C, there are secondary phase present and sitting in the grain boundaries. They can work like a binder system to make the main grains compact. At high temperatures, the secondary

phase evaporates. The big cubic grains cannot form a good network due to poor orientation, as shown in the SEM images. There are a lot of gaps among the grains. The relative densities were measured by Archimedes method. The trend is the same as linear shrinkage trend. The highest density and shrinkage appear at 1350°C. This is also the reason we chose 1350°C as the sintering temperature. The vanadium doping level may change the optimized temperature but to keep everything consistent, it was fixed at 1350°C.

Sintering Temperature	1250°C	1300°C	1350°C	1400°C
Linear Shrinkage	19.1%	21.0%	22.5%	18.3%
Relative Density	0.858	0.872	0.877	0.858

Table 3.1 Linear Shrinkage and Relative Densities of SVT30 under Different Sintering Temperatures

At last, electronic conductivity was measured for these samples. All compositions have higher conductivity. SVT35 has the best performance, reaching $100 \text{ S}\cdot\text{cm}^{-1}$ at 450°C (Figure 3.6). They are all better than the base material SrTiO_3 , thus doping V in to SrTiO_3 successfully transform an insulator to an electronic conductor. One thing should be pointed out is the solubility for V in titanate is not high. How do these compositions achieve such high conductivity? We believe it is a synergistic effect of the main phase and the impurities. The secondary phase is close to $\text{Sr}_3\text{V}_2\text{O}_8$ and it can show high

conductivity after reduction. ⁹⁶ This highly conductive secondary phase fills the gaps among the main grains and the overall effect is make the material metallic conductors.

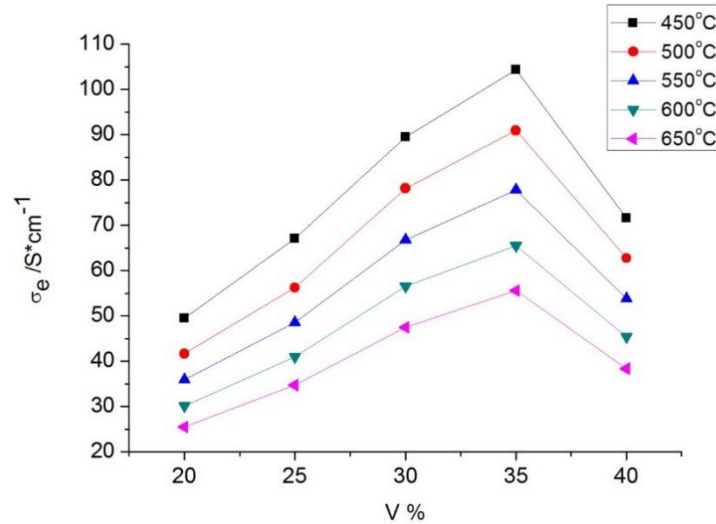


Figure 3.6 Conductivity of SVT with Different Vanadium doping level. 35% V doped sample has the highest conductivity and all compositions are metallic conductors.

3.4 Conclusion

Doping V into SrTiO₃ can greatly improve the conductivity. Because V is a cation that is easy to reduce, in reducing conditions, doping V can introduce free electrons into the materials. When the dopant level is 35%, the conductivity is the highest which is 100 S*cm⁻¹. However, based on the theoretical calculation, V solubility is low in titanate, due to very small ionic radii of V⁵⁺. The following X-Ray patterns, SEM images, and EDS analysis also prove there are glassy secondary phase. The secondary phases are mostly strontium vanadates and they are conductive after reduction. It helps to improve the conductivity by filling all gaps among main grains, and also densifies the materials. Nevertheless, this mixed composition is harmful for cell fabrication. The secondary

phase has a low melting point and it is not stable in stoichiometry. It has high tendency to react with other cell components. We tried to fabricate GDC electrolyte supported cell with SVT anode, but unexpected material formed and resulted to pinholes under fuel cell operation conditions. As a result, to make a working cell, more effort should be put on this material, either finding out a buffer layer between SVT anode and GDC electrolyte, or carefully controlling the SVT composition and firing procedure.

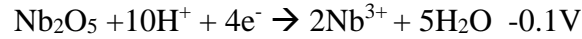
Chapter 4: Strontium and Vanadium co-doped NaNbO_3

4.1 Introduction

In Chapter 3, it has been proven that doping V into perovskite can improve the conductivity by increasing the concentration of free electrons. After V doping, SVT material has the conductivity up to $100 \text{ S}\cdot\text{cm}^{-1}$. However, even though the compositions are good in conductivity, it also reveals some problems. Based on calculation and characterizations (SEM, EDS, XRD), the solubility of V in SrTiO_3 is low, no more than 10%. It is because V^{5+} is too small and its different chemical properties form Ti^{4+} . As a result, there are a lot of glassy phases. The glassy phase may help with the conductivity, but it has potential bad effect in cell fabrication process. A better material is needed without these problems.

The calculated B site cation ionic radii limit is 59 pm, and V^{5+} is 54pm. Therefore, if the original B site cation is a larger than Ti^{4+} , the average ionic radii can be controlled above 59 pm. NaNbO_3 is a good candidate in which V can be doped. Nb^{5+} has the ionic radii of 64 pm. Even 30% V doped at B site, the average ionic radii is 61 pm which is above the limit. Moreover, Nb and V are in the same group in the periodic table and they share the same valence state of 5+, which means the chemical properties are close to each other. Accordingly, we can anticipate V has a higher solubility in NaNbO_3 than that in SrTiO_3 .

Meanwhile, we may also predict that V doped NaNbO₃ can have a higher conductivity than V doped SrTiO₃. Based on the reduction potentials of Ti⁴⁺ and Nb⁵⁺



Nb is easier to get reduced than Ti. In addition, the electron mobility is higher in niobate than that in titanate. These are the reasons SrTiO₃ is an insulator while NaNbO₃ can show the conductivity of 2 S*cm⁻¹ at 650°C in hydrogen. By doping the same amount of V, the NaNbO₃ system may have better performance.

4.2 Experiments

4.2.1 Material Synthesis

Based on different V dopant levels, Sr_{0.2}Na_{0.8}Nb_{0.9}V_{0.1}O₃, Sr_{0.2}Na_{0.8}Nb_{0.8}V_{0.2}O₃ and Sr_{0.2}Na_{0.8}Nb_{0.7}V_{0.3}O₃ are called SNNV10, SNNV20 and SNNV30, respectively throughout this chapter. All compositions were synthesized by a modified glycine-nitrate method. Stoichiometric amount of strontium nitrate, sodium nitrate, niobium oxalate and ammonium metavanadate were dissolved in de-ionized water separately. The solutions were mixed slowly and glycine was added based on glycine to nitrate ratio of 1:1. Citric acid was then added until the white precipitate disappears. The mixture was stirred and heated on the hot plate at 200°C to evaporate the solvent until a viscous gel was formed. Ethanol was sprayed on the gel and manually ignited. After a complete combustion, the residues of the reaction were collected and heated at 400°C for 2 hours. The precursors were then calcined at 1000°C for 4 hours, with the ramping

rate 3°C / min. The calcined powders were ball milled in ethanol for 24 hours and then sintered at 1300°C for 4 hours with the ramping rate 3°C/min.

4.2.2 Phase Purity Determination

To confirm phase purity, X-ray diffraction was performed on the sintered samples, using a Bruker D8 Advance diffractometer with CuK α radiation. The degree ranges from 20° to 80° with a step 0.015°/s. To examine the stability in reducing atmosphere, all samples were reduced and phase purity was determined.

4.2.3 Compatibility Test with Electrolytes

It is important to examine whether SNNV is compatible with common electrolytes such as yttrium stabilized zirconia (YSZ) and gadolinium doped ceria (GDC). Compared to all other compositions, SNNV30 has the highest reactivity with electrolyte due to its highest V dopant level. V⁵⁺ is small (ionic radii 54pm, coordination number = 6), so it is easy to migrate at high temperatures and reacts with other materials. To examine the possibility of reaction between the new anode and the electrolyte, SNNV30 is selected to confirm the chemical stability with YSZ and GDC. Equivalent weight of calcined SNNV30 powder and GDC (YSZ) nano particles were mixed, ball milled in ethanol for 24 hours. The mixtures were dried in oven and heated at 1300°C for 4 hours. The heated powders were sent to X-Ray to find out the phase purity.

4.2.4 Conductivity Measurements

Electronic conductivity was measured using four probe DC method. The samples were prepared by mixing equivalent amount of SNNV and GDC. The composite powders were ball milled in ethanol for 24 hours. Ethanol was then evaporated in oven, and the pellets were pressed using hydraulic press. The green bodies were sintered at 1300°C for 4 hours, and sample bars were cut to determine the conductivity. Thin silver wires were wrapped to the bars and connected with the Keithley 2400 current source. The geometry factors were measured between the two voltage leads and the Keithley was set at 4 probe mode. All SNNV samples were reduced in 10% H₂ /N₂ at 650°C for 24h and the measurements were done within temperature range from 650°C to 450°C. During the intervals of temperature ramping, the resistance values were taken when the readings were stabilized. The SNNV-GDC composite conductivity was also determined in a similar way.

4.2.5 Electrolyte Supported Cell Fabrication

SOFC performances were determined on GDC electrolyte-supported cell. A 260µm thick GDC electrolyte was prepared by tape casting technique, following a standard lab procedure with Polyvinyl Butyral (PVB) as binder, Butyl Benzyl Phthalate (BBP) as plasticizer and fish oil as dispersant. Solvent system is ethanol / toluene mixture. The tapes were dried and laminated to achieve desired thickness. The button cells were punched from the green tape and sintered at 1450°C for 4 hours with alumina settle plate as load. SNNV-GDC anode paste was prepared following the standard procedure. Equivalent volumetric proportion of SNNV and GDC were mixed. 12µm and 1.8µm

Poly(methyl methacrylate) (PMMA) pore formers were added into the mixture to obtain the theoretical porosity of 50 vol.%. The ESL vehicle (ElectroScience 441) was added in the mixtures to make a paste of screen printing consistency. The ink was then brush painted on the GDC electrolyte. The back side of the electrolyte was deposited with LSCF-GDC cathode using blade coating technique. The electrodes deposited assembly were dried separately and co-fired at 1050°C for 2 hours. After applying the anode paste. By weighing the sample we can know the add-on weight. Because the recipe is known, SNNV-GDC powder weight was calculated, which is the anode weight. To achieve high catalytic activity and ionic conductivity, nitrate precursor of Ni-GDC was infiltrated on the anode side. The nitrates were burned by heat-treating the sample at 400°C between each infiltration cycles. The Ni-GDC loading was determined by subtracting the initial weight from the final weight of the sample after infiltration. By Comparing the infiltrate weight and anode weight, the loading amount was calculated. The final Ni-GDC loading is around 10 wt%. For comparison, GDC only infiltrated samples were prepared by the same method, and the GDC loading is around 10 wt%.

4.3 Material Properties and Discussion

SNNV compositions show single perovskite phases as shown in Figure 4.1, however a few minor impurities at lower angle between 25° to 30° for high V dopant levels were observed, indicating there is a solubility limit of V in NaNbO₃. The excess V can exist in V⁵⁺ oxidation state with small ionic radii (54 pm, coordination number = 6) and high

mobility. This can facilitate easy formation of secondary phases such as NaVO_3 , SrVO_3 or other unknown amorphous phases.

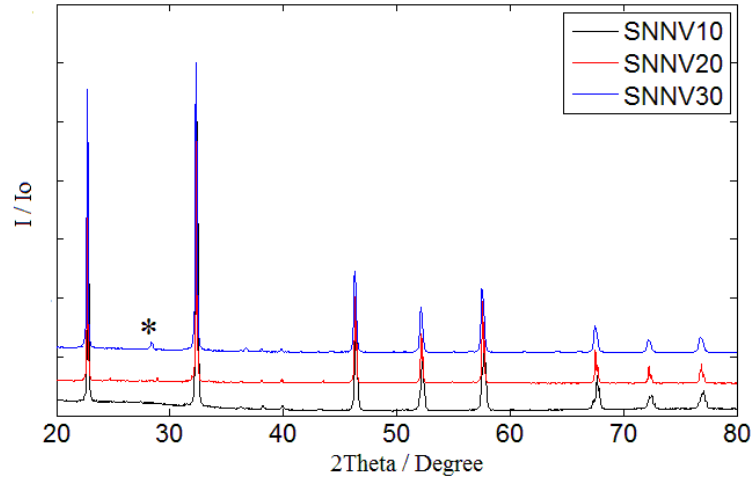


Figure 4.1 XRD Patterns of SNNV10, SNNV20 and SNNV30 after firing at 1300°C for 4h. All compositions have perovskite phases with minor impurities at low angles with high vanadium doped sample

The structural stability of SNNV in the presence of H_2 as reducing gas was studied using XRD and the patterns are shown in Figure 4.2. The compositions SNNV10 and SNNV20 have good structural stability even in H_2 containing gas.

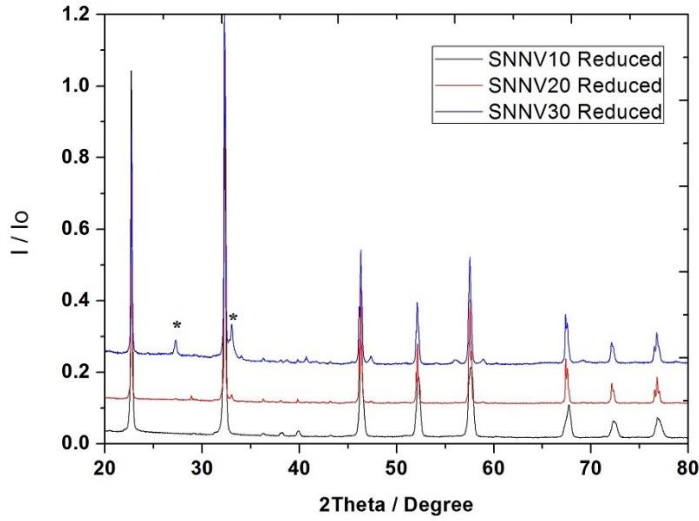
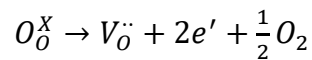


Figure 4.2 XRD patterns of reduced SNNV10, SNNV20 and SNNV30. SNNV10 and SNNV20 are still single phases. SNNV30 has impurities formed during reduction (* unknown impurities)

In order to improve the electronic conductivity either the concentration of free electrons or mobility of free electrons must be increased. At low P_{O_2} , free electrons are generated, when lattice oxygen is taken away by reducing gas such as H_2 , donating two free electrons and creating an oxygen vacancy as shown below



If the crystalline lattice is easy to lose oxygen, in other words, should the material be easily reducible. The dopant V can easily change its valence state from 5+ state to 4+ state or even 3+ state under reducing conditions. Thus, doping V in $NaNbO_3$ can favor the removal of lattice oxygen, and increase the concentration of free electrons. It is to

be noted that, even though oxygen removal improve the conductivity, it has negative effect. In the process of removing oxygen, oxygen vacancies are created. Higher the oxygen vacancies will compromise the stability of the material, and even cause collapse of lattice structure due to lower columbic force between cations and anion. In order to stabilize the perovskite structure, it is essential to dope a higher valence cation at the Na-site of the NaNbO_3 pervoskite and this would compensate the reduction in columbic force. Sr cation is doped in the in the Na-site due to their comparable ionic radii. (Sr 144pm, Na 136pm, coordination number = 12), and the XRD pattern of the resulted sample is shown in Figure 4.3. It must be noted that 10% Sr in A-site is not stable in hydrogen-containing atmosphere. However, the composition with 20% Sr at A-site is stable without decomposition, thus doping certain amount of high valence A-site cation can stabilize the lattice structure in reducing gas conditions.

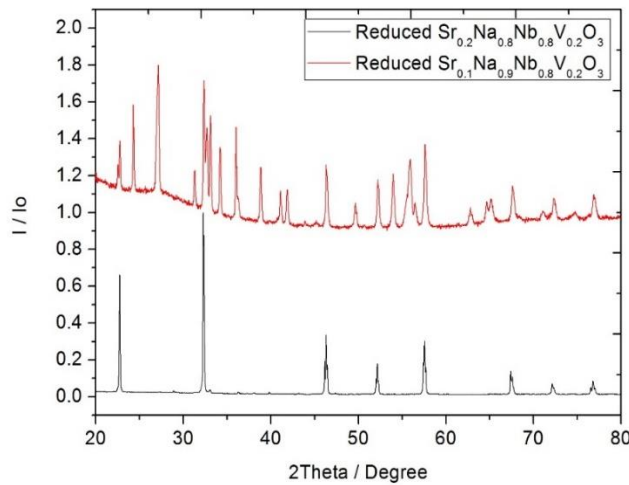
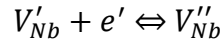
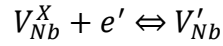
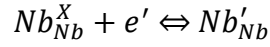


Figure 4.3 Examples of different strontium doped SNNV samples. 20% strontium can stabilize the perovskite phase. 10% strontium doped sample totally decomposes after reduction

At another aspect, the V-doped NaNbO₃ also has high electron mobility. According to electron hopping mechanism, electron hops among multivalence B-Site cations. So in these compositions, the electron hopping routes can be as follows.



Here, the multivalent cation is necessary. While B-site cation releases free electron, the valence decreases. When the electron incorporates into B-site cation, the valence increases. If the valence is easy to shift for the B-site cations, the electron mobility is high due to fast hopping process. Niobium and vanadium are all multivalent cations and the valence states can change easily. Therefore, perovskites with Nb and V as B-site cations have high electronic mobility and in turn have high electronic conductivity.

97,98

After reduction at 650°C in hydrogen, all SNNV samples show high conductivities and exhibit metallic behavior. The metallic type conduction is favorable for fabricating anode-supported LT-SOFCs shown in Figure 4.4. At 450°C, SNNV30 has the highest conductivity around 300 S*cm⁻¹ and 10% V doped sample, SNNV10, has the conductivity of 130 S*cm⁻¹.

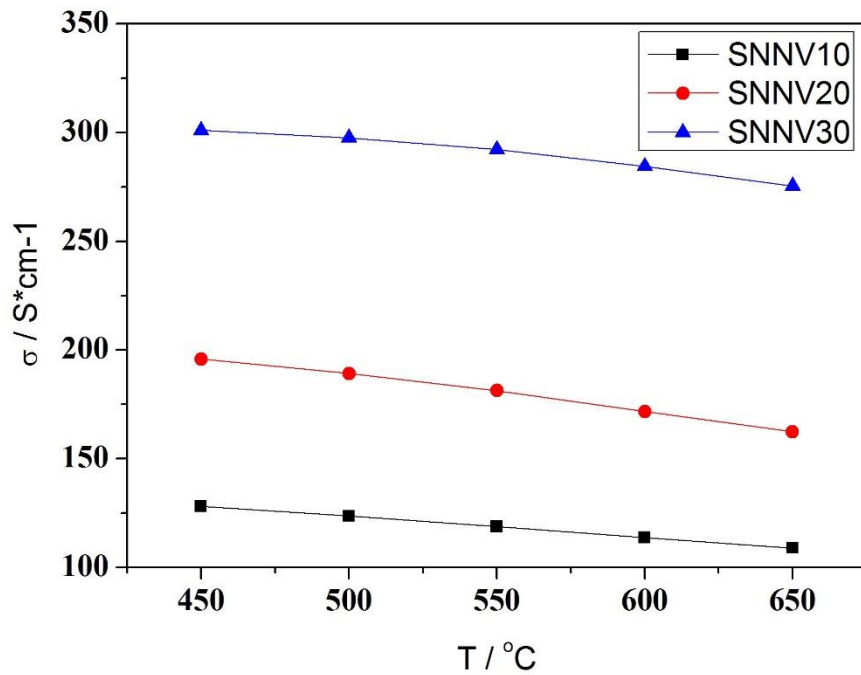


Figure 4.4 Conductivities of SNNV10, SNNV20 and SNNV30 after reduction in 10% H_2 / 90% N_2 . More vanadium dopant level, higher conductivity.

Due to high mobility of vanadium, it is necessary to determine the reactivity between SNNV30 and common electrolytes such as YSZ and GDC. XRD patterns show YSZ reacts with SNNV30 at high temperature and forms unknown phases. However, SNNV10 and GDC10 do not react with each other to form new phases up to 1300°C in air. Figure 4.5 and Figure 4.6 evidently explains that compatibility between GDC and SNNV is good.

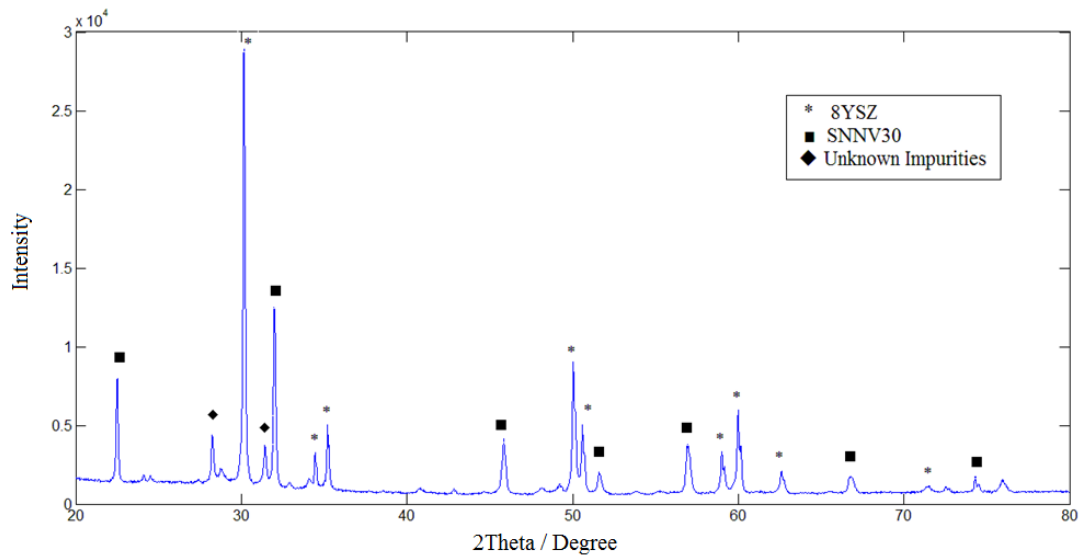


Figure 4.5 High temperature treated (1300°C) nano 8YSZ and SNNV30 mixture. They react with each other and form unknown materials

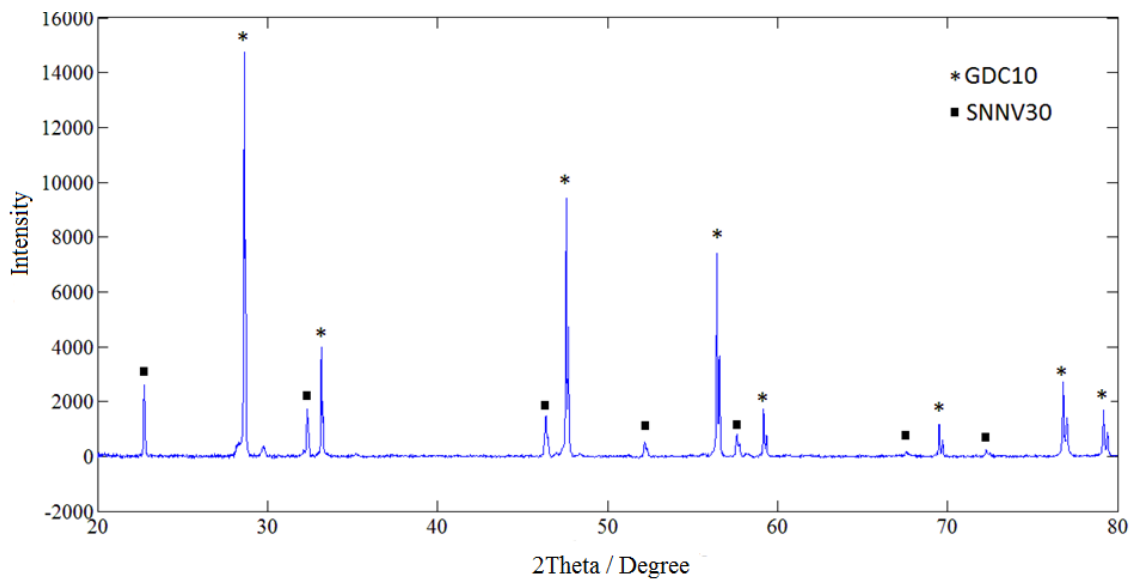


Figure 4.6 High temperature treated (1300°C) nano GDC and SNNV30 mixture. No reaction between the two compounds

Composite anode can decrease the shrinkage differences and thermal mismatch between electrolyte and anode during sintering. Conductivities of SNNV10-GDC, SNNV20-GDC and SNNV30-GDC were examined and the result is in Figure 4.7. Among all SNNV composition, SNNV30 has highest conductivity. However the composites behave differently. SNNV10-GDC has the highest conductivity among all composite samples. It may be caused by elements diffusion. Even though SNNV and GDC don't react with each other to form new phases, which may cause stability issues, minor elements diffusion may happen at high temperatures, which is quite common in fuel cell fabrication. During sintering conditions, vanadium could migrate into GDC phase, and it changes the stoichiometry slightly of both SNNV and GDC. As the result, the electronic conductivity decreases. Higher vanadium level, higher tendency of vanadium diffusion and more deviation from original SNNV compositions. It may explain why SNNV10-GDC has the highest conductivity. Further vanadium discussion is shown in the cell performance session with EDS analysis. In this way, SNNV10 is the best choice for the SOFC anode material compared with SNNV20 and SNNV30. The conductivity of SNNV10-GDC is the highest and lower vanadium doping level can reduce the potential vanadium inter diffusion between SNNV and GDC. As such, it is better to lower the cell fabrication temperature to minimize the vanadium diffusion which may result in lower OCV. Diffusion of V into electrolyte has to be prevented to fabricate an anode-supported cell. In this chapter we focus on electrolyte supported cells to study the electrode properties of SNNV.

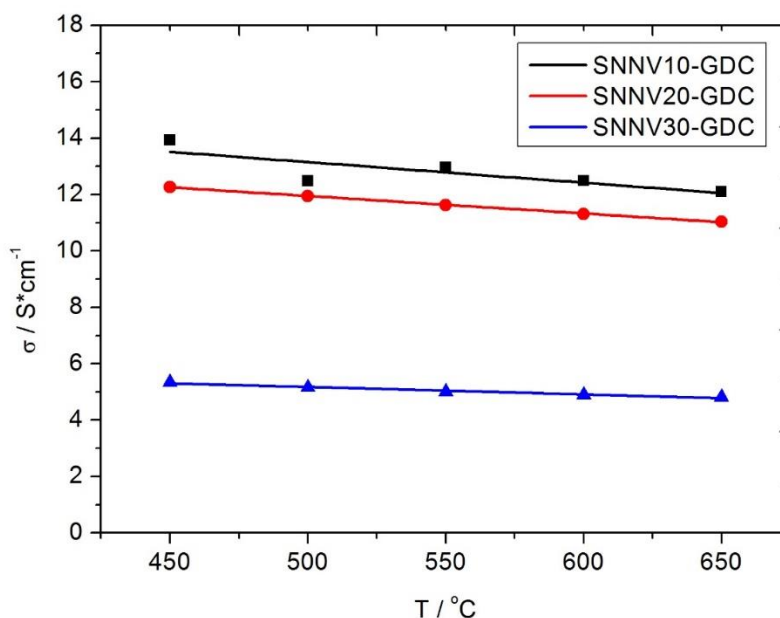


Figure 4.7 SNNV-GDC composites' conductivities at different temperatures. It has the opposite trend compared with SNNV single material. SNNV10-GDC has the highest conductivity

4.4 Performance of Electrolyte Supported Cell

A 260 μm thick dense GDC electrolyte supported cell with both cathode and anode co-fired at 1050°C was tested in dry/wet H_2 and dry/wet CH_4 . Initially SNNV-GDC samples infiltrated with GDC were examined. The cell performances are shown in Figure 4.8. At 650°C, the hydrogen performances of all ceramic cells are 135 mw/cm^2 in wet condition and 180 mw/cm^2 in dry condition. Vanadium contained compound can be used as catalyst for partially oxidize hydrocarbons^{99,100}. Based on the literature, there is a possibility that SNNV has the capability to catalyze hydrogen oxidation due to the various valence state of vanadium. In other words, without metallic catalyst, such

as Ni, Pd or Pt, SNNV can be both catalyst and electronic conductor at the SOFC anode side with hydrogen as fuel. However, while hydrocarbons are the fuel, such as CH₄, the performance is much lower, around 40 mw/cm² in dry CH₄ and 35 mw/cm² in wet CH₄. The catalytic activity is not high enough to accelerate methane oxidation reaction compared with hydrogen. Considering the low vanadium doping level in SNNV10, increasing vanadium dopant amount may improve hydrocarbon performance. Nevertheless, increasing vanadium amount in the system should be carefully considered as the composition conductivity may decrease when increasing vanadium dopant level, and high vanadium content may cause fabrication issues.

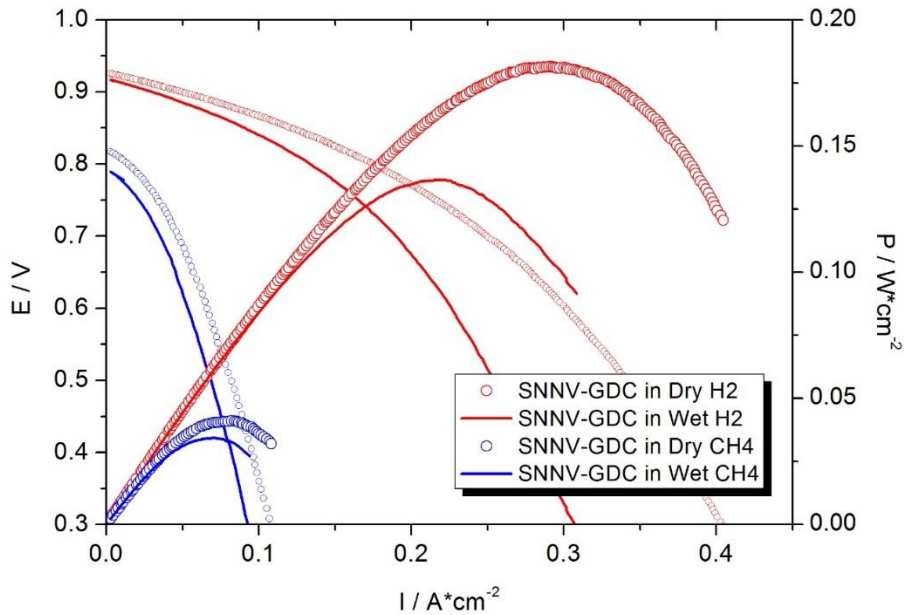


Figure 4.8 220 μm GDC supported cell with SNNV-GDC anode and LSCF-GDC cathode. 10 wt% GDC infiltrated into SNNV-GDC anode. Cell was tested at 650°C in H₂ and CH₄. CH₄ performance is much lower than H₂ performance. In dry conditions the cell works better.

Moreover, in the humidified fuel, the cell outputs are lower both in hydrogen or methane as the feed, unlike typical Ni-YSZ or Ni-GDC. Raymond J. Gorte also found there was a performance drop for their sodium tungsten bronze infiltrated cell in humidified hydrogen.¹⁰¹ The reduction in performance was attributed to an ohmic resistance increase for sodium tungsten bronze, when the cell is exposed to wet atmosphere. Considering SNNV, it may be the same case as we also found there was an ohmic resistance increase, shown in Figure 4.9. In other words, there is a possibility of some surface reaction between sodium and moisture, forming hydroxide at the surface, and overall performance decreases. Based on calculation, a running cell at the anode will generate 0.5% to 1% steam in the total flow rate of 100 SCCM, which is lower than the humidified 3% H₂O containing fuels. We believe these is a critical limit of water percentage for a stable running cell, due to the cell output decrease when the moisture level goes from 1% (dry condition) to 3% (wet condition).

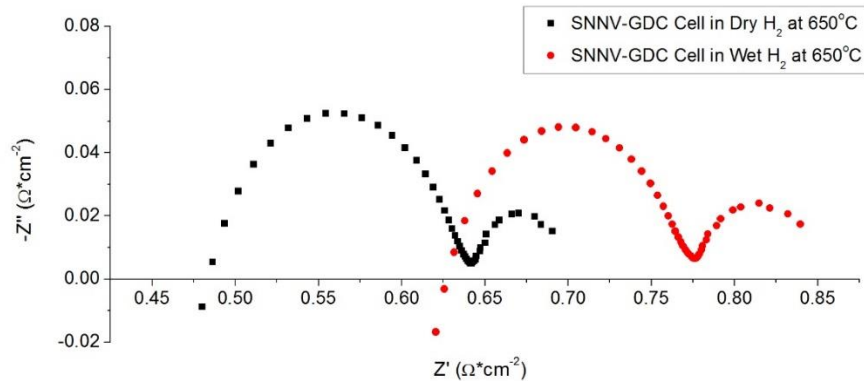


Figure 4.9 Impedance comparison between SNNV-GDC cells in dry and humidified hydrogen at 650°C. An ohmic resistance increase was observed while switching to humidified fuel.

Considering the low performance in GDC infiltrated cell, we also infiltrated Ni-GDC into this SNNV-GDC cell to examine the improvement. When Ni is infiltrated, the catalytic activities are both enhanced in dry H₂ and dry CH₄, especially in CH₄. At 650°C, the PPD in dry H₂ is 280 mw/cm², 50% improvement compared with GDC only infiltrated sample. The CH₄ performance is 220 mw/cm², 5 times higher than the no-nickel cell. At 600°C, the cell can still give out 150 mw/cm² and 115 mw/cm² in H₂ and CH₄ respectively shown in Figure 4.10. For a low temperature SOFC (< 600°C), the infiltration of catalyst is necessary, especially hydrocarbons are used as fuel, because low temperature hampers the reaction kinetics.

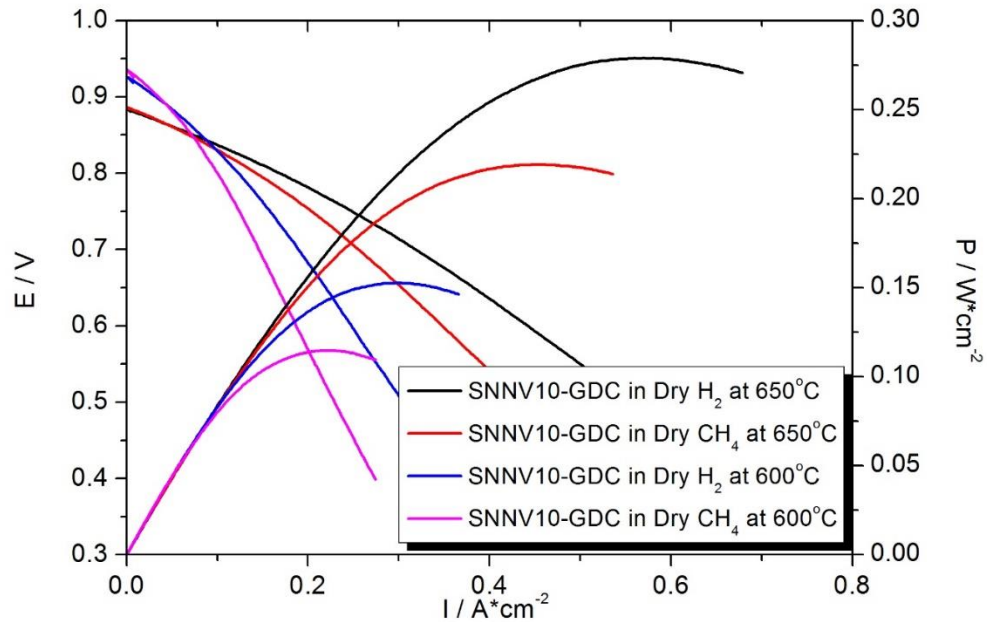


Figure 4.10 220 μm GDC supported cell with SNNV-GDC anode and LSCF-GDC cathode. 10 wt% Ni-GDC infiltrated into SNNV-GDC anode. Cell was tested in dry H₂ and dry CH₄.

The SEM of the cell cross section is shown in Figure 4.11. The overall thickness of electrolyte is around 260 μm , with 21.4 μm LSCF-GDC cathode. In order to get good performance, infiltration is needed. The morphology of pores in the anode can really affect infiltration results. We tried homogeneous size of PMMA, but there are a lot of closed pores and the connections between pores are easily blocked by infiltrates, which limits further infiltration and the total loading is low. By mixing different sizes of PMMAs, the microstructure shows a good pore percolation, resulting to a better infiltration and gas diffusion. In Figure 10d, we can see a well dispersed Ni-GDC nano particles.

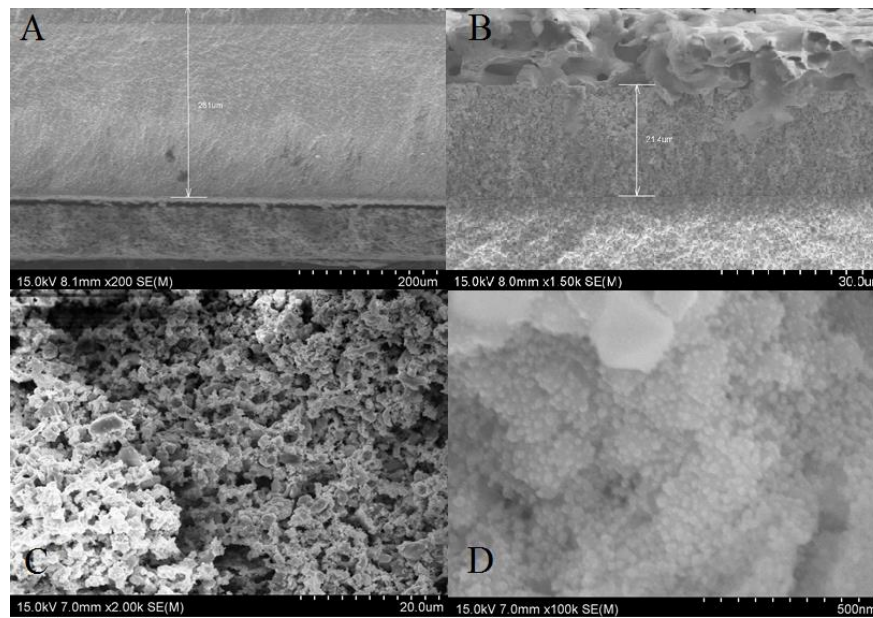


Figure 4.11 SEM images of cell structure. (A) Overall cell structure with thick GDC electrolyte, LSCF-GDC cathode and SNNV10-GDC anode. (B) Interface between cathode and anode. Cathode thickness is around 20 μm . (C) Anode microstructure (D) well distributed Ni-GDC nano particles

The EDS analysis in Figure 4.12 shows the elements distribution along the anode through the electrolyte. Because of low temperature firing (1050°C), Na and Nb are all sitting in the anode region, which is a good sign. However vanadium diffusion was observed, due to comparatively small ionic radii. It may have potential effect in cell performance and we are going to do further analysis in future.

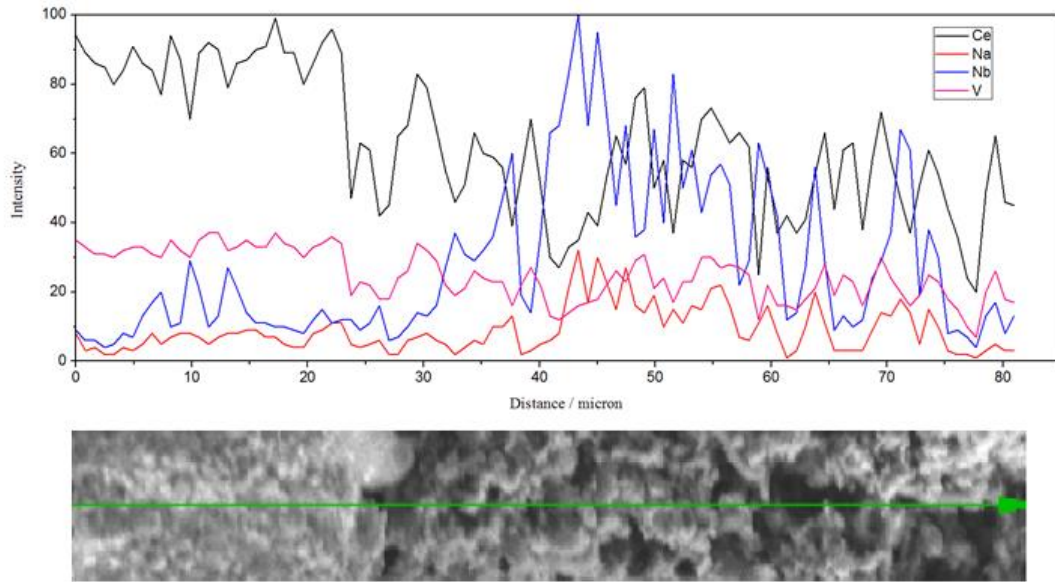


Figure 4.12 EDS analysis of the interface between GDC electrolyte and SNNV10-GDC anode. No sodium and niobium diffusion but there is vanadium migrate from the anode to the electrolyte

4.5 Conclusion

Different compositions of SNNV were synthesized via wet chemical method and high conductivities were achieved. SNNV10 has the conductivity of $130 \text{ S}\cdot\text{cm}^{-1}$ and the composite conductivity is the highest among the three. Because of vanadium diffusion at high temperatures, the cell is preferred to be fabricated at relatively lower temperatures. While infiltrating Ni-GDC, the GDC electrolyte supported cell has the

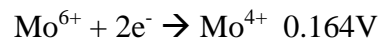
PPDs of 280 mw/cm^2 and 220 mw/cm^2 in dry H_2 and dry CH_4 respectively at 650°C . When the temperature is lowered to 600°C , the PPDs are 150 mw/cm^2 and 115 mw/cm^2 in H_2 and CH_4 respectively under dry conditions. If there is no nickel as catalyst, the SNNV can intrinsically catalyze H_2 and has an appropriate output. However, the hydrocarbon performance is hampered. Unlike Ni-cermet anode, SNNV has higher performance under dry conditions than that under wet conditions mainly because of potential instability in high moisture atmosphere. At last, vanadium diffusion is observed which may decrease the cell open circuit potential. Low temperature cell firing is needed to fabricate anode supported thin electrolyte cell.

Chapter 5: Modified Molybdenum Double Perovskite

5.1 Introduction

In the previous chapters, all materials are based on V dopant because V is easy to reduce. It increases the concentration of free electrons. However, there are some unexpected problems, like solubility, secondary phase formation, and V diffusion. To make an anode supported cell, all these problems should be solved. Due to vanadium's intrinsic properties, these problems are difficult to address. Therefore new materials without vanadium has to be developed, not only considering the material intrinsic properties, but also fabrication issues.

Molybdenum double perovskite is a good candidate and lot of these materials have been developed for fuel cells. But most of the cells are electrolyte supported, because of low anode conductivity and fabrication issues.^{72,102-106} The structure of double perovskite is shown in Figure 2.4 in chapter 2. It has ordered B site cations with alternative Mo / Me (transition metal) octahedrals. For Mo, the reduction potential is shown below, which promises good electron concentration and mobility.



Nevertheless, the conductivity for these double perovskites is quite tricky. When Me = Mg, Co, Ni, the compositions can be obtained in air, but the conductivity is lower than $10 \text{ S}\cdot\text{cm}^{-1}$ which is not enough for anode supported cell. This is one reason that these materials are usually used in electrolyte supported cells. To obtain a good fuel cell performance at low temperatures, anode supported cell is necessary, otherwise there is

a huge ohmic resistance. The reason for the low conductivity is the ordered structure. In Figure 5.1, we can see the route for electron transport, with the example of $\text{Sr}_2\text{CoMoO}_6$.

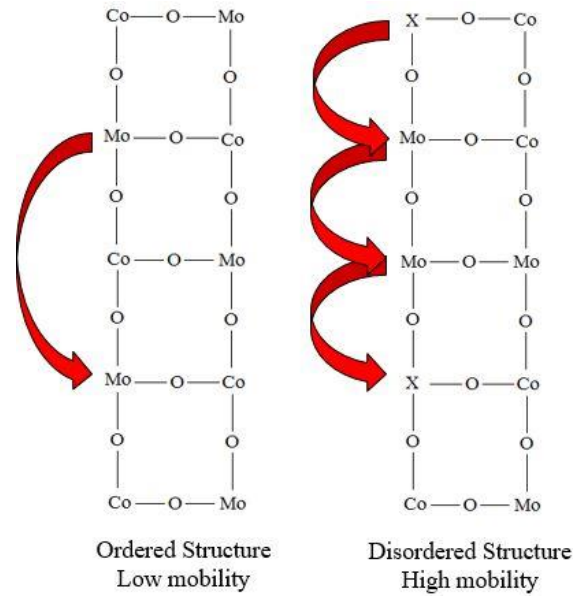


Figure 5.1 Ordered $\text{Sr}_2\text{CoMoO}_6$ and cation X doped $\text{Sr}_2\text{CoMoO}_6$ with a disordered structure. The electron transport route is shortened by doping.

In $\text{Sr}_2\text{CoMoO}_6$, when the material is exposed to hydrogen, Mo^{6+} can be reduced to Mo^{5+} and even Mo^{4+} to generate electrons. However, Co is fixed at 2+ state in reducing conditions and cannot be reduced to an even lower valence state. It means the electrons should bypass the Co^{2+} site and hop between Mo sites. It is a very long distance, as the result, the electron mobility is low. To improve the conductivity, the mobility needs further improvement. Our idea is to dope another cation X into the lattice. X has different valence state from either Co^{2+} or Mo^{6+} . In addition, cation X has a different ionic radii from Co^{2+} (70 pm) or Mo^{6+} (59 pm). The chemical property difference can

greatly disturb the ordered structure. The lattice with dopant is also shown in Figure 5.1. The electron transport route is greatly shortened, in another word, the mobility increases. If X is also a multivalent cation, the conductivity can be improved more. Here we selected Fe as the dopant. Fe^{3+} has the ionic radii of 60 pm which is in between of Mo^{6+} and Co^{2+} , and the valence state is also different from Mo^{6+} and Co^{2+} . Therefore it can be expected that doping Fe will increase the degree of disorder. Meanwhile, the Fe^{3+} is able to get reduced to Fe^{2+} in hydrogen, so it provides extra free electrons and mobility.

5.2 Experiments

5.2.1 Material Synthesis

Compositions with equal amount of cobalt and molybdenum (SFCM), $\text{SrFe}_{0.1}\text{Co}_{0.45}\text{Mo}_{0.45}\text{O}_3$, $\text{SrFe}_{0.2}\text{Co}_{0.4}\text{Mo}_{0.4}\text{O}_3$, $\text{SrFe}_{0.34}\text{Co}_{0.33}\text{Mo}_{0.33}\text{O}_3$ and $\text{SrFe}_{0.5}\text{Co}_{0.25}\text{Mo}_{0.25}\text{O}_3$ were synthesized via wet chemical method. Stoichiometric amount of strontium nitrate (Alfa Aesar 99.0%), iron nitrate nonahydrate (Sigma Aldrich 99.95%), cobalt nitrate hexahydrate (Alfa Aesar 98%-102%) and ammonium molybdate (para) tetrahydrate (Alfa Aesar 99%) were dissolved in de-ionized water separately. The solutions were mixed and citric acid was added into it to keep the PH level around 2. Glycine was then added with the glycine to nitrate anion ratio 1:1. The mixture was stirred and heated on a hot plate to evaporate all solvent, and a viscous gel formed. And then the temperature was brought up to 350°C and an auto ignition took place. After the flame was gone, the remaining ashes were crushed, collected and

calcined at 1100°C for 4 hours. The powders were pressed via a hydraulic press and sintered at 1300°C for 4 hours, so that the dense samples were obtained.

5.2.2 Phase Purity Examination

The calcined powders were sent to Bruker D8 Advance powder diffractometer for X-Ray detection. The degree ranges from 20° to 80° with a step 0.03° / second. The patterns were compared and check whether they were single perovskite phases. To evaluate the effect of cobalt and molybdenum content on phase, SFCMs with unequal amount of cobalt and molybdenum were synthesized via the method showing above. X-Ray patterns of $\text{SrFe}_{0.3}\text{Co}_{0.3}\text{Mo}_{0.4}\text{O}_3$ and $\text{SrFe}_{0.4}\text{Co}_{0.2}\text{Mo}_{0.4}\text{O}_3$ were compared with $\text{SrFe}_{0.2}\text{Co}_{0.4}\text{Mo}_{0.4}\text{O}_3$ to find out whether different Co to Mo ratio can influence phase purity. $\text{SrFe}_{0.4}\text{Co}_{0.2}\text{Mo}_{0.4}\text{O}_3$ was selected for redox stability test. The sample was reduced in 10% H_2 / 90% N_2 and the X-Ray pattern was compared with the calcined sample.

5.2.3 Conductivity Measurement

Dense pellets were obtained by sintering the pressed green bodies at 1300°C for 4 hours. The pellets were cut into bar shape by a diamond blade. Four probe DC method was used to measure the conductivities by a Keithley 2400 source meter, with silver wires as leads. All samples were reduced in 10% H_2 / 90% N_2 at 650°C for at least one day, and the data was taken when the reading was stable. The reason not using pure hydrogen is safety concern. The measuring temperature ranges from 650°C to 450°C

and the conductivities were compared to find out the composition for best performance. To examine the redox stability, the reduced samples were sent to Bruker D8 Advance powder diffractometer again to see whether the composition was decomposed or new phases appeared.

5.2.4 Chemical Compatibility with the Electrolyte

To make an anode supported cell. It is quite important to check whether SFCM is chemically compatible with GDC electrolyte. Equal molecular amount of SFCM and nano GDC were mixed and ball milled in ethanol for 24 hours. The powders were then dried and heated at 1300°C for 4 hours. The heat treated powder was then sent to Bruker D8 Advance powder diffractometer for X-Ray detection. The degree ranges from 20° to 80° with a step 0.03° / second. The purpose is to find out whether there are new phases forming at high temperatures.

5.3 Material Properties and Discussion

5.3.1 Phase Purity Discussion

After calcination at 1100°C in air, all compositions have single perovskite phases (Figure 5.2) without any impurities. It is a good sign because some of the high conductive molybdenum double perovskite should be synthesized in reducing conditions, but these SFCMs can be obtained in air. It may work with regular electrolytes like GDC, SDC. These compositions could be regard as a mixed phase of SrFeO₃ perovskite and SrCo_{0.5}Mo_{0.5}O₃ double perovskite. Based on the literatures,

SrFeO₃ is a simple cubic perovskite phase with Fm3m symmetry¹⁰⁷ and SrCo_{0.5}Mo_{0.5}O₃ is a distorted tetragonal double perovskite phase with I4/m symmetry.^{108,109} When Fe dopant is high (50%), the SFCM has the same cubic phase as SrFeO₃. While Fe dopant amount decreases, the crystal structure is more approaching to SrCo_{0.5}Mo_{0.5}O₃. The biggest change is a small peak (103,211,121) comes up at 38°, indicating there is an octahedral distortion. After firing, Fe in the system has two valence states of 3+ and 4+. ¹¹⁰ Fe³⁺ is a small cation with the ionic radii of 60pm and Fe⁴⁺ has an ionic radii of 58.5pm. Therefore, Fe dopant decreases lattice parameter and we can see peaks shift to the high angles for high Fe doped samples.

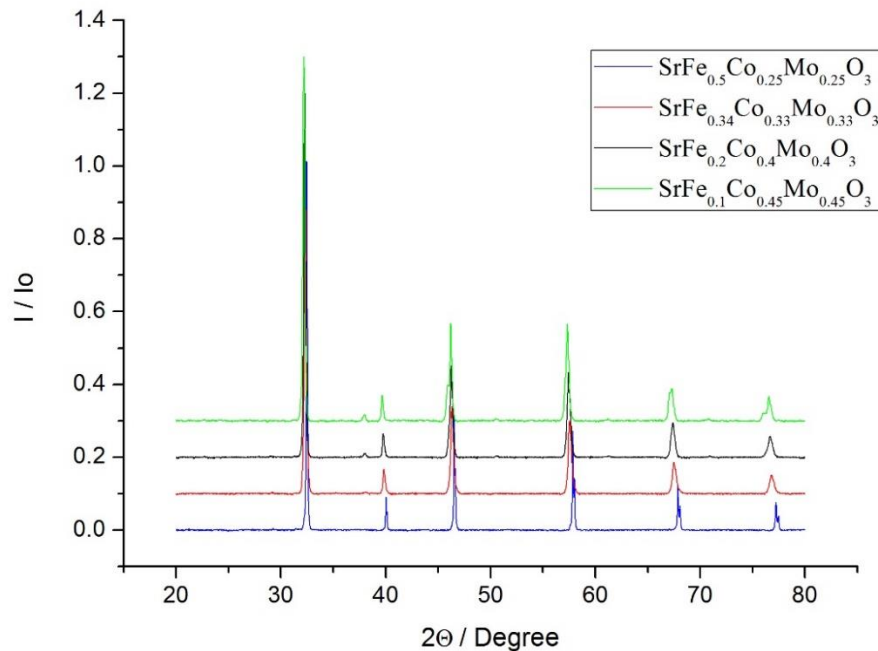


Figure 5.2 SFCM X-Ray patterns after calcination at 1100°C. All Compositions show perovskite phase without impurities.

All compositions have equal amount of Co and Mo. The reason is that only equal amount of Co and Mo can form the single phases. Besides the samples shown in Figure 5.2, other compositions have been investigated. When Co amount and Mo amount are not the same, shown in Figure 5.3, a strong signal of SrMoO₄ phase shows up in the X-Ray pattern. This SrMoO₄ phase is harmful to the anode supported cell fabrication, because there is volume change during redox cycling.¹¹¹ Initial SrMoO₄ is an insulator with the scheelite structure. After reduction, SrMoO₄ can be reduced to conductive SrMoO₃ perovskite phase. While undergoing this phase transition, the volume shrinks around 28%. It is very similar to Ni-cermet anode. At this point, anode support with SrMoO₄ may not have redox cycling stability. Therefore, SrMoO₄ can only be used as infiltrates, instead of anode support. The reason why they form these secondary phase can be attributed by the multivalences of Fe. As discussed before, Fe has a mixed valence state of 4+/3+ after firing in air and 4+ is the majority.¹⁰⁷ Hence there is a problem. If Mo amount is higher than Co amount, due to the high valence state of Fe⁴⁺, there will be excess oxygen anion in the lattice according charge neutrality. It is not stable and excess Mo can be removed from the perovskite phase and forms SrMoO₄. Therefore, it is necessary to control the Co/Mo ratio.

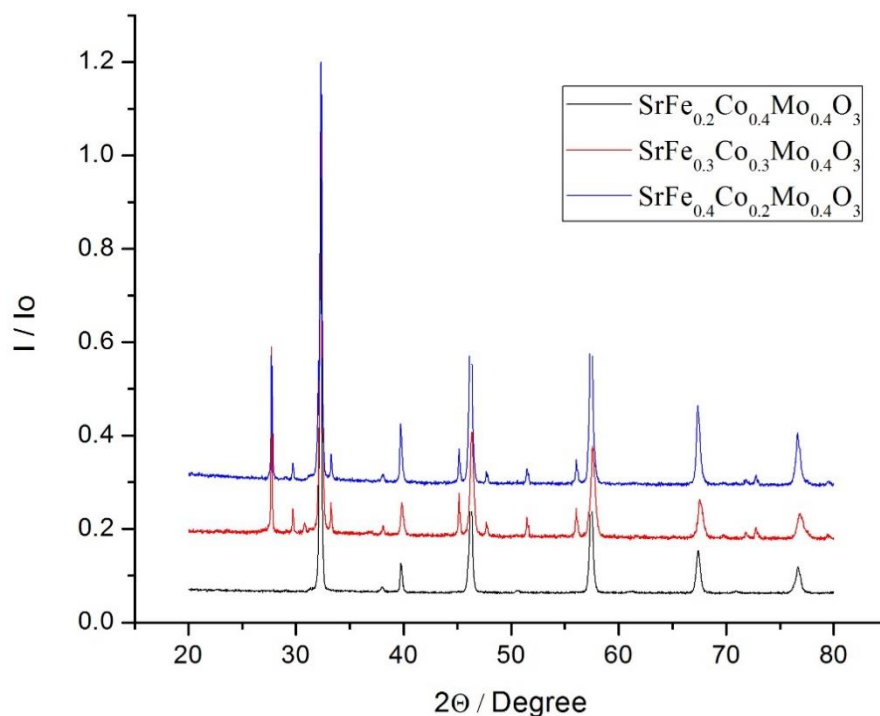


Figure 5.3 X-Ray Pattern comparison among SFCM with and without matched Co/Mo.

When cobalt content is lower than molybdenum SrMoO_4 impurity comes out.

$\text{SrFe}_{0.4}\text{Co}_{0.2}\text{Mo}_{0.4}\text{O}_3$ was selected for redox stability test. By comparing the X-ray patterns before and after reduction, no new phases come up, indicating this composition is stable in both oxidizing and reducing conditions. After reduction, the peaks shift to the low angle. The reduction process removes oxygen anion from the lattice, so the repulsion among cations increase while oxygen is decreasing. Meanwhile, reduction can also lower the valence state of B site cation, such as $\text{Mo}^{6+} / \text{Mo}^{5+}$ transition. The lower valence cation also has larger ionic radii, and finally the crystal lattice expands.

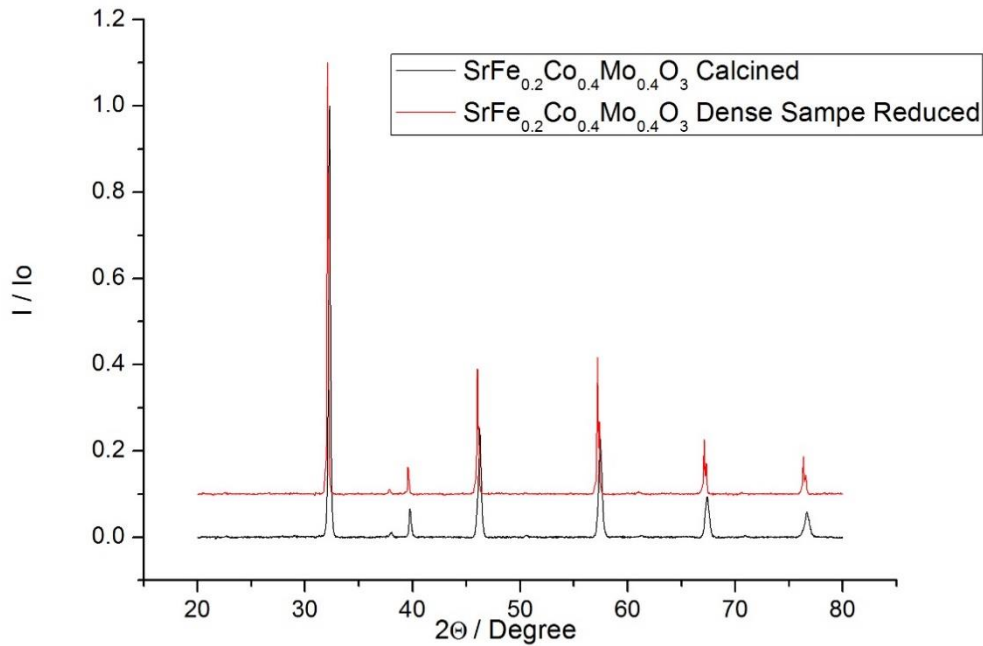


Figure 5.4 X-Ray Patterns of Calcined $\text{SrFe}_{0.2}\text{Co}_{0.4}\text{Mo}_{0.4}\text{O}_3$ Powder and reduced $\text{SrFe}_{0.2}\text{Co}_{0.4}\text{Mo}_{0.4}\text{O}_3$ Dense sample. Before and after reduction, no impurity phase forms

5.3.2 Conductivity Discussion

Different compositions of SFCMs were reduced and the conductivity was measured via Four Probe DC measurement. The results are shown in Figure 5.5. In the introduction part, we hypothesized the reason that $\text{SrCo}_{0.5}\text{Mo}_{0.5}\text{O}_3$ has low conductivity is because of the ordered double perovskite structure. This kind of structure can decrease the mobility of electrons due to a long hopping distance. The conclusion is that if certain dopant is added into the lattice, the degree of disorder will increase and finally improve the electron mobility. Here Fe is the dopant ranges from 10% to 50% at B site. From the figure we can see a big difference in the conductivity of original $\text{SrCo}_{0.5}\text{Mo}_{0.5}\text{O}_3$

and the 10% Fe doped sample ($\text{SrFe}_{0.1}\text{Co}_{0.45}\text{Mo}_{0.45}\text{O}_3$). The undoped sample has the conductivity around $1 \text{ S}\cdot\text{cm}^{-1}$ while $\text{SrFe}_{0.1}\text{Co}_{0.45}\text{Mo}_{0.45}\text{O}_3$ has the conductivity over $30 \text{ S}\cdot\text{cm}^{-1}$ within the whole temperature range. Even though the dopant level is low (10%), the conductivity is increased over one magnitude, which confirms our hypothesis.

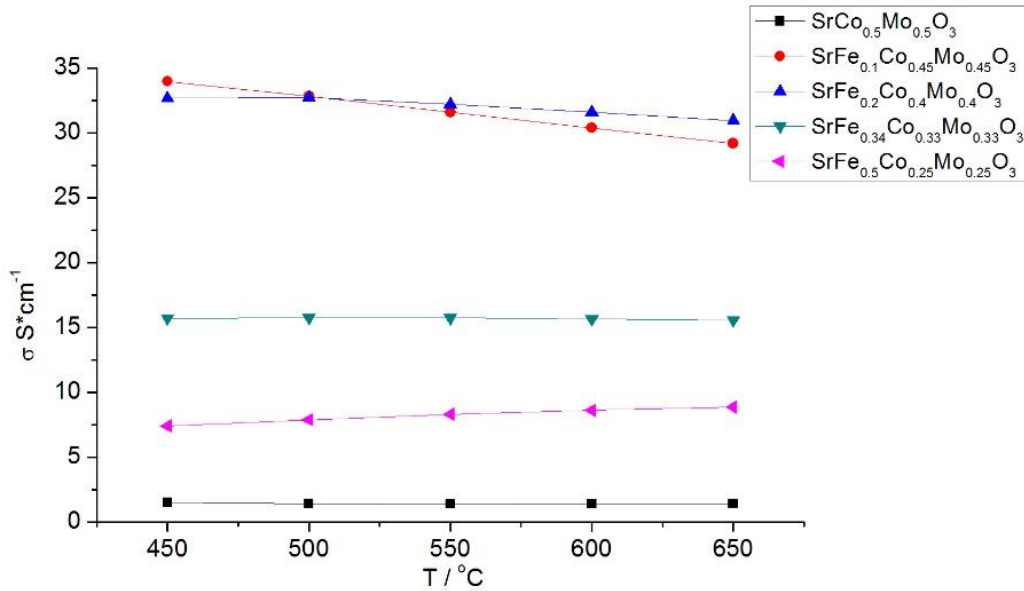


Figure 5.5 Conductivity of SFCMs at 650°C in 10% H_2 / 90% N_2 Hydrogen.

Conductivity of $\text{SrCo}_{0.5}\text{Mo}_{0.5}\text{O}_3$ obtained from literature⁷³

Doping more Fe doesn't seem to increase the conductivity a lot. $\text{SrFe}_{0.1}\text{Co}_{0.45}\text{Mo}_{0.45}\text{O}_3$ and $\text{SrFe}_{0.2}\text{Co}_{0.4}\text{Mo}_{0.4}\text{O}_3$ almost have the same in conductivity. Even though 20% Fe doped sample $\text{SrFe}_{0.2}\text{Co}_{0.4}\text{Mo}_{0.4}\text{O}_3$ should have higher electron mobility, the Mo content is lower. It is kind of tradeoff. Doping Fe can improve the mobility, but also lower the concentration of free electrons. The effect is more obvious in high Fe doped samples. When the Fe content is higher, the mobility cannot be improved much, but the concentration of electrons decrease a lot, due to low Mo content. Therefore, the

conductivity drops when the composition has a high level of Fe content. Because $\text{SrFe}_{0.2}\text{Co}_{0.4}\text{Mo}_{0.4}\text{O}_3$ has high conductivity and it has already been confirmed redox stability, this composition (SFCM244) was selected for the cell fabrication

5.4 Electrolyte Supported Cell Fabrication and Performance

5.4.1 Electrolyte Cell Fabrication

300 μm GDC dense electrolyte was used as the support. The SFCM244 anode was prepared by the following method. Calcined SFCM244 ceramic powder and 5 μm PMMA pore former were mixed with volume ratio 1:1. The ESL vehicle (ElectroScience 441) was added in the mixtures to make a paste of screen printing consistency. The ink was then brush painted on the GDC electrolyte. The half cell was then dried in 100 $^{\circ}\text{C}$ oven and fired 1300 $^{\circ}\text{C}$ for 4 hours. The LSCF-GDC (equivalent weight amount) cathode was prepared in the same way. The full cell was fired at 1100 $^{\circ}\text{C}$ for 2 hours.

To compare the infiltration effect on the cell performance, different infiltration solutions were added into the anode side. The solutions were prepared as follows. Gadolinium nitrate hexahydrate and cerium nitrate hexahydrate with the molecular ratio of 1:9 were dissolved in pure ethanol to get 1M solution. This is the GDC ethanol infiltration solution. To confirm the Ni effect on the performance, different Ni-GDC infiltration solutions were prepared in the same way, with Ni:GDC molecular ratios of 1:1, 2:3, 1:2 and 1:7. Here all solutions are 1M and the salts are nitrates. During each

interval between infiltrations, a furnace burnout process was performed at 400°C, until the final loading is up to 10 wt%. The cells with different infiltrations were tested at 650°C in wet H₂ or CH₄ and the performance is examined.

5.4.2 Electrolyte Cell Performance and Infiltration Effects

The performance shows a big difference between the original cell and the infiltrated cells (Figure 5.6). Mo double perovskite can be directly used as anode material without any infiltration and show reasonable power output. However, all these cells are operated at high temperatures (~ 800°C)^{72,102,112-114} At a high temperature, which is a more vigorous reducing condition, the double perovskite is easier to lose lattice oxygen. This oxygen loss can increase the electronic conductivity and also increase the ionic conductivity due to high concentration of oxygen vacancies. At another aspect, the catalytic activity for hydrogen oxidation reaction and hydrocarbon oxidation reaction is much higher at high temperatures. Thus this kind of anode configuration is suitable for a HT-SOFC. Nevertheless, in IT-SOFC or even LT-SOFC, this type of anode performance dramatically decreases due to lower electronic conductivity, ionic conductivity, and catalytic activity. As we can see in the figure, without any infiltration, the OCV is also low because of low catalytic activity. The PPD is merely 30 mW/cm², which is too low to be usable. After 10wt % GDC infiltration, the OCV increases and the PPD is around 80 mW/cm², better than the original cell. 650°C is a mild reduction condition. There is not much oxygen loss, so the ionic conductivity is low. Even though Fe dopant can improve the electronic conductivity, the low oxygen ion conductivity limits the cell performance. The infiltrated GDC covers the SFCM244 anode surface

and provides extra oxygen ion conductivity. It is also necessary to examine the catalytic activity of SFCM244 at 650°C, so the Ni-GDC was infiltrated. We can see the OCV is further improved and the PPD is around 150mW/cm², almost doubled than the GDC infiltrated cell. Ni is widely used in the traditional Ni-YSZ and Ni-GDC cells and Ni has problems such as redox cycling stability and carbon formation while using hydrocarbon fuels. However, Ni nano particles can solve the problems. Instead of supporting material in anode, Ni nano particles are only catalyst. The redox cycling of these particles do not introduce stress into the anode to cause mechanical failure. At another aspect, nano particles can reduce the carbon deposition. Our group infiltrated Ni into porous GDC scaffold and cell ran in hydrocarbon without degradation for 300 hours.¹¹⁵ GDC has the ability to give out oxygen ions and the oxygen ion can migrate on Ni surface for a short distance. This is called oxygen spillover.^{116,117} When Ni particle is very small, the oxygen is able to migrate all over the Ni surface and react with the deposited carbon to form CO/CO₂. Therefore, the carbon is removed and the cell stability increases in hydrocarbons. When using Ni infiltrates instead of Ni support, the cell performance can be improved by large catalyst surface area and the possible degradations are prevented.

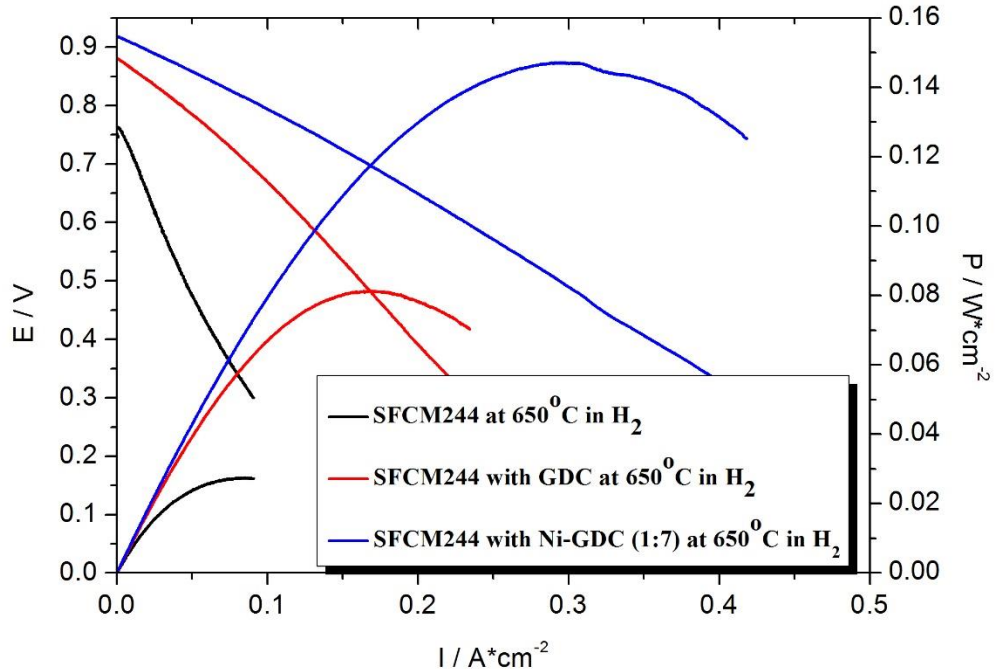


Figure 5.6 300 μ m GDC dense electrolyte supported cells with SFCM244 anode and LSCF-GDC cathode. Comparison among the cells without any infiltration, with GDC infiltration, with Ni-GDC (1:7) infiltration

It is also very important to find out the best recipe for the infiltration solution. If Ni content is low, the catalytic activity is not enough. When Ni content is too high, the particle is easy to agglomerate. The active surface also decreases and bigger particle size is not stable for hydrocarbon fuels. And also, SFCM is a purely electronic conductor. It requires infiltration of ionic conductors, which is GDC in this case. Thus, the ratio of Ni to GDC has to be determined in the infiltration solutions. As stated before, different Ni-GDC infiltration solutions were prepared and cell performance comparison with these infiltrations is shown in Figure 5.7. When Ni content is low

(Ni:GDC=1:7), the H₂ performance is good, while CH₄ performance is relatively low. In this situation, the catalytic activity is enough for hydrogen oxidation reaction, but it is not sufficient for methane oxidation reaction. It is very similar to the GDC infiltrated SNNV10 anode in Chapter 4. Because the bonding energy of C-H in methane is higher than that of H-H in hydrogen, the oxidation activation energy is higher for hydrocarbons than that for hydrogen. Therefore, to achieve a good performance, more catalyst is needed if methane is the fuel. When Ni:GDC=1:2, the H₂ performance increases a little bit. It seems the catalytic activity for hydrogen reaches a plateau, and more Ni cannot help a lot for hydrogen performance. However, the CH₄ performance increases almost proportional to the Ni content increase. So high Ni content promises a good performance in methane. When the Ni content is further increased to 40 mol% (Cell 3), both H₂ performance and CH₄ performance decrease. There may be two reasons. While Ni content is increasing, because of same loading amount, GDC content is decreasing. As we explored before, SFCM244 is a purely electronic conductor at 650°C, and it needs both ionic conductor and catalyst. When GDC content is too low, the reaction is also limited by low oxygen ion transport and finally the cell output is hindered. Another possible reason is that high Ni content accelerates the Ni nano particle agglomeration. It decreases the Ni surface area and the number of active sites drops. In cell 4, the Ni content is the highest (50 mol%), the performance is even lower, either in hydrogen or in methane. Thus, the optimized Ni to GDC ratio is 1:2. The following research sticks to this infiltration solution.

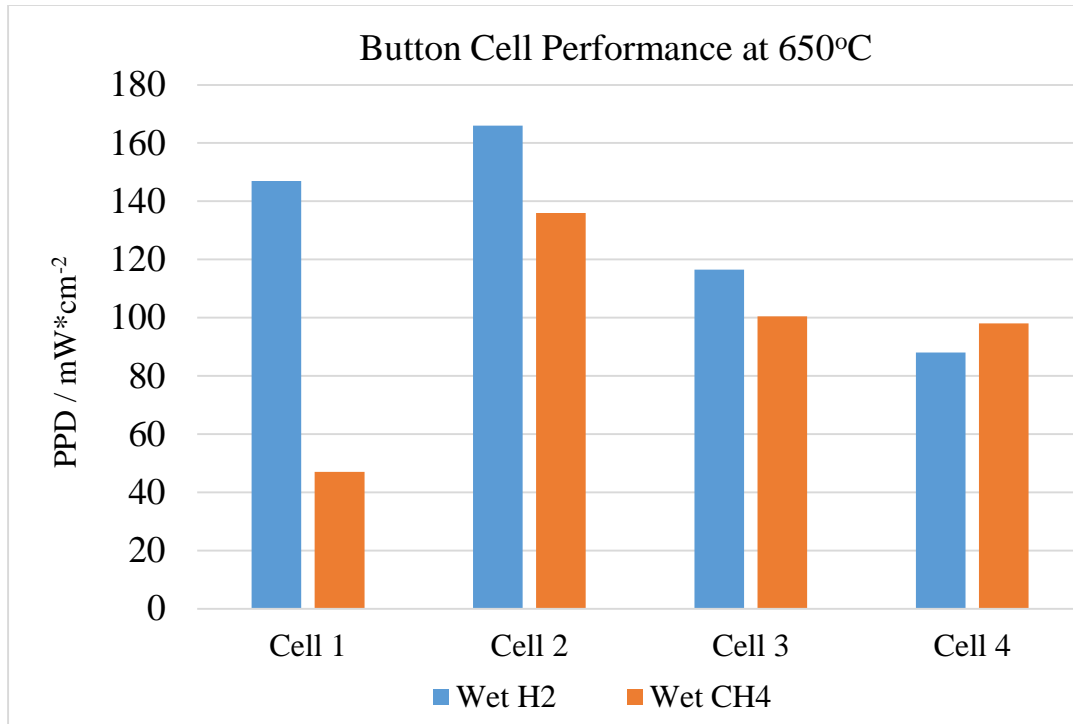


Figure 5.7 Button cell performance at 650°C in wet H₂ and in wet CH₄. Cell(1) Ni:GDC =1:7, Cell(2) Ni:GDC =1:2, Cell(1) Ni:GDC =2:3, Cell(1) Ni:GDC =1:1. All cells have the loading around 10 wt%.

5.5 Anode Supported Cell Fabrication and Performance

5.5.1 Introduction to Anode Supported Cells

To obtain a high performance, anode supported cell is always the configuration. Like traditional Ni-YSZ and Ni-GDC cells, they all have the anode supported configuration. The disadvantage of electrolyte support cell is the huge ohmic resistance of electrolytes. A typical electrolyte has the conductivity of 0.01-0.1 S*cm⁻¹, while normal electrodes usually have the conductivity above 10 S*cm⁻¹, which is over two magnitudes higher. So it is necessary to reduce the thickness of electrolyte to lower the ohmic resistance.

Considering cell mechanical strength, an SOFC needs a thick supporting layer. Electrolyte supported cell configuration is not a good choice for high performing cell. Comparing anode support, the cathode support configuration is not favored either, because of its higher activation polarization than the anode.^{118,119} It is easy to understand that at the cathode side, the oxygen reduction reaction takes place. O₂ gas should transform to O²⁻ and the bonding energy of O-O is higher than that of H-H at anode side. Based on modeling, anode supported cell is the best configuration, with lowest ohmic and polarization losses. At another aspect, typical cathode, like LSCF, LSM (La_{0.8}Sr_{0.2}MnO₃) and LSC (La_{0.6}Sr_{0.4}CoO₃) have much higher thermal expansion coefficients than that of the electrolytes, such as GDC and YSZ¹²⁰⁻¹³⁰. If cathode is used as the support, it may cause cracks in the electrolyte because of big difference in thermal expansion during thermal cycling process.

Unlike electrolyte supported cell, the anode supported cell requires a lot of engineering work. In an SOFC, the most important thing is to obtain a gas tight electrolyte membrane. As electrolyte deposited on a sinter body cannot be densified, because the substrate has no way to shrink together with the electrolyte. There are always cracks on such electrolyte thin film. Therefore, the common way is to co-fire anode electrolyte half cell and let them to shrink together. Here come with one key issue. It is how to match the shrinkage mismatch. Because the anode and the electrolyte are two different materials, usually they have different shrinkage rates. If the shrinkage mismatch is big, the cell is easy to bent, and in some cases, it cracks during sintering. Usually, composite materials are used instead of single anode materials. Composite has the shrinkage

between the anode and the electrolyte, so it can minimize the shrinkage mismatch. Here in the SFCM cell, SFCM244-GDC composite is used as the anode.

5.5.2 Anode Supported Cell Fabrication

The SFCM (Here the following SFCM244s are called SFCM for short) anode supported cell was fabricated by tape casting technique. SFCM and 2% cobalt doped GDC were mixed with the weight ratio 2:1 and a mixed 12 μ m and 1.8 μ m PMMA powder was added to control the theoretical porosity of 40 vol%. PVB, BBP and fish oil were used as binder, plasticizer and dispersant separately. Here pure ethanol was the solvent. This anode tape and 20 μ m GDC electrolyte tape were laminated together and cofired at 1200°C for 4 hours. Here 2% Co-GDC was used instead of regular GDC is to exactly match the shrinkages and make a flat cell.^{131,132} LSCF – GDC cathode was applied on top of it and it was fired at 1100°C for 2 hours. The optimized Ni-GDC infiltrate was impregnated into the anode. A 400°C burnout process was performed during each infiltration interval and the final burnout was performed at 800°C for 1 hour. The total loading is around 10 wt%. The cell configuration is shown below in Figure 5.8.

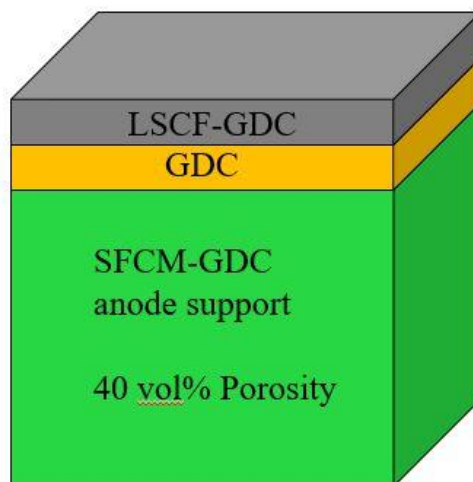


Figure 5.8 Anode support cell configuration

5.5.3 Anode Supported Cell Performance

The cell was tested in hydrogen from 650°C to 500°C. Compared with electrolyte supported cell, a high power output increase is observed, showing in Figure 5.9. At 650°C, the electrolyte supported cell has the PPD of 160 mW/cm², while the anode supported cell has the PPD of 650 mW/cm². This is mainly due to reduced thickness of electrolyte and lower ohmic resistance. However, we also found there were low OCVs for the anode supported cell, especially within high temperature regions. At 650°C, the OCV is only 0.76V which is much lower than the standard Ni-GDC cell (~0.8-0.85V). This OCV drop decreases the cell efficiency and must be prevented.

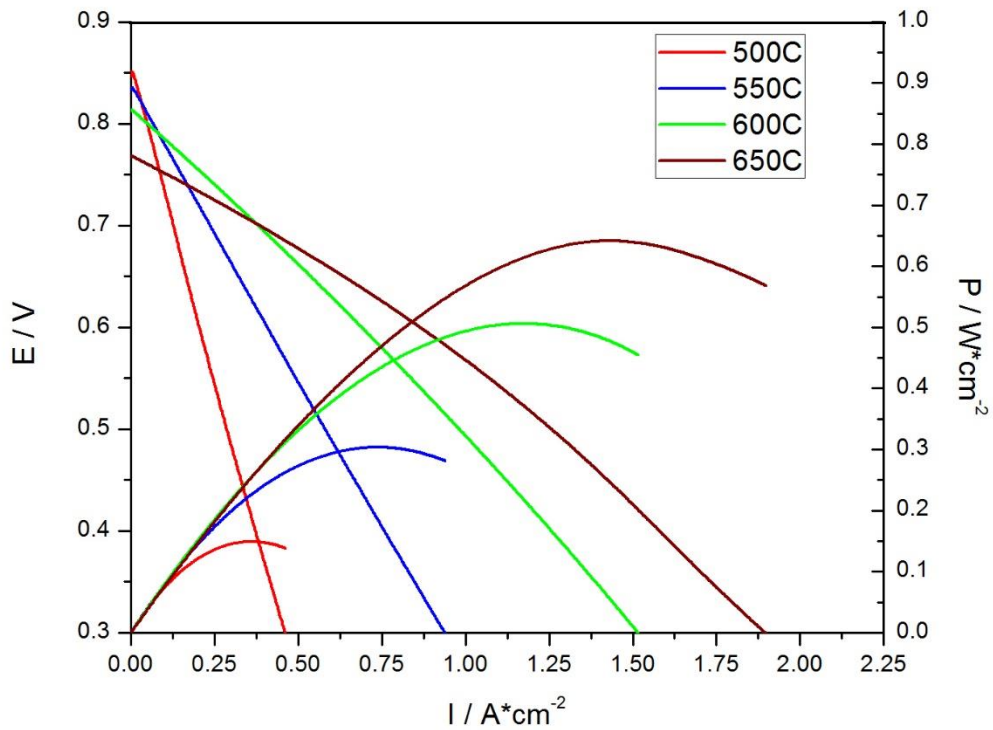


Figure 5.9 Cell Performance of SFCM cell in hydrogen from 650°C to 500°C.

There are two possible reasons why the OCV is lower than the standard Ni-GDC cell. One is the gas leakage, coming from pin holes in the electrolyte and the sealants. In most of the cases, if there is sealing issue or there is gas leakage, besides of low OCV, the performance is low. The air may diffuse into the anode side and partially oxidize Ni, so the catalytic activity drops. The other reason is the leakage current due to the electronic conductivity in the electrolyte. In principle, the electrolyte should be ionic conductive only, like YSZ and LSGM ($\text{La}_{0.8}\text{Sr}_{0.2}\text{Ga}_{0.8}\text{Mg}_{0.2}\text{O}_3$). For YSZ cells and LSGM cells, the OCVs are always above 1V almost at all temperature ranges. The disadvantage of YSZ is low ionic conductivity and YSZ cells can only be operated above 750°C. LSGM has a bit higher ionic conductivity than YSZ, but the material is

difficult to fabricate and it is also expensive. In contrast, GDC is a good choice for IT-SOFC and LT-SOFC due to its high conductivity and moderate material cost. However, as we know Ce is multivalent cation. Ce^{4+} can get reduced to Ce^{3+} in hydrogen. In an SOFC, one side of the electrolyte is exposed in reducing conditions and the GDC can be partially electronic conductive due to Ce^{4+}/Ce^{3+} electron hopping. As a result, if the electrolyte is thin, the OCV is lower than that of YSZ or LSGM cells. Typically, a 20 μm thin GDC electrolyte has the OCV around 0.8-0.85V at 650°C. ¹³² In this cell, the performance is good, expect for the low OCV. The possible explanation is there is extra leakage current. It means the electronic conductivity is higher than GDC. The anode contains high concentration of Co and Mo. During sintering process, Co and Mo may migrate into GDC phase and they increase the electronic conductivity. When the cell is dwelling at 650°C, the OCV drops continuously. It means the electronic conductivity is increasing with time, showing in Figure 5.10. It is a fast degradation and this electronic conductivity should be blocked.

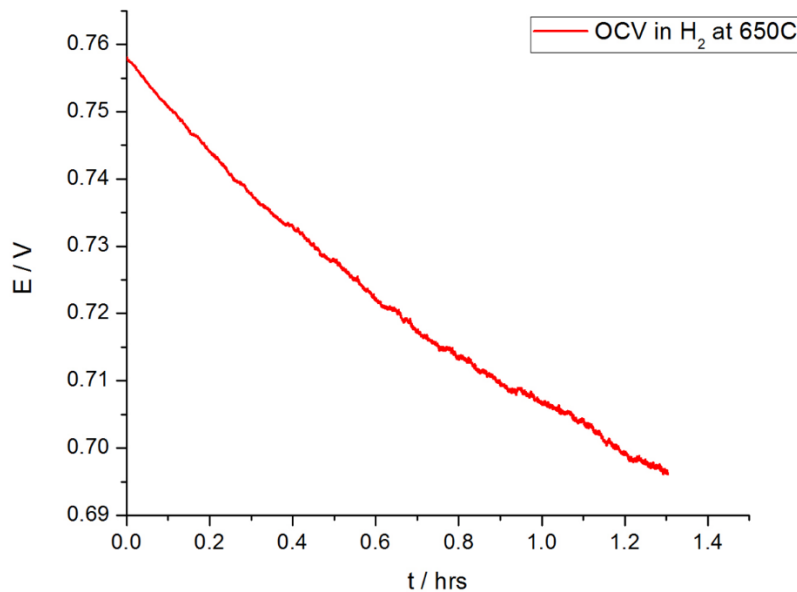


Figure 5.10 OCV drops with time in SFCM cell at 650°C

5.5.4 SFCM Cell with Normal Electronic Blocking Layers

To block the electronic conductivity, a purely ionic conductors can be applied on top of GDC electrolyte. Our group did a lot of research on GDC/ESB (Erbium stabilized bismuth) bilayer structures to improve OCV.^{54,133-135} ESB is an ionic conductor with high oxygen ion conductivity ($\sim 0.1 \text{ S}\cdot\text{cm}^{-1}$ at 650°C). Thus applying ESB onto GDC will not add on a lot of ohmic resistance in principle. Also thanks to the low melting point of bismuth materials, it is easy to obtain a dense layer on GDC at low temperatures. Therefore, our first attempt is to use ESB as the buffer layer. After firing the SFCM half cell, the ESB paste was applied onto the GDC side and oven dried. After that, instead of using LSCF, LSM-ESB cathode paste was directly brushed onto the

ESB layer. The ESB and LSM-ESB cathode layers were cofired at 775°C for 2 hours. The cell configuration is shown in Figure 5.11

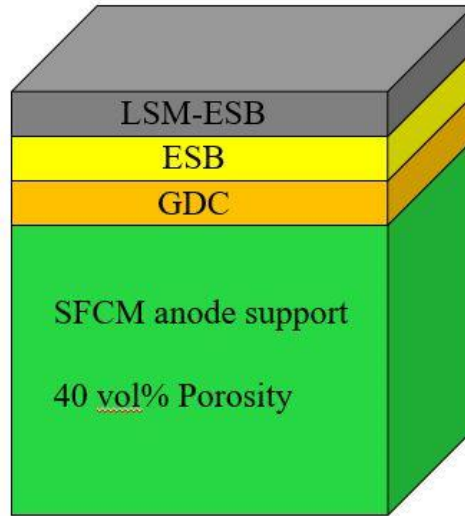


Figure 5.11 SFCM cells with ESB electronic blocking layer and LSM-ESB cathode

After firing, SEM and EDS were used to examine whether ESB can block the Co diffusion, in Figure 5.12. The SEM clearly shows four layers, including SFCM anode, GDC electrolyte, ESB electronic blocking layer, and LSM-ESB cathode. According to the following EDS mapping, we can see a high intensity of Co in the GDC electrolyte. Co is very easy to migrate at high temperatures and Co diffusion has been confirmed from SFCM anode to the GDC electrolyte. These Co will introduce electronic conductivity and lower the OCV. After applying ESB, the intensity of Co decreases. ESB has a low firing temperature of 775°C and this temperature is not sufficient for Co diffusion. Thus, the ESB is not contaminated and stays as an ionic conductor. After examining the Bi content, no Bi is observed in GDC or anode. It indicates Bi didn't diffuse into the GDC electrolyte and there is no interfacial reaction between ESB and

GDC at 775°C. However, we also observed strong signals for Ce and Gd everywhere, which we believe they are caused by equipment accuracy and it is not the real situation.

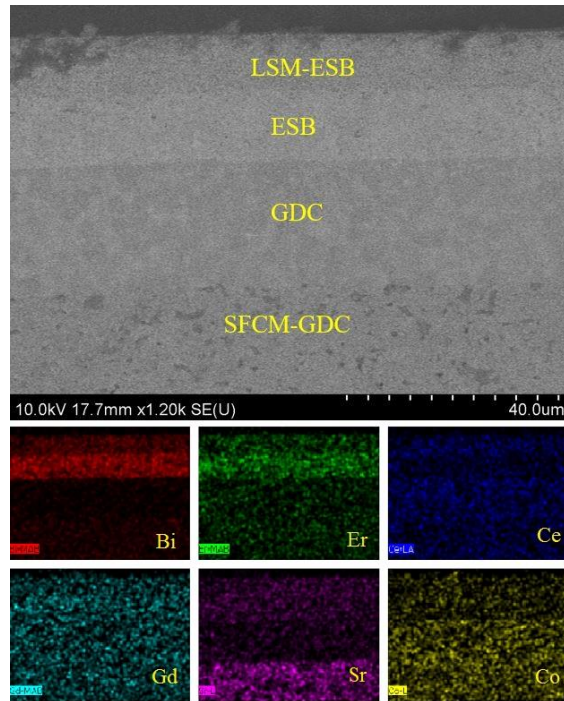


Figure 5.12 SEM and EDS mapping for SFCM anode supported GDC-ESB bilayer cell. ESB can block Co diffusion.

The bi-layer cell is performed in hydrogen at 650°C to find out there is any OCV improvement, shown in figure 5.13. To determine the electrolyte thickness impact on the OCV, different combinations of GDC and ESB were tested. When the electrolyte is 15µm GDC with 2µm ESB, the OCV is low. Even though there is ESB blocking layer, no improvement can be observed and it is even worse than the original 20µm GDC electrolyte. When the ESB thickness increases, an obvious increase in OCV is recorded, which is 0.8V with 15µm GDC and 10µm ESB. It is almost the same value as the OCV that Ni-GDC standard cell can achieve at 650°C. When the bilayer has

30 μm GDC and 10 μm ESB, the OCV increases a little bit to 0.85V which is not a big difference from the cell with 15 μm GDC and 10 μm ESB. Therefore, here is the conclusion that increasing ESB thickness improves the OCV, while increasing GDC doesn't have obvious effect. GDC in the half cell is partially an electronic conductor. Even a thick GDC still have leakage current, because Co can go everywhere during sintering. Thus, increasing GDC thickness is not a good idea as increasing ESB. However, we cannot increase the ESB thickness too much as there is a critical ratio of ESB to GDC.¹³⁵ Bismuth composition can get reduced very easily when Po_2 is low. As the electrolyte is exposed to hydrogen and air at both sides respectively, there is a Po_2 gradient through the electrolyte, so there is an interfacial Po_2 right between GDC and ESB. If GDC is too thin or ESB is too thick, the interfacial Po_2 will be too low and start to decompose the ESB. ESB is reduced to Bi metal. At high temperatures, Bi metal is in its liquid form and diffuses into the electrolyte and the cathode. It results to pin holes and increases electronic conductivity in the electrolyte, and deteriorates the cathode performance. As a result, applying a very thick ESB to obtain a high OCV is not feasible. Nonetheless, the power performance doesn't increase with the improvement of OCV. The cell configuration is totally changed, so it is difficult to conclude whether the low performance is coming from the bilayer electrolyte or the cathode. The EDS also shows there is slight Co in the ESB phase. The bilayer improves the OCV but the slight Co content may decrease the ionic conductivity of ESB and lower the cathode performance. If ESB has to be used as the electronic blocking layer, more effort should be taken to find out the cause of the low performance, the best cell configuration, and the optimized fabrication process.

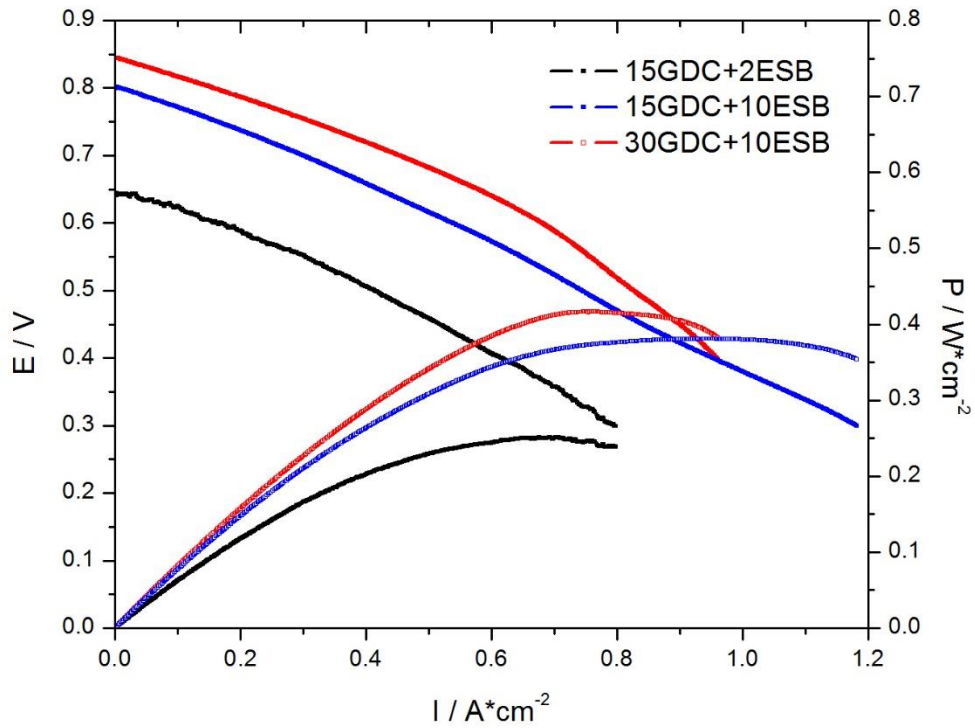


Figure 5.13 Cell performance with different thickness of GDC and ESB at 650°C in hydrogen. Increasing thickness of ESB has higher improvement than increasing thickness of GDC.

Considering the possible issues of ESB, we also tried LSGM electronic blocking layer. LSGM is a purely ionic conductor with higher conductivity than YSZ, almost comparable as GDC above 600°C. The disadvantages of this material are expensive, difficult to sinter, and reactive to NiO. Here, our concern about GDC-LSGM bilayer is LSGM requires high temperature to sinter (above 1350°C) and at high temperatures, it may react with the other cell components and LSGM may not block Co diffusion. To confirm this, we prepared the cells via two routes. One route is to follow the procedure

before to make SFCM-GDC half cell. LSGM paste with 5 at% LiNO_3 was blade coated on top. Here Li is the sintering agent. The cell was then heat treated at 1100°C for 4 hours. The LSCF-GDC cathode was applied by the standard method. The other route is to use tape casting and make thin LSGM electrolyte tape. Instead of laminating anode tape and GDC electrolyte tape only, an extra LSGM tape was laminated on top of the GDC. This triple layer structure was co-fired at 1300°C for 4 hours to obtain the sintered half cell. After that, LSCF-GDC cathode was applied with the standard method shown before.

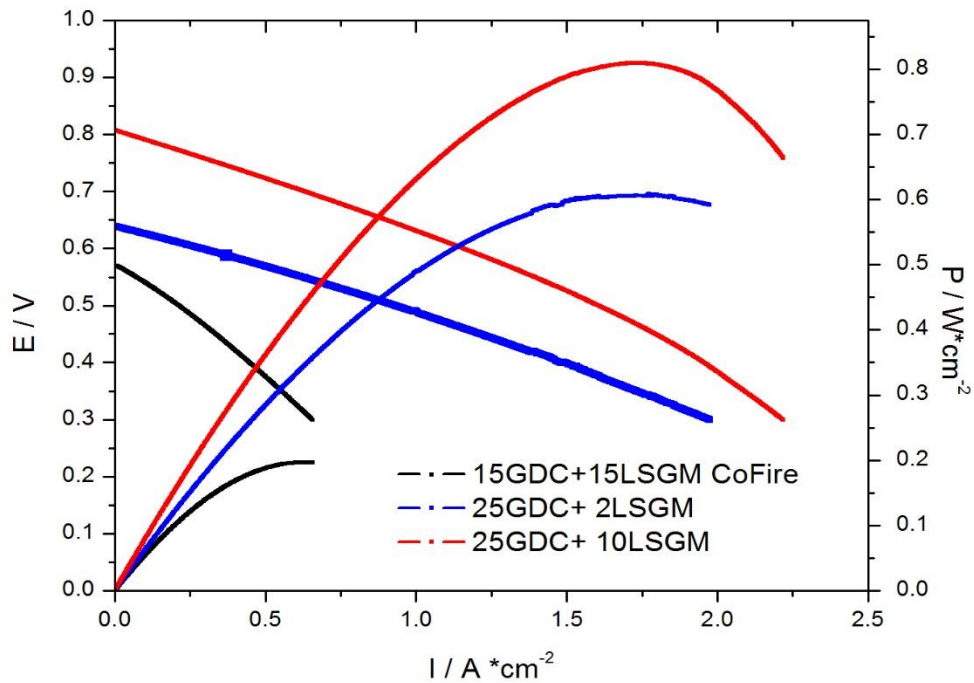


Figure 5.14 Performance of cells with GDC-LSGM bilayer in H_2 at 650°C . Both OCV and cell performance are improved

The performance of cells with different fabrication routes are shown in Figure 5.14. The cell with cofired bi-layer has very low performance at 650°C in hydrogen. To densify the LSGM, the firing temperature should be high, which is 1300°C in this route. At 1300°C, LSGM and GDC may have interfacial reaction. The possible reaction could decrease the cell performance. At another aspect, 1300°C is high enough for Co diffusion. Co migrates from SFCM, through GDC, and finally reaches LSGM phase. The Co can also increase the electronic conductivity of LSGM.^{136,137} As a result, the LSGM cannot block the electronic conduction anymore and the OCV is low. If firing LSGM at low temperature with Li sintering agent. The OCV is higher than the cofired bilayer cell. The cells with 25µm GDC and 2µm LSGM has good PPD but with a low OCV. Lowering the firing temperature can decrease the tendency of interfacial reaction. Even though the OCV only increases a little bit, the PPD is much higher than the cofired bilayer cell. The LSGM layer was heat treated at 1100°C, and we think it is still high. Slight Co may diffuse into LSGM layer and 2µm LSGM cannot be a purely ionic conductor. When the thickness increases to 10µm, the cell OCV is over 0.8V at 650°C, comparable to Ni-GDC cell at the same temperature. The PPD is over 800mW/cm², higher than the single layer cell. Therefore, by using this configuration, this ceramic anode supported cell can compete with the normal Ni-GDC cell.

In addition, stability of these configurations should be determined. As in Figure 5.10, we observed a fast OCV decay in single layer GDC cell. The reason may be the Co valence state change when the electrolyte is exposed to hydrogen. Now the blocking layers are applied. It is necessary to confirm whether the blocking layers can also

improve the cell stability. Shown in Figure 5.15, compared with the single layer GDC cell, both ESB blocking layer and LSGM blocking layer can greatly improve the OCV as well as the stability. Instead of fast degradation of single layer GDC cell, the GDC-ESB bilayer cell and the GDC-LSGM bilayer cell both have a slower decay in hydrogen at 650°C, with GDC-LSGM bilayer the best.

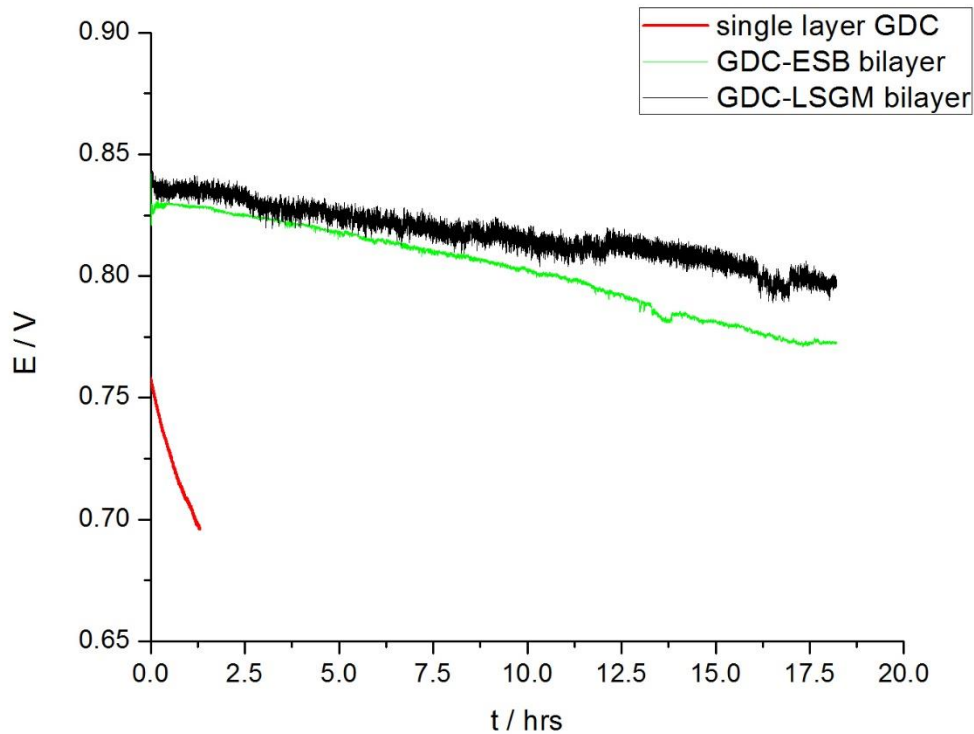


Figure 5.15 OCV degradation of single layer GDC cell, GDC-ESB bilayer cell and GDC-LSGM bilayer cell. All cells have degradation with different rates. GDC-LSGM has the best stability among the three. Anode side is exposed to hydrogen at 650°C.

However, to be a good cell running for long time. The OCV stability above is not enough. The OCV degradation rate for GDC-LSGM bilayer cell is 0.2% / hour, still

too fast to be good. In order to minimize the degradation rate, a lower operation temperature is preferred, due to slower degradation kinetics. But new issues come out for the bi-layer configurations. For GDC-ESB bilayer, even though ESB has a high ionic conductivity, low temperature operation is not favored. Bismuth oxides have a special oxygen order-disorder transition below 650°C, and because of this phase transition, low temperature conductivity is hindered and cannot give enough ionic conductivity¹³⁸⁻¹⁴⁰. The example plot is shown in Figure 5.16¹⁴¹. Right below 600°C, the conductivity drops a lot. Therefore, to let the cell run at low temperatures, more effort should be taken to maintain ESB's high conductivity below 600°C. Besides of this, the GDC-ESB bilayer cells have low performance at 650°C. The reasons should be investigated and the problems have to be solved.

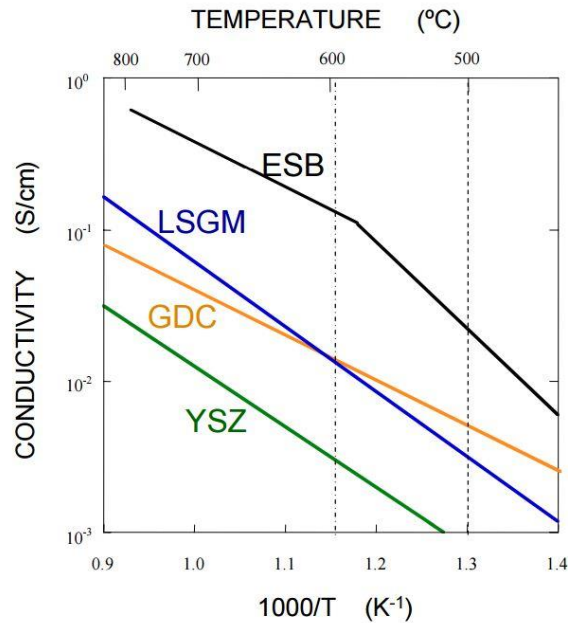


Figure 5.16 Conductivity of different electrolytes. ESB shows a nonlinear relationship of conductivity and temperature right below 600°C

GDC-LSGM cells have high performance at 650°C which may be a good configuration at low temperatures, but according to Figure 5.16, LSGM doesn't have good conductivity below 600°C. In order to improve the OCV, a thick layer (10µm) of LSGM has to be applied on GDC. This thick layer will add on much ohmic resistance to the cell and decrease the low temperature cell performance. Moreover, even though Li is used as sintering agent to densify LSGM, the LSGM cannot be fully sintered because it is difficult to shrink on a rigid substrate (sintered GDC electrolyte). As a result, the LSGM layer is porous anyway. It aggravates the ohmic resistance problem. To make the cell work at low temperatures, these problems should be solved or a new electronic blocking layer has to be investigated.

5.5.5 SFCM Cell with Co-GDC Electronic Blocking Layers

As it is mentioned above, traditional electronic blocking layers like ESB and LSGM have their intrinsic problems and they are difficult to get solved in a short time. To find out a new material may be a better way. In SFCM-GDC cells, the low OCV is caused by Co diffusion, which introduces high p-type conduction. However, we all know ceria is an n-type conductor, showing electronic conductivity in reducing conditions due to $\text{Ce}^{4+}/\text{Ce}^{3+}$ transition. As a result, if certain amount of Co is doped into GDC, the electronic conductivity should be neutralized, because electrons (n type) and electron holes annihilate. The reason Co diffused GDC electrolyte has high electronic conductivity is the Co content is too high and p-type conductivity dominates. DP Fagg et al. doped 2 mol% Co into GDC. They claimed the ionic transference number is above 0.98 at 650°C.¹⁴² Due to the high ionic transference number, 2 mol% Co-GDC can be

used as the electronic blocking layer. Meanwhile, Co can be used as sintering agent to densify GDC at 950°C. The low firing temperature can also prevent further Co diffusion from anode to the Co-GDC electronic blocking layer. Below 600°C, GDC has higher conductivity than LSGM and YSZ, so it won't add on a lot of ohmic resistance if the cell is operated at low temperatures.

SFCM-GDC half cells were fabricated via the method discussed before. The Co-GDC electronic blocking layer is prepared as follows. GDC powder and 2 mol% cobalt nitrate were mixed and heat treated at 400°C for 1 hour. The mixed powder was made into paste by ESL and brushed onto the half cell to form a cathode functional interlayer. After it was dried in oven, Sr_{0.5}Sm_{0.5}CoO₃ – GDC (SSC-GDC) cathode was applied on top of it and the two layers were cofired at 950°C for 2 hours. Co-GDC can be densified at 950°C. To prevent further Co diffusion, higher firing temperature is not favored. Therefore, LSCF-GDC cannot be used here, as this cathode requires the firing temperature of 1100°C. SSC-GDC is a better choice here, as the optimized firing temperature is between 900°C to 950°C. The optimized Ni-GDC infiltrate was impregnated into the anode. A 400°C burnout process was performed during each infiltration interval and the final burnout was performed at 800°C for 1 hour. The total loading is around 10 wt%. The cell configuration is shown below in Figure 5.17.

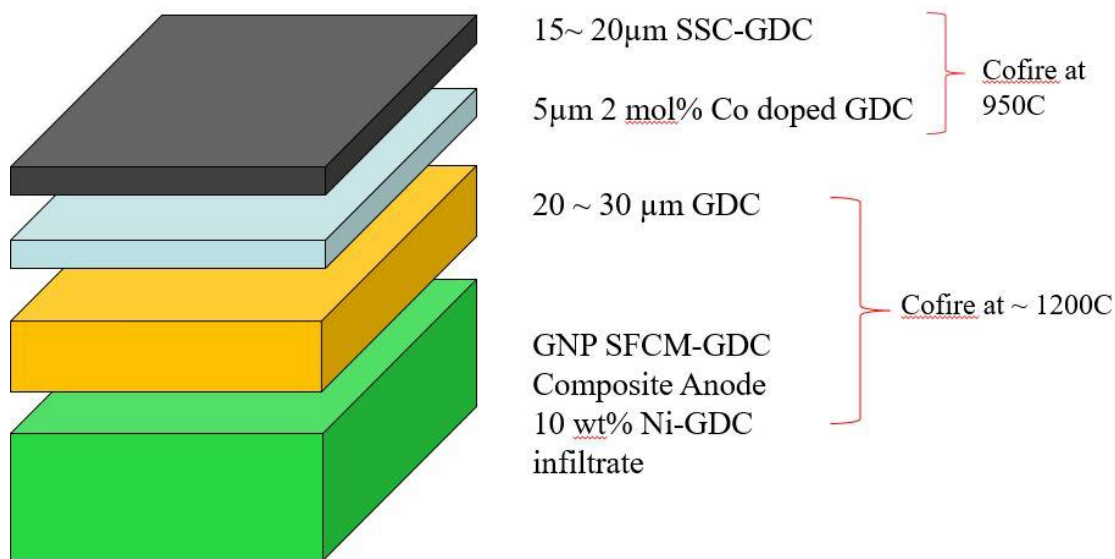


Figure 5.17 Configuration of SFCM-GDC cell with 5µm Co-GDC electronic blocking layer. SSC-GDC is the cathode.

The cell was operated in hydrogen between 550° and 450° to examine the low temperature performance. The I-V curve is shown in Figure 5.18. After applying the Co-GDC, the OCVs from 450°C to 550°C are all at high values, above 0.9V. At 450°C, the OCV is almost approaching to 1V, comparable to YSZ and LSGM cells. Meanwhile, the power outputs are very promising. At 550°C, the PPD is around 750mW/cm². For a typical Ni-GDC cell in lab scale, the PPD is usually between 100mW/cm² to 200 mW/cm² at 500°C. C. Xia et al. reported their Ni-GDC cell can give out 160mW/cm² at 500°C. ¹⁴³ In comparison, our cell performance at 500°C is 460 mW/cm², which is almost three times of the standard cell. Even the temperature is lowered to 450°C, the cell can still give out 300mW/cm², nearly doubling the standard performance with high OCV.

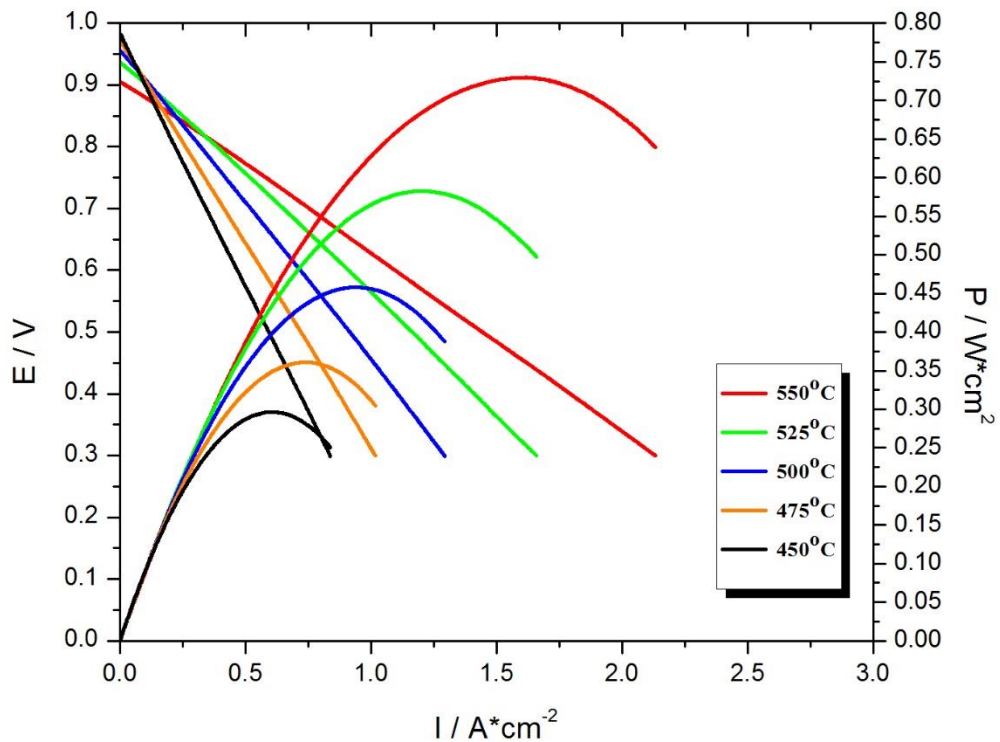


Figure 5.18 Performance of SFCM anode supported cell with Co-GDC electronic blocking layer. The performance is high at low temperatures.

By carefully tailoring the Co content in GDC, the p-type electronic conduction and n-type electronic conduction can be minimized, so we can obtain a high OCV with 2 mol% Co doped GDC. The high performance at low temperatures can be attributed to the following three aspects. At the anode side, instead of big Ni grains, Ni nano particles can be formed during the infiltration burnout process, which can be found out in the SEM in Figure 5.19. Besides the advantage of no carbon formation and redox cycling stability, small Ni particle size results to high surface area of active sites. Therefore, the anode catalytic activity is much higher than the traditional Ni-YSZ and Ni-GDC

cells. In the fabrication process, mixed sizes of PMMA were added to form porosity in the anode. The mixed PMMA can improve the percolation and enhance the connection of pores. Thus during infiltration, the infiltrates don't block the pores and can evenly cover the SFCM surface, showing Figure 5.18(D). Because of this, the loading amount can be high, meaning more Ni could be loaded in the anode. It promises a high performance. The Co diffusion during sintering can also help the ionic conductivity of GDC electrolyte. As mentioned before, Co can be sintering agent. The diffused Co into the electrolyte not only increases the electronic conductivity, but also densify the electrolyte. We observed a bigger grain size than the traditional Ni-GDC cell sintered at 1450°C. The bigger grains can reduce the overall grain boundary resistance and finally reduce the electrolyte ohmic resistance. Co-GDC has almost the same composition as GDC electrolyte, so there should not be any chemical compatibility issues between GDC and Co-GDC layers. Co can also densify the Co-GDC electronic blocking layer, introduces minimal extra ohmic resistance. At last, the cathode is also improved. Instead of LSCF-GDC which is a standard cathode, SSC-GDC cathode was used here due to its low firing temperature. This cathode has also been reported to have higher performance than LSCF at low temperatures.¹⁴⁴ To adopt the better cathode extends the cell operation temperature ranges, especially bellow 600°C, comparing with LSCF. In addition, we also find adding Co-GDC layer can improve the cathode performance, instead of directly applying the cathode material to the GDC electrolyte. More experiments and explanations will be discussed in Chapter 6. In our cell, the anode, electrolyte, and cathode are all better than the ones in a standard Ni-GDC cell,

as a result the cell performance is nearly tripled and the operation temperature is lowered to 450°C.

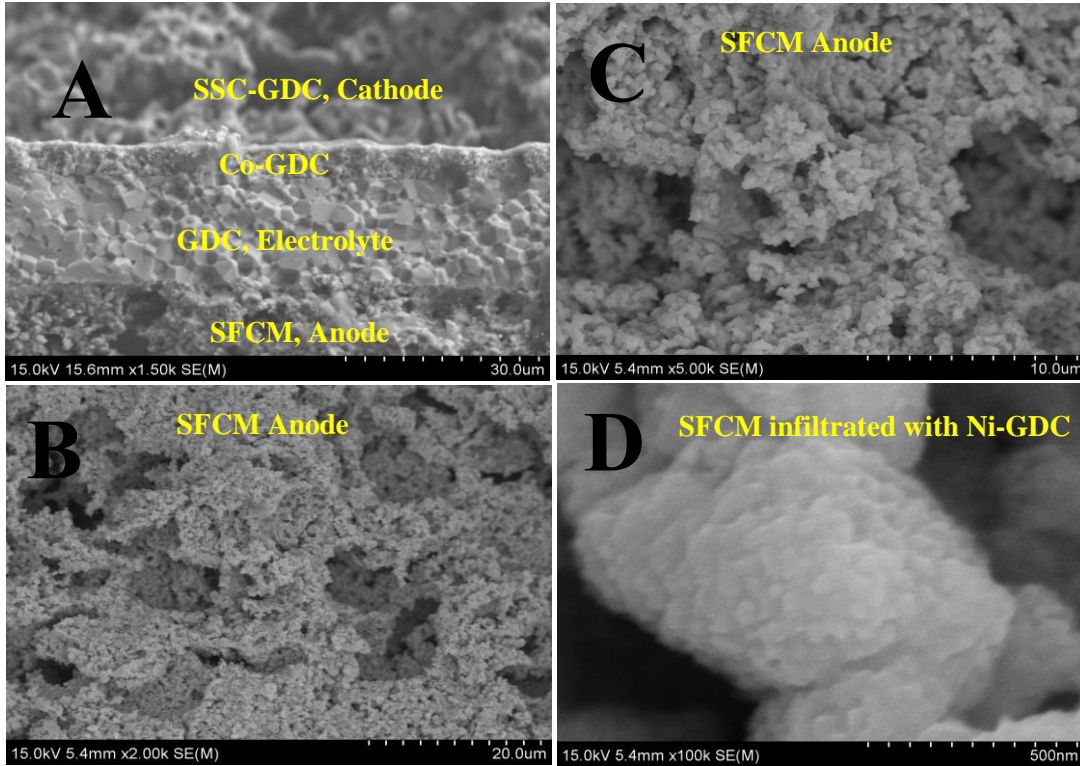


Figure 5.19 SEM images A) Cross section of SFCM anode /GDC electrolyte /CFL/SSC-GDC cathode B-C) Porous microstructure of SFCM anode and D) Ni-GDC infiltrated SFCM.

By checking the impedance plots, more information can be obtained. In Figure 5.20, the ohmic resistances are low at all temperatures. The anode and cathode are usually highly conductive materials, so the ohmic resistances of electrodes can be negligible and the overall ohmic resistance is attributed by the electrolyte. In our previous report, a good 25 μm GDC contributes $0.275\Omega\cdot\text{cm}^{-2}$ at 500°C.¹⁴¹ Here the SFCM cell (20 μm GDC and 5 μm Co-GDC) has the same value at 500°C (blue curve in the plot). It confirms the Co-GDC doesn't add on extra ohmic resistance, and it has the same

conductivity as regular GDC electrolyte. Each impedance plot shows three arcs. There is an accepted explanation is that the high frequency arc and intermediate arc represent charge transfer for SSC cathode, and the low frequency arc represents the concentration polarization, related to microstructure.^{145,146} At 550°C, we can see a small concentration charge transfer and concentration polarization. When the operation temperature decreases, the concentration polarization gets smaller due to slower reaction kinetics. The charge transfer keeps increasing. The high frequency arc and intermediate arc increase proportionally because they are both for oxygen reduction kinetic on SSC-GDC cathode. In figure 5.21, when the temperature increases, both ohmic and polarization increase, with a fast rate in polarization. At 450°C, the ohmic and polarization have equal contribution in total resistance and it is at a low value below $1\Omega\cdot\text{cm}^{-2}$, which is the criteria for a good SOFC.

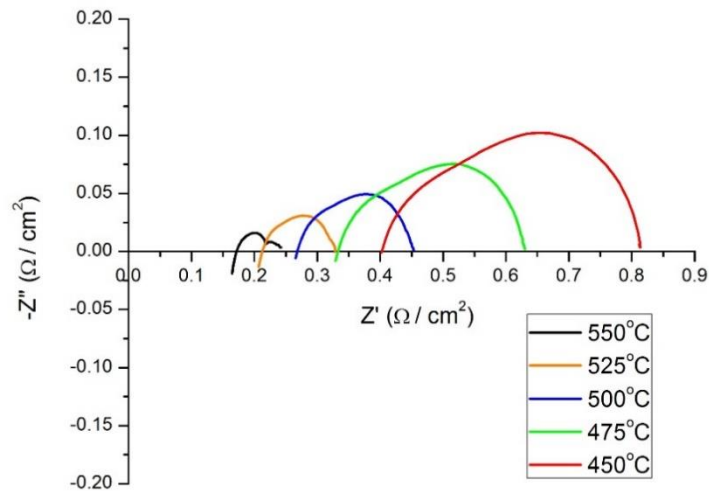


Figure 5.20 Impedance plots of the cells between 550°C and 450°C in hydrogen. All measurements were done at OCV conditions.

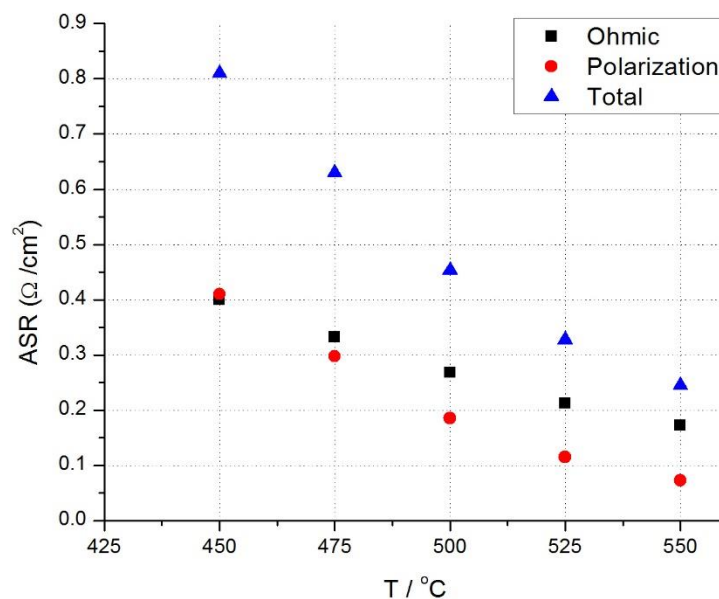


Figure 5.21 Ohmic, polarization, and total resistance of the cells between 550°C and 450°C in hydrogen. All measurements were done at OCV conditions.

To be a good cell, the long term stability is also required. In the SOFC, a lot of researchers are trying to improve the cell performance, and lower the cell operation temperatures. However, few of them reported long term stability for these new cells. In most of the cases, if a certain material performs very well, there are always some stability issues. For example, $\text{Ba}_{0.5}\text{Sr}_{0.5}\text{Co}_{0.2}\text{Fe}_{0.8}\text{O}_3$ (BSCF) cathode is very good at low temperature, but it is very vulnerable to CO_2 and moisture and even during normal operation, it starts to decay.¹⁴⁷⁻¹⁴⁹ Our cell is also highly performing, so it is necessary to examine the stability and it is more challenging because it is a whole cell systems. At the anode side, the moisture and Ni nano particle agglomeration may lower the cell performance. The electrolyte may have higher leakage current when the reduction

depth increases. The cathode may also have thermal stability issues like BSCF. At last, the life time of gas sealant, current collector stability, and possible delamination are all the concerns.

Initially, the cell was running in humidified hydrogen at 450°C, with a constant current density of $0.2\text{A}\cdot\text{cm}^{-2}$. The cell voltage was recorded with time in order to find out whether there is any degradation. After that, another cell was run in hydrogen and methane mixture, with 81% H_2 , 16% CH_4 and 3% H_2O , at 450°C. In a commercialized SOFC, due to fuel prices, natural gas is sometimes the feed instead of pure hydrogen. As we stated before, typical SOFC is not stable in hydrocarbons because of carbon deposition. Thus, natural gas undergoes a steam reforming reaction to get H_2 rich gas, with CO , CO_2 , steam and CH_4 residue. Here we use H_2 and CH_4 mixture to simulate this feed. For such reformat, the composition is not fixed and if more CH_4 remains in the gas, it is more challenging to the SOFC operation. Therefore, in our simulated reformat, 16% CH_4 is in the composition to examine the stability.

The long term stability in H_2 is shown in Figure 5.22. Initially the cell has the voltage of 0.8V with the constant current density of $0.2\text{A}/\text{cm}^2$, which is $160\text{mW}/\text{cm}^2$. After that, the cell voltage went up to 0.85V. This is because of activation of anode, such as NiO reduction, infiltrate particles bonding and increasing conductivity of SFCM under reduction. After that, the cell voltage started to drop slowly with almost a constant rate of 0.03% per hour. The cell has been run in hydrogen for over 200 hours, but the degradation rate seems unchanged and doesn't reach a plateau. One possible

explanation is the sealant degradation. We used ceram-bond to seal the cell, but it is not designed for long term operation. The sealant may expire at high temperatures for a long time and form pin holes, so there will be a slow increasing gas leakage. This gas leakage lowers the OCV and we can see there is such a stable voltage degradation. We tested other cells from different batches, and the degradation rates were very similar. There are other possible degradations, such as Ni nano particle agglomeration. The cell was opened after long term test in H₂ and sent to SEM to examine the infiltrate morphology. In Figure 5.23, we find relatively big Ni particles range from 0.5 μm to 1 μm. It is bigger than the initial state. After the infiltration burnout, the particle size was nano scale, and after long term test, it went up to submicron scale. It decreases the active surface area, and possibly decreases the cell performance.

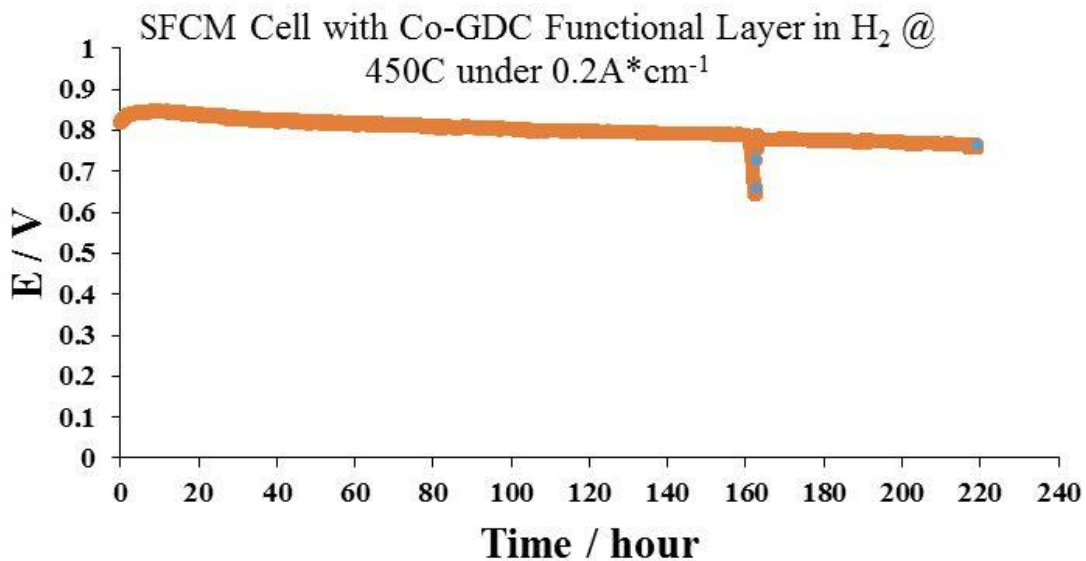


Figure 5.22 Long term stability of SFCM cell at 450°C in H₂. The cell is working under a constant current of 0.2A/cm².

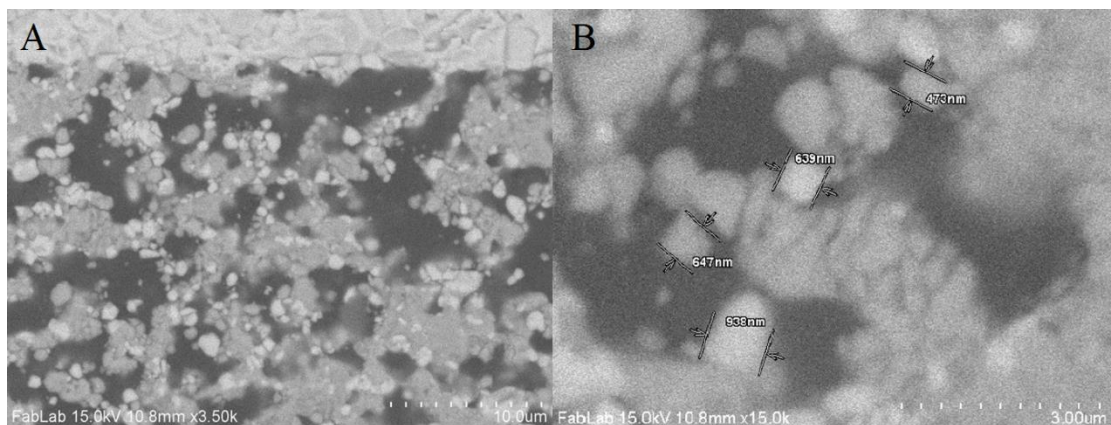


Figure 5.23 SEM images of SFCM cell after long term test in hydrogen. Ni agglomeration is observed.

After that, one cell from the same batch was tested in the H_2 / CH_4 mixture to examine the long term stability in reformat. The cell ran in reformat at $450^\circ C$ for about 400 hours at a constant current of $0.2A/cm^2$. Shown in Figure 5.24, the initial performance is similar to hydrogen performance which is around $160 mW/cm^2$. It means at this temperature, the SFCM cell can work in both H_2 and CH_4 respectively. Flexible fuel is feasible. After initial decay and several voltage drops at the beginning 150 hours, the performance afterwards is quite stable. Except for the sudden drops, the initial degradation rate is 0.04% per hour, very close to the degradation in H_2 . The sudden drops could be caused by micro cracks during testing, or the gas sealant failure, as other causes cannot result to a sudden decay in cell performance. From 150 hours to 400 hours, the voltage is stable. It confirms SFCM anode supported cell has long term stability. In order to make it work longer, more engineering work should be done. At last, the voltage started to go down again. It is because the bubbler ran out of water and

air leaked into the gas line during water refilling process. Bigger bubbler should be used next time for long term test.

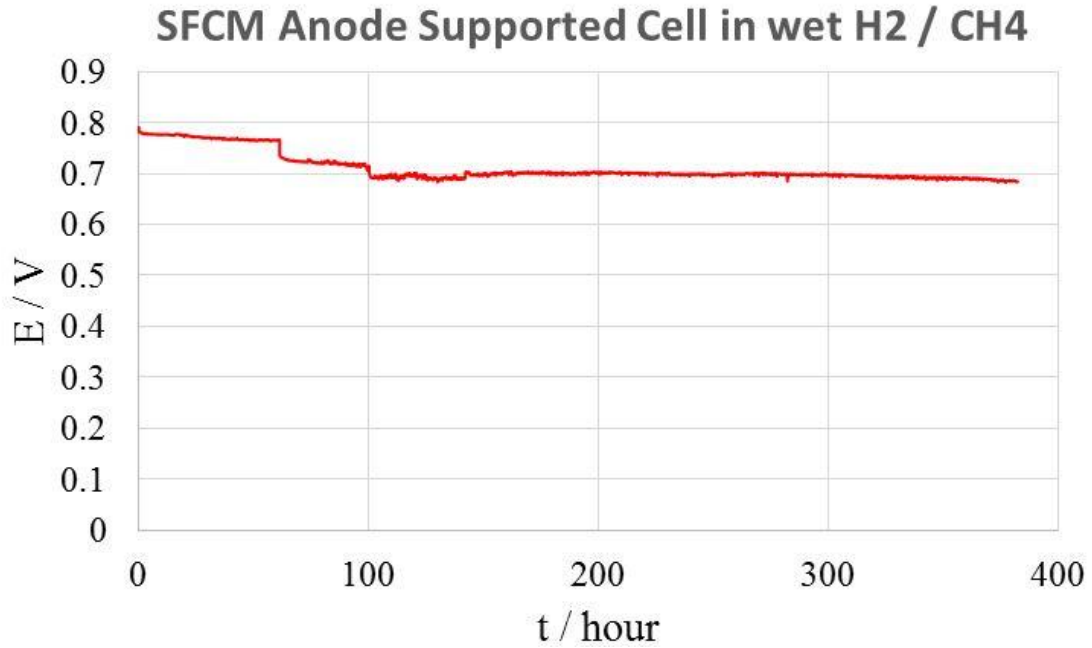


Figure 5.24 SFCM anode supported cell in 81% H₂, 16%CH₄ and 3% water mixture. The cell ran at 450°C at a constant current density of 0.2A/cm². The cell is stable after 150 hours.

5.6 Conclusion

By doping Fe into Sr₂CoMoO₆, the conductivity is greatly improved. The mobility of electron transport increases with Fe dopant due to the degree of disorder goes up. However, too much Fe dopant lowers the conductivity because lower Mo content. SFCM materials are redox stable in both air and H₂, and they are compatible with the GDC electrolyte. SFCM244 was selected for cell fabrication, because it has the highest metallic conductivity.

Porous SFCM-GDC anode supported cells were fabricated via tape casting techniques. At low temperatures, the anode is only an electronic conductor. Thus infiltration is needed to improve the ionic conductivity, as well as the catalytic activity. The best one is Ni-GDC (1:2) ethanol solution. With 10 wt% loading in the anode, the cell has the highest performance in both H₂ and CH₄. With single layer GDC electrolyte, the cell performance is good, but the OCV is low. We believe it is caused by Co diffusion in sintering process. Co can introduce leakage current in the electrolyte and lowers the OCV. In order to solve this problem, a certain electronic blocking layer should be used. The first attempt is ESB. ESB is an ionic conductor and has the advantage of low sintering temperature and high ionic conductivity. With a thick layer of ESB, the OCV improves, but the cell performance decreases. We speculate it is caused by small amount Co in the ESB layer or interfacial reaction between Co contaminated GDC and ESB. Our next attempt was using LSGM. With 10 μm LSGM, the OCV got improved and the performance is higher than single layer GDC cells. However, LSGM has to be fired at high temperature. Even a 5% Li sintering aid cannot fully densify LSGM, thus low temperature operation is not favored due to high ohmic resistance. Meanwhile, the OCVs decrease slowly even with these electronic blocking layer. Therefore, the operation temperature should be lowered to slow down the degradation kinetics.

We found 2 mol% Co-GDC is a good electronic blocking material. It has high ionic transference number and this layer can be densified at low temperatures. The cells with Co-GDC buffer layer were fabricated. In H₂, the cell gives out high power density between 550°C and 450°C with a high OCV. At 450°C, the H₂ stability is good with

the degradation rate of 0.03% per hour, and the reason for this degradation is mainly caused by sealant failure and Ni agglomeration. In reformat, the cell can give out similar power density as it is in H₂. After slow degradation for the first 150 hours, the cell is stable without any decay. Therefore, SFCM is a good anode material to replace traditional Ni-Cermet. SFCM supported cell has high performance with flexible fuels at low temperatures and the stability is applauding. At last, we suspect Co-GDC cannot only improve cell OCV, it may also increase the cathode performance. The details will be discussed in the next chapter.

Chapter 6: Improving Cathode Performance By Adding Cathode Functional layer

6.1 Introduction

In the previous chapter, Co-GDC was used as the electronic blocking layer, as it has high ionic transference number. By adding this layer on top of the electrolyte, the OCV is improved. In addition, we observed the cell had low polarization resistances, especially at low temperatures. Therefore, there is a possibility that this Co-GDC can also improve the cathode performance, besides the OCV. This finding is promising because it may lower the cell operation temperature. Typical SOFCs are operated at high temperatures, and commercialized Ni-YSZ SOFC has an operation temperature around 800°C. High operation temperature causes some problems, such as fast degradation kinetics of cell components, longer startup time, high maintenance cost, etc. Nowadays, Ni-GDC SOFC is approached for commercialization and has a lower operation temperature around 650°C due to higher ionic conductivity of GDC than YSZ. However, this operation temperature is still high. The target in this field is to design a low temperature SOFC (LT-SOFC) that can be operated below 500°C. There are several issues that prevent the SOFC being operated at low temperatures, and one of the biggest problem is the cathode activation polarization loss. At the cathode side, the oxygen reduction reaction takes place and it requires higher activation energy than the hydrogen oxidation reaction at the anode, because splitting O=O double bond needs

more energy than splitting H-H single bond.^{118,119} Therefore, the cathode always reaches its limitation before the anode.

The overall cathode processes includes oxygen adsorption / desorption on cathode surface, oxygen incorporation into cathode lattice, and oxygen transport from cathode to electrolyte. To improve the cathode performance, developing new materials with high cathode catalytic activity and optimizing cathode microstructure are two major routes. Typical cathode materials like LSM and LSCF have been studied a lot and the mechanism have already been investigated.¹⁵⁰⁻¹⁵⁶ The cells with these cathodes can work functionally for a long time with minimal degradation.¹⁵⁷⁻¹⁶⁰ However, the cells with these cathode should be operated at elevated temperatures. $\text{La}_{0.6}\text{Sr}_{0.4}\text{CoO}_3$ (LSC) and $\text{Sr}_{0.5}\text{Sm}_{0.5}\text{CoO}_3$ (SSC) can work at 600°C, with a better performance than LSCF and LSM, due to their higher catalytic activity.¹⁶¹⁻¹⁶⁵ To extend the cell operation temperature even lower, more active materials are needed. $\text{Ba}_{0.5}\text{Sr}_{0.5}\text{Co}_{0.8}\text{Fe}_{0.2}\text{O}_3$ (BSCF) that works at 500°C, and the cell with BSCF cathode has a good output around 400mW/cm² at this temperature.¹⁶⁶⁻¹⁶⁸ However, this cathode is not stable during long term operation or when CO₂ is present.^{147,169-171} There is also another type of cathode called $\text{PrBa}_{0.5}\text{Sr}_{0.5}\text{Co}_{2-x}\text{Fe}_x\text{O}_{5+\delta}$ (PBSCF), which has higher performance than BSCF and the stability is better, but the fabrication requires 600 hours annealing at 700°C to get the right structure.¹⁷² Low temperature cathodes always come with stability, fabrication and cost issues because of the operation conditions are more challenging. At another aspect, improving microstructure can also lower the cell operation temperature because of more active sites. Nano fiber or rods types of cathodes have

high surface area, and the performance is enhanced especially at low temperatures.¹⁷³⁻

¹⁷⁵ Due to nano particle's intrinsic property, they are easy to agglomerate during long term operation. In addition, in order to maintain the original nano structure during fabrication process, the firing temperature is lower than that in regular process. Decreasing firing temperature lowers the bonding strength between particles and reduces the cathode mechanical strength.

More active materials and optimized microstructure usually improves the overall effect of surface oxygen adsorption / desorption and oxygen incorporation into cathode lattice, which is the surface oxygen exchange kinetics. However, the mass transport between cathode and electrolyte also plays an important role in cathode performance. C Xia et al indicated that the cathode electrolyte interfacial resistance dominates the cell performance especially at low temperatures.¹⁶⁵ S Wang et al also found out the cathode polarization not only depends on the cathode itself, but also the substrate.¹⁷⁶ Nonetheless, there is no effective way to improve the mass transport between cathode and electrolyte and Plasma Pulsed Deposition (PLD) is the regular method without causing extra interfacial problems.

Our group found out Co doped GDC is a good candidate as the cathode functional layer (CFL) to assist mass transport between cathode and GDC electrolyte. This CFL works with multiple cathodes, improves the cathode performance, increases cell open circuit potential, and no expensive methods are used. With the CFL, the high temperature cell

performance is increased and the operation temperature can also be lowered to 500°C effectively and efficiently.

6.2 Experiments

6.2.1 Cathode Functional Layer (CFL) Preparation

Different amounts of Co-GDC were prepared as follows. 2mol%, 5mol% and 10mol% cobalt nitrates were dissolved in ethanol respectively and ball milled with GDC powder for 24 hours. The mixtures were dried and all nitrates were burnt out at 400°C for 1 hour in furnace. The Co-GDC powder was then mixed with ESL 441 vehicle (ElectroScience) by the weight ratio 1:1 to form the CFL pastes (2Co-GDC, 5Co-GDC and 10Co-GDC). The CFL paste was applied onto the densified GDC surface. After the CFL layer was fully dried in oven, the cathode was applied onto the CFL. Both CFL and cathode layers were fired together at the regular cathode firing temperatures.

6.2.2 Determination of Oxygen Surface Exchange Coefficient

The oxygen surface exchange coefficient (k) of a certain material is used to describe the rate of gas phase oxygen transfer into the solid lattice. It is controlled by a multistep mechanism, including surface oxygen adsorption / desorption, surface oxygen incorporation into lattice, and oxygen transport from lattice surface into inner lattice.

6.2.3 Impedance Analysis of Symmetrical Cell

To determine the improvement of cathode performance by adding CFL, the impedance analysis was done on the symmetrical cells via solartron 1260. The schemes of baseline samples and samples with CFL layer were shown in Figure 6.1. SSC-GDC, LSC-GDC and LSCF-GDC were examined to find out the effect of CFLs on different cathode materials. The firing temperatures were 950°C, 950°C and 1100°C respectively for 2 hours. During testing, Ag paste was used as the current collector, and all samples were measured by 2-point probe mode within the temperature range of 450°C to 600°C.

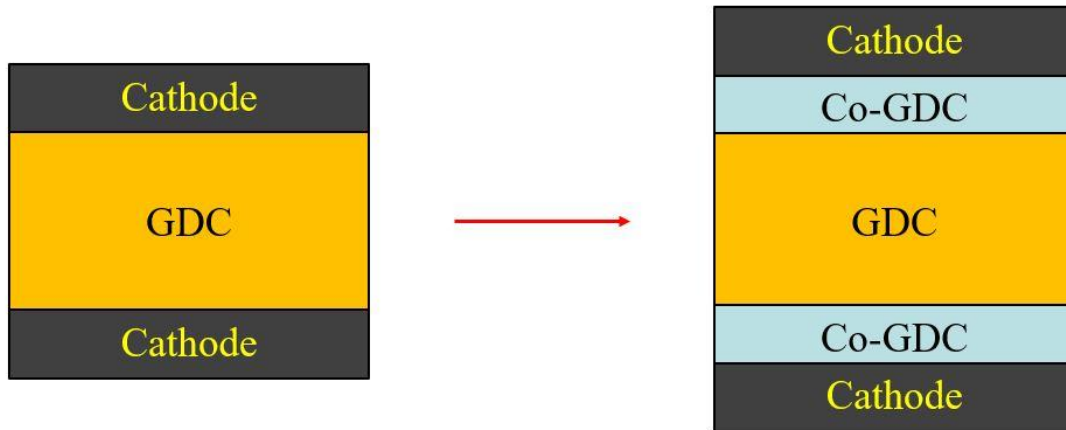


Figure 6.1 Schemes of symmetrical cells. The left one is the baseline sample and the right one is the sample with Co-GDC CFL

6.2.4 Cell Performance Analysis

Ni-GDC half cells were prepared by tape casting technique. NiO-GDC anode support tape, NiO-GDC anode functional layer (AFL) tape and GDC electrolyte tape were laminated together. After firing at 1450°C for 4 hours, the Ni-GDC half cell comprises 400µm anode support, 20µm AFL, and 20µm GDC electrolyte. 2 mol% Co doped GDC

CFL and SSC-GDC cathode were selected for fuel cell testing. The CFL was blade coated on top of the Ni-GDC half cell and dried in a 100°C oven. The SSC-GDC cathode was then blade coated on top of CFL and then dried in the same way. The full cell was fired at 950°C for 2 hours. Two cells with different CFL thickness were prepared (14µm and < 1µm). Ag paste was used as the current collector at both sides of the cell and the measuring temperature ranges from 500°C to 650°C with humidified H₂ as the fuel.

6.3 Results and Discussion

6.3.1 Mechanism of Interfacial Resistance Decrease

Co helps the densification of GDC electrolyte. After firing, the Co agglomerates in the GDC grain boundary and forms a Co rich layer.¹³¹ Due to this Co rich layer on GDC surface, the surface oxygen exchange coefficient improves. According to ¹⁸O isotope exchange test, the 2mol% Co doped GDC starts to exchange oxygen as low as 300°C, shown in Figure 6.2, while the standard GDC undergoes such an exchange above 500°C. In Figure 6.3, the oxygen exchange coefficient of 2mol% Co doped GDC is higher than that of regular GDC all over the temperature range. A higher oxygen exchange coefficient means faster surface oxygen adsorption / desorption and faster oxygen incorporation into lattice. Thus, it enhances the mass transport at the interface between cathode and electrolyte.

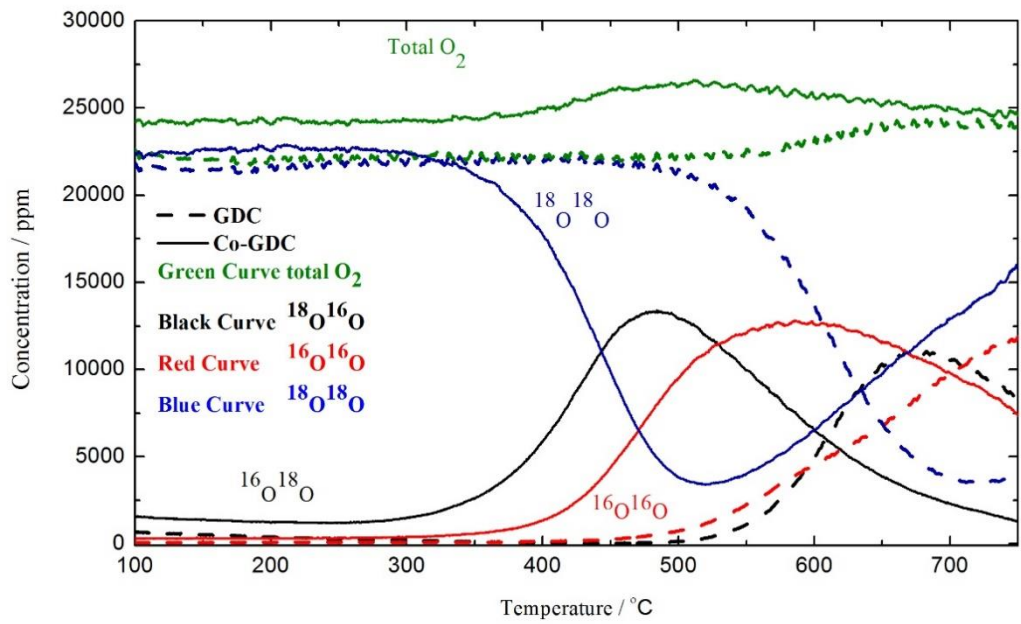


Figure 6.2 Oxygen isotope exchange curves of Co-GDC and standard GDC. Co-GDC started to exchange surface oxygen as low as 300°C.

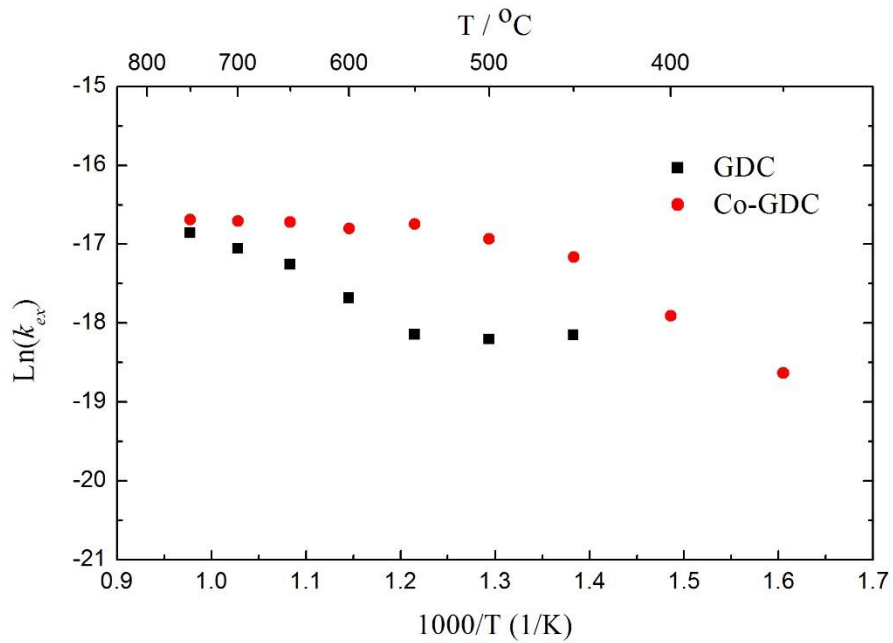


Figure 6.3 Oxygen surface exchange coefficients of Co-GDC and GDC. Within whole temperature range, Co-GDC has faster oxygen exchange.

At the interface between electrolyte and cathode, the oxygen anion was dissociated from cathode and incorporated into electrolyte lattice. The cathode usually has high surface oxygen exchange coefficient, so the process of oxygen dissociation from cathode is easy. However, due to GDC's low surface oxygen exchange kinetics, it is difficult for oxygen ion to enter GDC electrolyte lattice, even though GDC has a high oxygen ion conductivity. When the Co-GDC is applied onto the GDC electrolyte surface, the situation is different. The configuration is shown in Figure 6.4.

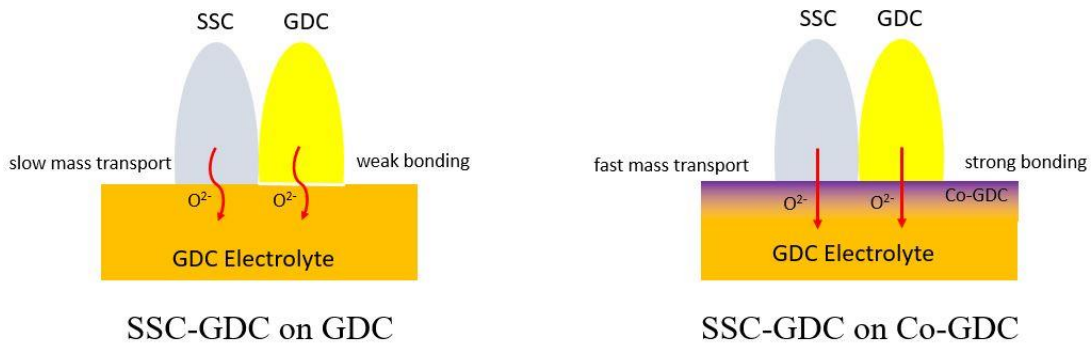


Figure 6.4 Scheme of the interface between SSC-GDC cathode and GDC electrolyte. By adding Co-GDC CFL the mass transport is improved and the bonding strength is enhanced.

When Co-GDC contacts with cathode, because of fast surface oxygen exchange kinetics in both Co-GDC and cathode phases, the mass transport at the interface is promoted, resulting to a lower interfacial resistance. This mechanism has also been confirmed in our previous report, which is a thin ESB interlayer can decrease the interfacial resistance between YSZ electrolyte and cathode.¹⁷⁷ At another aspect, Co-GDC assists the bonding between cathode and electrolyte. In most circumstances, GDC is added into the cathode to improve the ionic conductivity. At low firing temperatures,

the bonding strength between GDC electrolyte and GDC phase in cathode is not good. It introduces extra interfacial resistance. Co-GDC also assists such bonding because the Co rich layer works as the sintering aid.

6.3.2 Cathodes Improvement by CFL

By adding a CFL between cathode and electrolyte, the cathode performance are all improved, no matter how much Co in the CFL, shown in Figure 6.5 -6.7. With CFL, the polarization area specific resistance (ASR) decreases, while the slopes of $\log(\text{ASR})$ vs. $1/T$ remains almost unchanged for the three types of cathode. The slopes represents the activation energies of cathode. If they are the same, it means the CFL doesn't enhance the intrinsic cathode catalytic activity or change the cathode morphology. The cathode polarization resistance includes the whole process that gas phase oxygen gets reduced on cathode surface, the oxygen anion transports within the cathode, and the oxygen anion goes across the interface between cathode and electrolyte. Thus, the improvement is due to lower interfacial resistance between cathode and electrolyte. Co-GDC CFL can assist oxygen ion transport from cathode into the electrolyte. At another aspect, Co can work as the sintering agent for lots of materials, especially for ceria.^{131,132,178} Therefore, The Co-GDC can be a bonding agent to help the anchoring of cathode on GDC electrolyte.

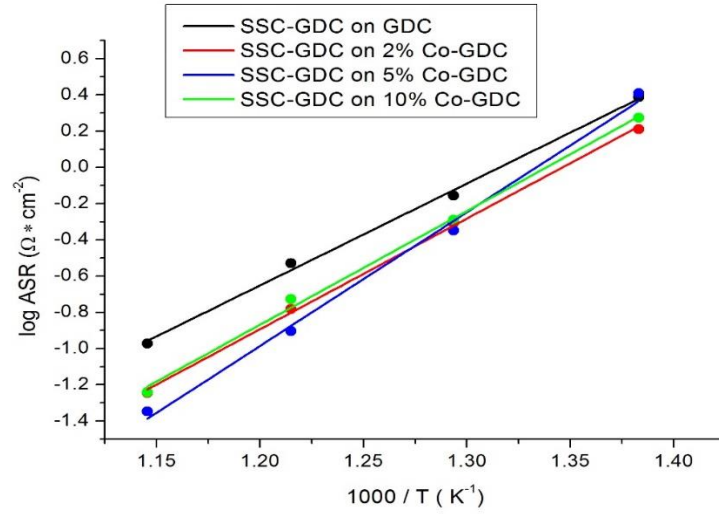


Figure 6.5 Polarization resistance of SSC-GDC on Co-GDC CFL. Temperature ranges from 450°C to 600°C

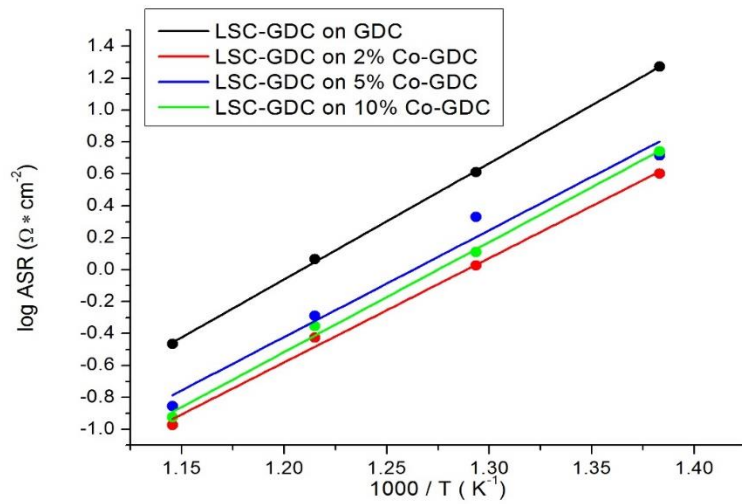


Figure 6.6 Polarization resistance of LSC-GDC on Co-GDC CFL. Temperature ranges from 450°C to 600°C

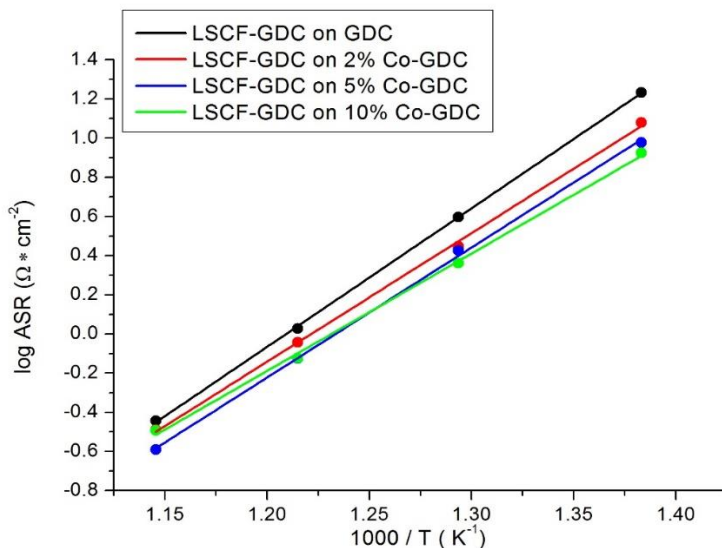


Figure 6.7 Polarization resistance of LSCF-GDC on Co-GDC CFL. Temperature ranges from 450°C to 600°C

Specifically, at 500°C, the cathode polarization resistance is smaller on top of Co-GDC CFL than on GDC surface, shown in Figure 6.8-6.10. For SSC-GDC cathode, the ASR on GDC surface is around 0.105Ω/cm² with Ag current collector. When there is a 5Co-GDC CFL, the ASR is 60% smaller. The 2Co-GDC and 10Co-GDC have a bit less effect, around 50% shrinkage in the cathode polarization arc. For LSC-GDC cathode with CFL, the ASR is only around 30% of the standard ASR on GDC, which is a big enhancement. However, when the cathode is LSCF-GDC, even though the ASR can get decreased, the improvement is not as high as SSC-GDC and LSC-GDC. With 2% Co-GDC CFL or 5% Co-GDC CFL, the cathode performance is close to the standard performance on GDC surface. When the Co content goes up to 10%, a relatively bigger improvement is observed. This is because LSCF-GDC requires higher firing temperature. Unlike SSC-GDC or LSC-GDC, LSCF-GDC has to be fired around

1100°C. Co covers the GDC surface in CFL and it helps with the oxygen ion transport. Co is volatile at high temperatures and if the heating process is too vigorous, Co evaporates and the CFL expires. Therefore, LSCF-GDC doesn't have such a good performance on CFLs as SSC-GDC or LSC-GDC. When the Co content is high, the CFL doesn't fully expire and still have some positive effect.

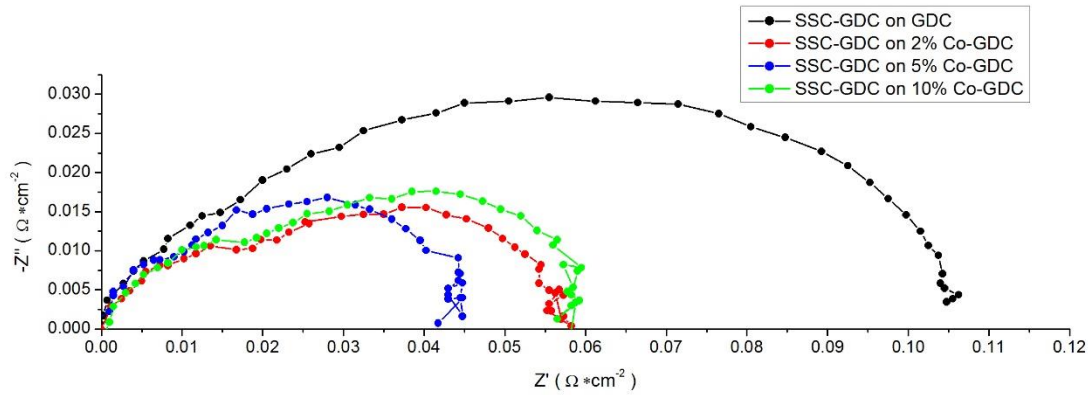


Figure 6.8 Polarization resistance of SSC-GDC cathode on Co-GDC CFL at 500°C. When the CFL contains 5% Co, the improvement is the highest. When CFL contains 2% or 10% Co, the performances are similar.

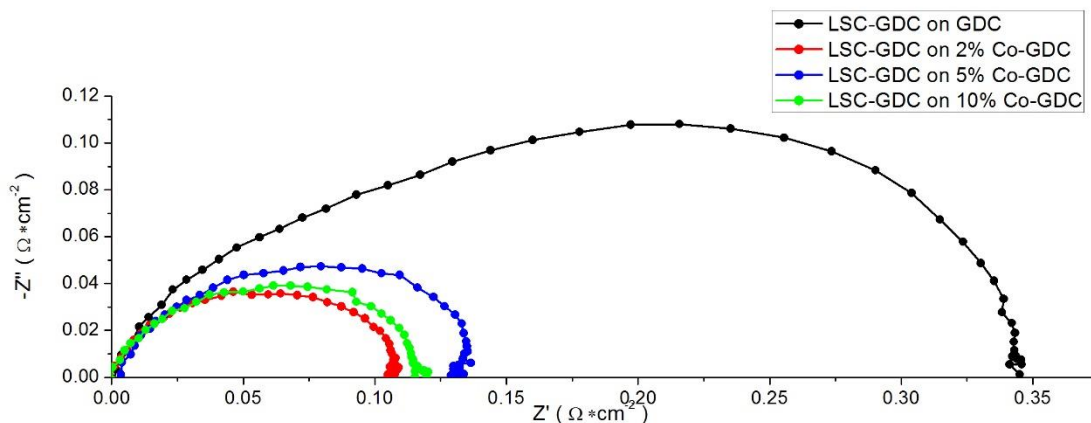


Figure 6.9 Polarization resistance of LSC-GDC cathode on Co-GDC CFL at 500°C.

When CFL contains 2% Co, the performance is the best.

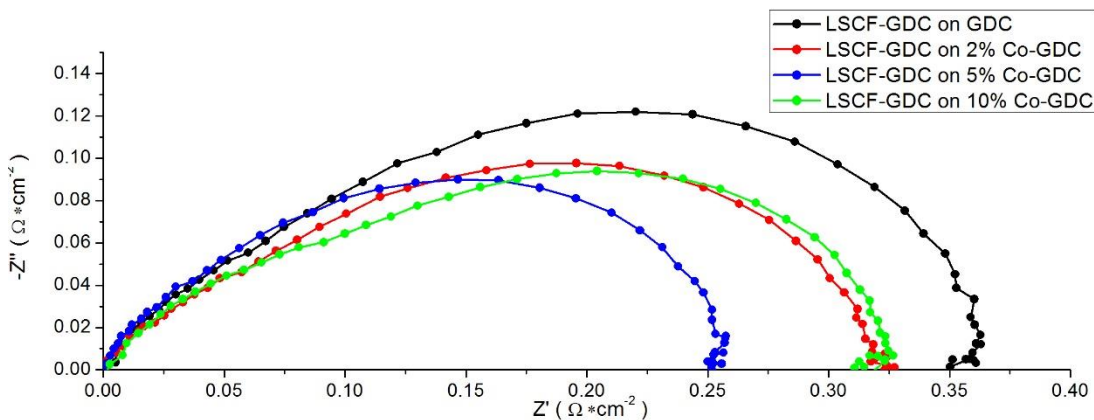


Figure 6.10 Polarization resistance of LSCF-GDC cathode on Co-GDC CFL at 500°C.

Compared with SSC and LSC, CFL has less effect on LSCF, mainly because LSCF should be fired at higher temperature, and the surface Co on CFL evaporates.

6.3.3 Cell Performance Improvement by CFL

By adding 2Co-GDC CFL, the Ni-GDC cell performance increases a lot within the whole temperature range. If the cell performance is increased, less material is needed to output certain amount of power. It reduces system cost, weight, and building difficulties. The performance of standard Ni-GDC cell with SSC-GDC cathode is shown in Figure 6.12. At 650°C, the peak power density (PPD) is closed to 1W/cm². Two cells with different CFL thickness (14 μm and less than 1μm) were fabricated for comparison. The SEM images of cell cross section is shown in Figure 6.11. In Figure 6.11(A), we can see a clear 14μm CFL. When the CFL is very thin, it is not visible, in Figure 6.11(B). We believe this layer follows the cathode shrinkage and has the similar microstructure with the cathode.

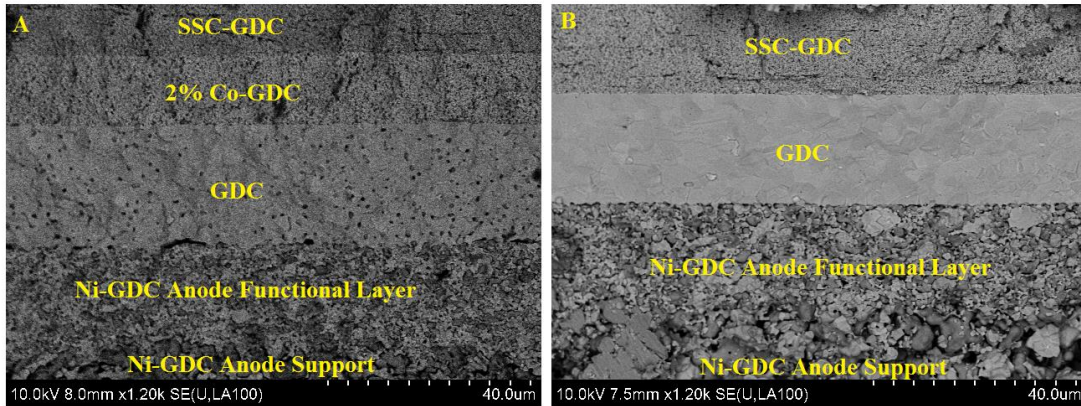


Figure 6.11 SEM Images of Ni-GDC cells with 2% Co-GDC CFL. (A) Thick 14μm 2% Co-GDC prepared by blade coating. (B) Thin 2% Co-GDC prepared by drop coating. The estimated thickness is less than 1μm, and the layer cannot be differentiated from SSC-GDC cathode.

When $14\mu\text{m}$ 2Co-GDC CFL is used, the PPD easily exceeds the standard value and reaches $1.84\text{W}/\text{cm}^2$ which is almost doubled, shown in Figure 6.13. Besides the cathode improvement, part of the enhancement is caused by high OCV. Ceria electrolytes have a common problem. The OCV is lower than YSZ or LSGM at high temperatures. Ce is a multivalence cation and it can be reduced at the anode side during cell operation conditions. This type of decreased OCV lowers overall cell efficiency. Ceria is an n-type conductor, and if a certain p type conductor is doped, the electronic conductivity will be neutralized. D.P. Fagg et al reported 2 mol% Co doped GDC has the ionic transference number higher than 0.98 at 650°C ¹⁴² Thus, when the 2Co-GDC CFL covers the GDC electrolyte, the OCV goes up to 0.9V at 650°C , compared with 0.84V of the standard cell. If the CFL is thin ($<1\mu\text{m}$), the OCV has no improvement, which is 0.82V at 650°C , shown in Figure 6.14. However, the cell PPD is $1.6\text{ W}/\text{cm}^2$, much higher than the standard cell. At low temperatures, the cathode kinetics is slow. The standard cell only outputs $250\text{mW}/\text{cm}^2$ at 550°C . In order to lower the cell operation temperature, reducing cathode polarization loss is very important. Here, the CFL plays a more important role. When the CFL is thin, the cell PPD is $750\text{mW}/\text{cm}^2$ at 550°C , 3 times of the standard cell. At 500°C , the cell can output as much as $400\text{mW}/\text{cm}^2$, while the cell with thick CFL outputs $300\text{mW}/\text{cm}^2$. Thus, by incorporating a CFL, the cell can be operated ideally at low temperatures.

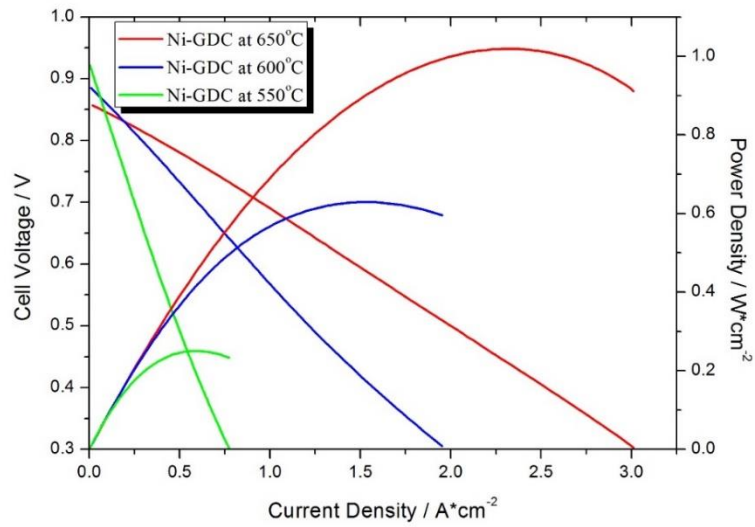


Figure 6.12 Performance of standard Ni-GDC cell. 20 μ m GDC electrolyte and SSC-GDC cathode are used in the cell configuration. The cell was tested in humidified hydrogen between 500°C to 650°C.

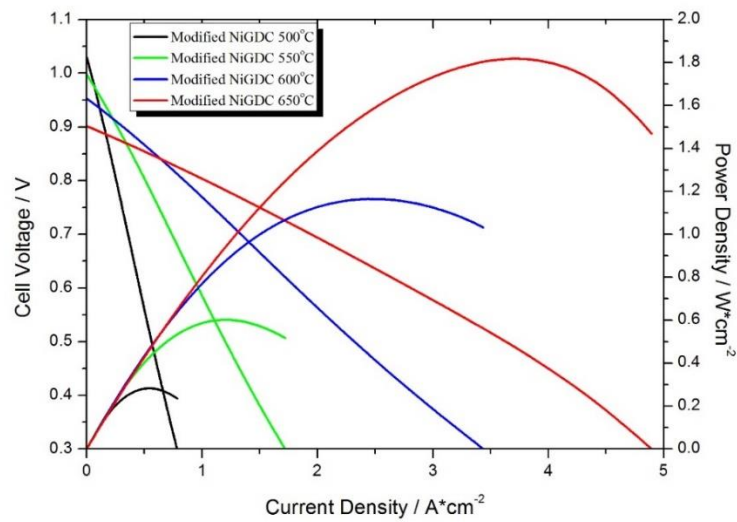


Figure 6.13 Performance of Ni-GDC cell with 7 μ m CFL. 20 μ m GDC electrolyte and SSC-GDC cathode are used in the cell configuration. The cell was tested in humidified hydrogen between 500°C to 650°C.

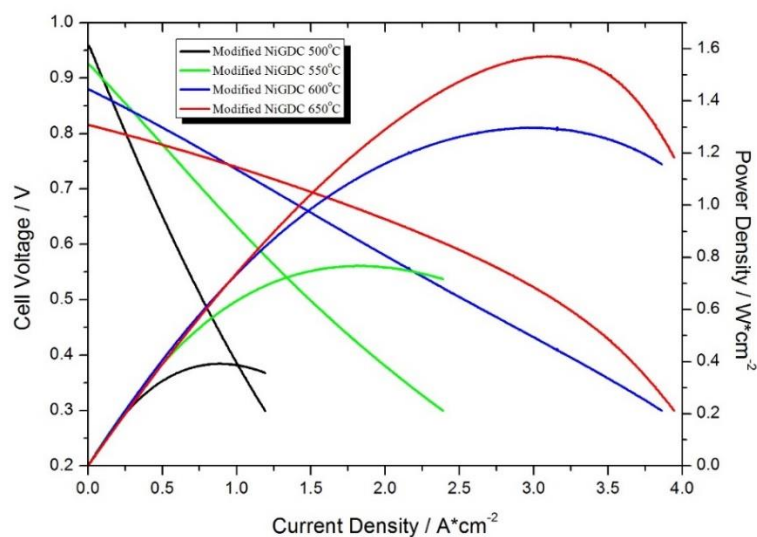


Figure 6.14 Performance of Ni-GDC cell with very thin CFL (<1 μ m) . 20 μ m GDC electrolyte and SSC-GDC cathode are used in the cell configuration. The cell was tested in humidified hydrogen between 500°C to 650°C.

6.4 Conclusion

The mechanism of Co-GDC CFL was studied by isotope exchange. Co covers GDC particles and changes the surface properties. Co-GDC has high surface oxygen exchange coefficient which helps the interfacial mass transport. The Co rich layer also enhances the bonding strength between cathode and electrolyte. This CFL works for different types of cathode and the decrease of polarization resistance is as much as 70%. By using CFL, traditional Ni-GDC cells have higher OCV and the performance is higher at all temperatures. When the CFL is thick (14 μ m), the OCV is higher with the PPD of 1.84mW/cm² at 650°C. When the CFL is thin, the cell has more advantages to be operated at low temperatures. At 550°C the PPD is 750mW/cm² while it is

400mW/cm² at 500°C. Depending on cell operation temperatures, the CFL thickness can be tailored to achieve the optimized performance. No expensive materials or complicated fabrication techniques are used. This is a new route to improve the SOFC performance and lower the cell operation temperatures.

Chapter 7: Mixed Protonic Electronic Conductors

7.1 Introduction

In this chapter, a side project of developing mixed protonic electronic conductors is discussed. From previous chapters, we can know for a good SOFC, it is preferred to use pure ionic conductors for the electrolyte, such as YSZ, LSGM and ESB. For ceria based electrolytes, like GDC, the operation temperature should be below 650°C, otherwise the cell OCV is low, due to partial reduction of Ce^{4+} to Ce^{3+} . This valence transition introduces leakage current in the electrolyte. As the result, some electrons do not go through the outside circuit, lowering the cell performance and efficiency. These cases are all oxygen conductors. The same, if the electrolyte conducts proton, instead of oxygen anion, it is a proton solid oxide fuel cell. Examples of the electrolyte materials are lanthanide doped SrCeO_3 , lanthanide doped BaCeO_3 and lanthanide doped BaZrO_3 .¹⁷⁹⁻¹⁸⁴ These materials are purely protonic conductors and the cell OCVs are all above 1V.

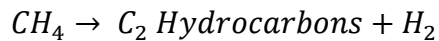
If it is a purely ionic conductor, only ions can transport in the electrolyte, and high OCV can be obtained. If there is electronic conduction, the electrons will migrate in the electrolyte can the cell performance is low. However, if the leakage current is high, it can be another application called hydrogen (oxygen) permeation membrane, depending on the type of ionic conductivity. The simple mechanism is shown in Figure 7.1. Here protonic electronic mixed conductor is used as the example. When there is a P_{H_2} difference present at both sides of the membrane, proton and the electron move

from the high P_{H_2} side to the low P_{H_2} side. The driving force is the hydrogen partial pressure gradient.



Figure 7.1 Hydrogen permeation membrane and oxygen permeation membrane

This application is very useful to separate hydrogen out from gas mixtures in the petroleum industry and because the membrane is dense and has high selectivity, the hydrogen obtained via this method has a very high purity. This membrane can also be used to accelerate some reactions. Nowadays, due to the low price of natural gas, researchers are investigating how to convert methane to high C hydrocarbons or even liquid fuels. One of the reactions is shown as follows,

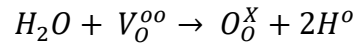


In order to increase the yield of this reaction, hydrogen should be removed from the products. Therefore, the protonic electronic mixed conductor can be used to do this job. When hydrogen is formed, because there is a P_{H_2} difference between the inside and the outside of the reactor, the product hydrogen can permeate through the membrane. As the result, the yields of C_2 hydrocarbons are increased and the by product ultra pure hydrogen is obtained.

Because the protons and electrons are transport towards to the same direction, it is easy to imagine such a membrane with equivalent protonic and electronic conductivity has the highest performance. If the protonic conductivity is higher, the hydrogen flux is limited by the lower electronic conduction, vice versa. To achieve high performance, matched high conductivity of protons and electrons are desired.

7.2 Conduction Mechanism

Specifically, in the perovskite, the protons are generated through the water vapor incorporating into the oxygen vacancies. The equation is shown below



Therefore, in order to obtain protonic conductivity, the oxygen vacancy is necessary. Thus, doping lanthanide into SrCeO₃ or BaCeO₃ is needed. There are a lot of materials have oxygen vacancies, but not all of them have protonic conductivity. When the materials have high basicity, H₂O molecules are more likely incorporate into the oxygen vacancies, because at elevated temperatures, steam can be considered as a type of acidic gas. In SrCeO₃ and BaCeO₃, Sr and Ba are both rare earth elements with high basicity. At another aspect, Ce is lanthanide which is also very basic. Therefore, the compositions tend to “react” with water to form protons. However, the basicity cannot be too strong, otherwise the material may decompose in moisture or when CO₂ is present at high temperatures.^{185,186} To solve the stability problem, doping Zr at B site or directly use Y doped BaZrO₃ may be good ideas. Zr is not as basic as Ce, and Y doped BaZrO₃ has a cubic structure which is more stable than SrCeO₃ and BaCeO₃. However, when Zr is added into the composition, the sinterability of the material is

lowered. The poor densification increases the ohmic resistance, and sintering agent may be needed. ¹⁸⁷⁻¹⁹⁰

After the protons are formed, protons can bond with the lattice oxygen and hop among the oxygen anions, as shown in Figure 7.2. The proton moves around the oxygen anion and due to the oxygen oscillation and vibration, the proton can move from one oxygen to another oxygen, finally realizing proton hopping. ¹⁹¹

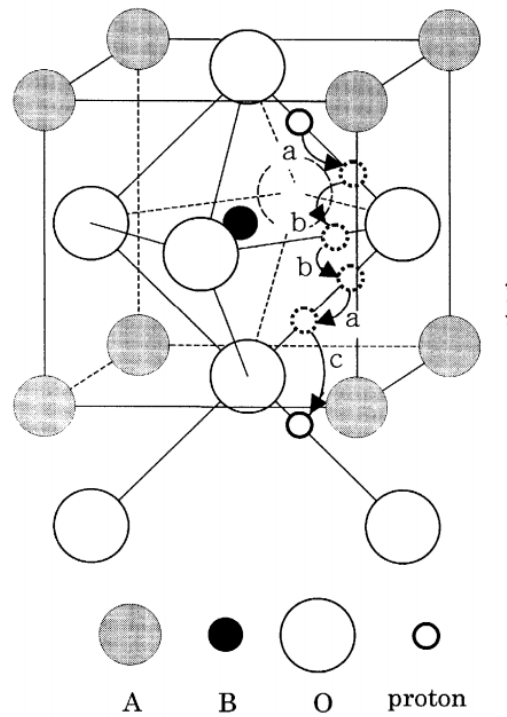
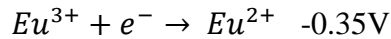


Figure 7.2 proton conduction in an ABO₃ perovskite material. Protons are hopping among the oxygen sites ¹⁹²

The electron transport mechanism is explained in Chapter 2. All of the perovskite materials follow the electron hopping mechanism.

Most of the protonic conductors are purely ionic conductors. In order to increase the electronic conductivity, multivalent cation should be doped into the composition. One of the good mixed conductor is Eu doped SrCeO₃. Eu is a special lanthanide which has two valence state of +3/+2. The standard reduction potential is not very negative, and it can provide some n-type conduction under reducing conditions. The standard reduction potential is shown below,



As the result, Eu doped SrCeO₃ is widely used for hydrogen separation.¹⁹³⁻¹⁹⁵ Nevertheless, even though this composition is good, the electronic conductivity is still lower than protonic conductivity.

7.3 Experiments

BaZr_{0.8}Y_{0.1}Nb_{0.07}Co_{0.03}O_{3-x} (BZYN), Ba_{0.95}La_{0.05}Zr_{0.8}Y_{0.1}Nb_{0.07}Co_{0.03}O_{3-x} (BLZYN), and Ba_{0.95}Eu_{0.05}Zr_{0.8}Y_{0.1}Nb_{0.07}Co_{0.03}O_{3-x} (BEZYN) were synthesized via solid state reaction. Stoichiometry amount of BaCO₃, ZrO₂, Y₂O₃, Nb₂O₅ and Co₃O₄ (Eu₂O₃ and La₂O₃) were mixed together and ball milled in ethanol for 24 hours. The powders were then dried and calcined at 1100°C for 4 hours. The calcined powders were grinded and ball milled again for another 24 hours. The powders were then dried, pressed into pellets and sintered at 1450°C for 12 hours. The sintered bodies were sent to XRD diffractometer to examine the phase purity.

Conductivity of the samples were measured via 4 probe DC method with Keithley 2400 source meter. Pt paste was used as the current collector. All samples stayed in

humidified 10% H_2 / 90% N_2 . The conductivity was taken when the readings were stabilized. The temperature ranges from 600°C to 900°C

7.4 Results and Discussion

The base composition is $BaZr_{0.9}Y_{0.1}O_{2.95}$. The reason why don't select $BaCeO_3$ or $SrCeO_3$ series is Y doped $BaZrO_3$ has higher conductivity. At another aspect, $BaZrO_3$ has higher stability and that of the cerates compositions. It will not decompose in moisture or in CO_2 , showing long term stability. In these compositions. 3 mol% Co is added. As discussed before, barium zirconate is very difficult to sinter. To improve sinterability, transition metal oxide is usually added as the sintering agent. Nb is an n-type conductor which can provide some electronic conductivity in reducing conditions. By doping Nb, the pure ionic conductor can be modified into the mixed conductor.

The purpose of comparing these compositions is to find out whether A site dopant can affect the conductivity. As we know, most dopant methods modify the perovskite B site, because both protonic and electronic conductivity mostly depend on the B site. However, A site doping can also affect the material properties. To confirm this, 5 mol% La and Eu were doped respectively in this composition.

The XRD patterns are shown in Figure 7.3. After sintering, all compositions have single cubic perovskite phases. When doping La or even doping Eu, the peaks shift to the right. The ionic radii r_{Ba} (144pm) > r_{La} (136pm) > r_{Eu} (124pm), and smaller cation decreases the lattice parameter. As the result, the peaks move to the high angles.

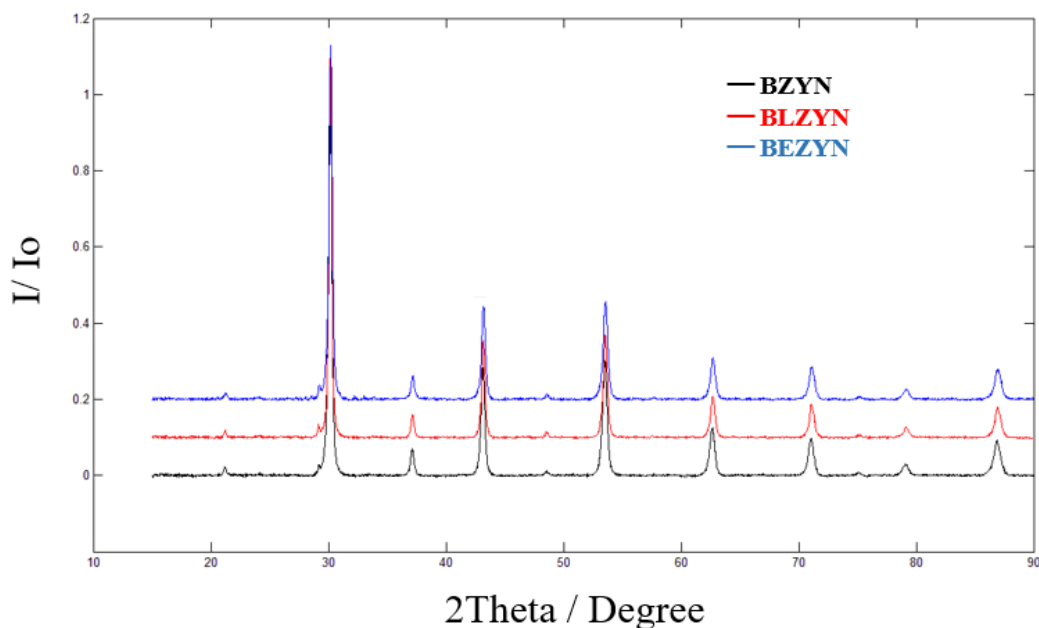


Figure 7.3 XRD patterns of sintered bodies of BZYN, BLZYN and BEZYN. All compositions show single phases after sintering

The conductivity were measured from 600°C to 900°C in humidified hydrogen. The conductivity of the three compositions is shown in Figure 7.4. With A site dopant, the conductivity decreases. Ba has the valence state of +2, while the dopants are both lanthanide, with the valence state of +3. Thus, doping lanthanide lowers the concentration of oxygen vacancy. The lower oxygen vacancy concentration directly decreases the protonic conductivity. As the result, when 5% La is doped into A site, the conductivity drops over one magnitude all over the temperature range. However, when Eu is doped, the conductivity increases a lot compared with La. Under reducing conditions, Eu can be partially reduced from the valence state of +3 to +2. Therefore, it introduces electronic conductivity in the composition. According to Chapter 2, usually the electrons hop between B site cations. If Eu is doped at A site, the electron

hopping route could be A site to B site, which provides an extra pathway.

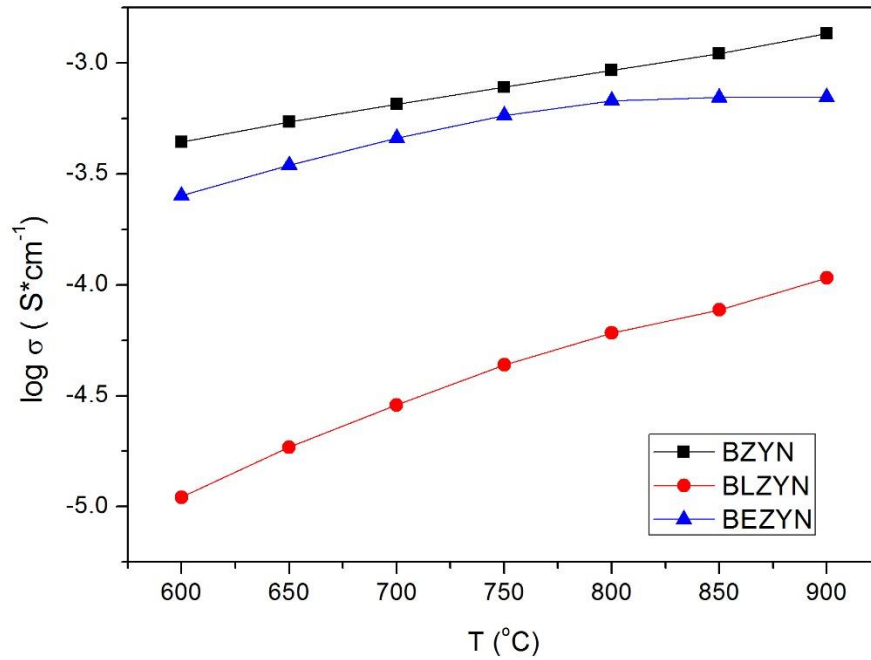


Figure 7.4 Conductivity of BZYN, BLZYN, and BEZYN. With A site dopant, the conductivity decreases due to lower protonic conductivity. BEZYN has much higher conductivity than BLZYN.

7.4 Conclusion

By doping lanthanide into A site, even with 5 mol% dopant level, the conductivity changes a lot. BZYN has the conductivity around $10^{-3} \text{ S*cm}^{-1}$, but when 5% La is doped at A site, the conductivity decreases a lot by over one magnitude. It is because higher valence S site cation can decrease the concentration of oxygen vacancies and finally decreases the concentration of protons. With 5% Eu dopant, the situation is different. Eu has an easy $3+/2+$ transition. Even though in this composition the protonic

conductivity is also low, because of the same reason, the electronic conductivity increases a lot. Standard electronic hopping route is from one B site cation to another B site cation. With Eu at A site, it provides an extra pathway. As the result, we can observe the conductivity jump by switching La to Eu.

Chapter 8: Summary and Future Work

Anode research is a very important part of SOFC development. At the anode side, the fuel is oxidized and the power is generated. In order to lower the SOFC operation temperature, increase SOFC life time, and make it suitable for hydrocarbon fuels, a good anode is necessary. To meet these requirements, the ceramic anode is now the research focus. Ceramic materials are more stable than the cermet composite, and they are more tolerant to hydrocarbons. However, the biggest issue is the ceramic materials have much lower conductivity than cermets, and it introduces high ohmic resistance. Therefore, the overall discussion is about how to increase the conductivity. To achieve high conductivity, the mechanism should be found out. Our idea is using standard reduction potential to seek appropriate elements combination in the perovskite structure, which can make the materials have high concentration of free electrons as well as high electron mobility. Our observation is that if a certain B site element has the reduction potential between 0V to 1V, the composition is probable to have high conductivity, without reduction at high temperatures, and also it can provide enough stability to work in fuel cell operation conditions. Through this way, we determined vanadium and molybdenum are good candidates for perovskite B site dopants.

With vanadium dopant, we developed vanadium doped SrTiO_3 and NaNbO_3 . All of the compositions have very high conductivity over $50 \text{ S}\cdot\text{cm}^{-1}$. However, there are tradeoffs. High performing material usually means lower stability and fabrication problems. Vanadium is a small cation and is very mobile. During materials preparation process,

it always introduces impurities and form unexpected phases. The electrolyte supported configuration is suitable for these materials, because the anode can be fired at lower temperatures and reduce the chance of vanadium diffusion. The anode materials are only electronic conductors. In order to achieve high performance, catalyst and ionic conductors should be infiltrated into the anode. Here Ni-GDC nitrate solution can enhance the anode performance, and an optimized ratio of Ni to GDC was determined. The best cell performance at 650°C in hydrogen is lower than 300 mW/cm², which is attributed to the electrolyte supported cell configuration. Meanwhile, slight vanadium diffusion was observed even though the anode is fired at low temperatures.

Molybdenum double perovskite type of anode was also developed. Molybdenum double perovskite has lower conductivity than vanadium doped perovskite, while the stability is higher. By doping Fe into Sr₂CoMoO₆ (SFCM), the B site cation ordering is disturbed and the conductivity increases over one magnitude, which is high enough for anode support. This material is suitable for anode supported cell configuration. The SFCM supported cell was fired at 1200°C, much lower than the typical Ni-GDC cell. However, due to Co or Mo diffusion into electrolyte, the OCV is lower than regular GDC electrolyte. In order to improve OCV, Co-GDC electronic blocking layer was applied onto the electrolyte surface. Co-GDC has high ionic transference number, so it blocks the leakage current and the OCV is increased. With SSC-GDC as cathode and Ni-GDC as anode infiltrate, the cell has high performance (760 mW/cm²) at a relatively low temperature (550°C). Even the temperature is lowered to 450°C, the cell can still give out a reasonable performance around 300mW/cm², while maintain a long term

stability. Currently most ceramic anode material should be operated above 750°C, because the conductivity is low unless the anode is reduced at high temperatures. This material can be operated at a much lower temperature which is a big improvement.

During the anode development, we observed a cathode improvement. We attributed this phenomena to the Co-GDC layer. The detailed analysis on Co-GDC cathode functional layer (CFL) was performed. By adding the CFL, the performance of different cathodes is improved, including LSCF, LSC and SSC. On regular Ni-GDC cells, both OCV and cell performance are improved. To find out the mechanism, isotope exchange was done on Co-GDC. After firing, Co covers the GDC particle and modifies the GDC surface properties. The oxygen exchange coefficient of Co-GDC is much faster than that of the standard GDC. Better oxygen exchange coefficient means Co-GDC is easy to take oxygen. When the oxygen transport from cathode to the interface between electrolyte and cathode, the Co-GDC CFL can easily capture these anions. Therefore, the interface resistance is decreased and the overall cathode performance is increased, without incorporating expensive materials or using complicated fabrication techniques. This method is easy and effective. Compared with standard Ni-GDC cells, the CFL cells have much higher performance which makes a LT-SOFC feasible.

Besides these, during my first years of Ph.D study, I also did some research on mixed protonic electronic conductors. I modified the Y doped BaZrO₃ and found A site dopant can affect both protonic and electronic conductivity. With lanthanide at A site, the

protonic conduction decreases due to lower oxygen vacancies. However, by carefully doping suitable lanthanide, such as Eu, the electronic conductivity goes up because it provides extra electronic pathway.

In addition, there is still other work should be done in the future. During my Ph.D process, there are some other types of anode were developed, but not fully analyzed or elaborated. One example is Fe doped $\text{Sr}_2\text{NiMoO}_6$ (SFNM). This material is similar to SFCM, which is redox stable (Figure 8.1). Compared with SFCM, the conductivity is about half but still high enough for anode supported cell. The conductivity is shown in Figure 8.2.

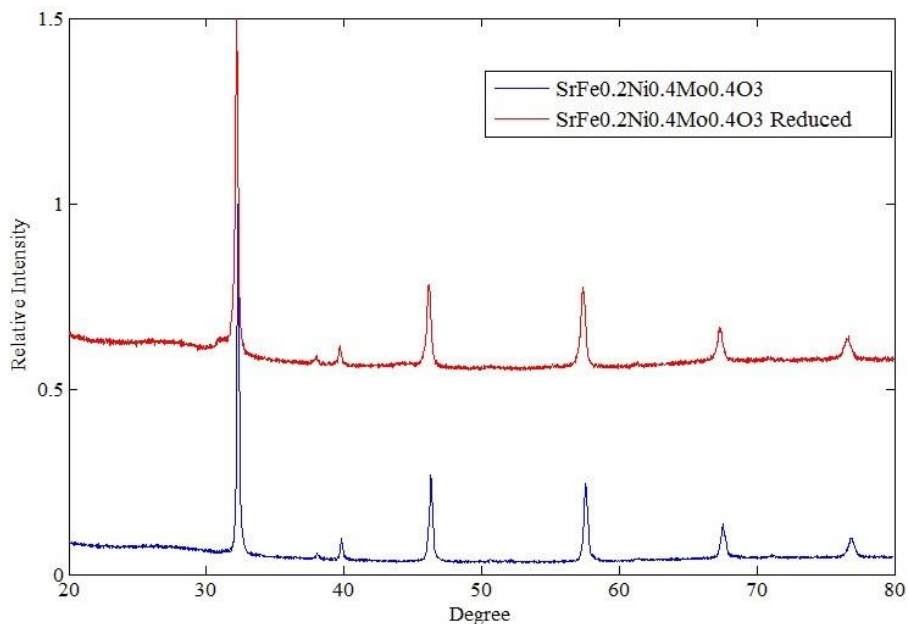


Figure 8.1 20% Fe doped $\text{Sr}_2\text{NiMoO}_6$. The sample was sintered at 1300°C and reduced at 650°C. The phase is stable before and after reduction.

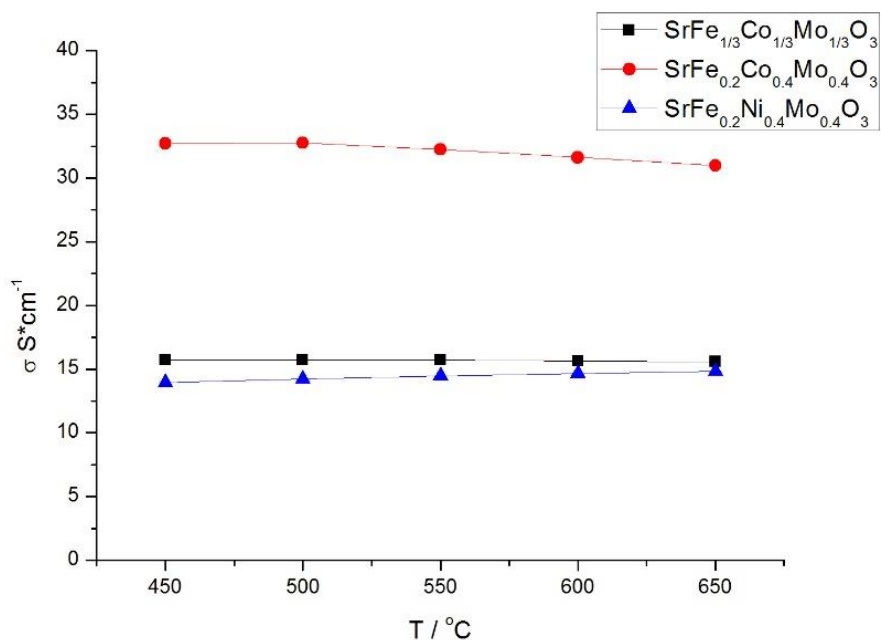


Figure 8.2 Conductivity comparison between SFCM and SFNM. All samples were reduced at 650°C in 10% H₂ / 90% N₂

Even though the conductivity is lower, it has its own advantage. Possibly due to the Ni in the double perovskite phase, SFNM has intrinsic catalytic activity. Thus no metallic catalyst is needed. The cell peak power density (PPD) is shown in Figure 8.3. With only GDC infiltration, SFNM performs much better than SFCM due to higher catalytic activity in both hydrogen and methane. If the fuel contains H₂S which is poisonous to Ni catalyst, SFNM is a good candidate. However, anode supported cell has not been fabricated and how to make such a cell is the future work.

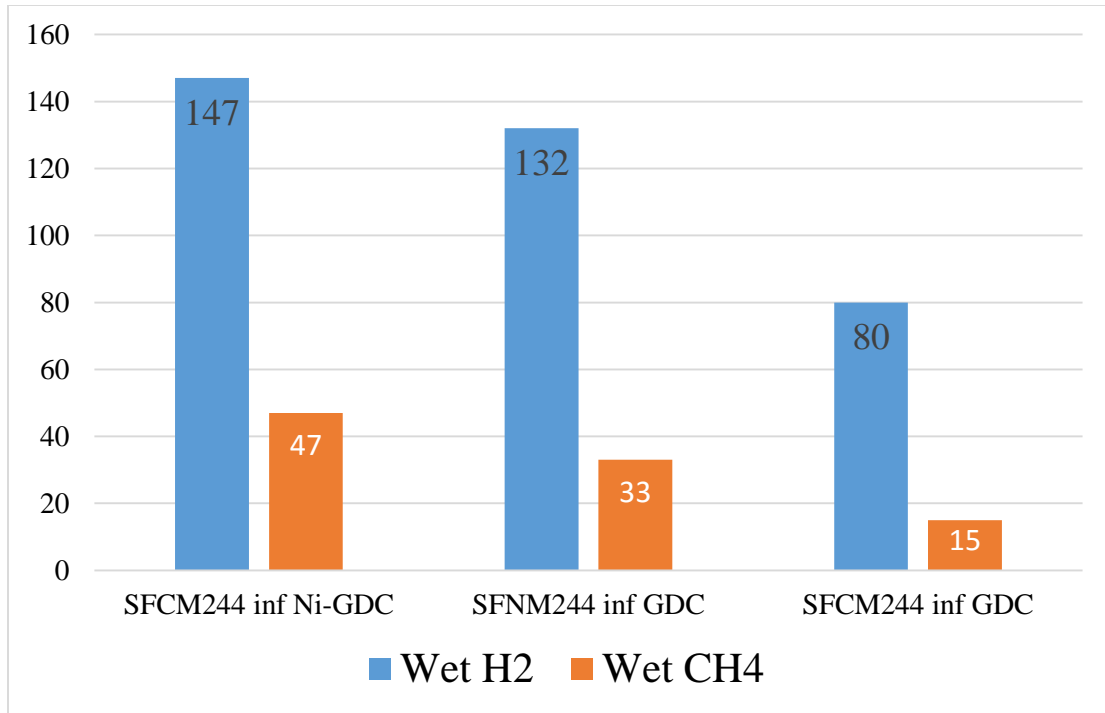


Figure 8.3 PPDs of SFCM cell and SFNM cell. All cells were tested at 650°C.

Meanwhile, there is another type of anode candidate which is $\text{La}_{0.6}\text{Sr}_{0.4}\text{Cr}_{0.9}\text{Mo}_{0.1}\text{O}_3$ (LSCM). After firing at 1450°C, LSCM was densified with minor SrMoO_4 impurity, shown in Figure 8.4. After reduction at 650°C, the impurity is gone. The conductivity is over $30 \text{ S}\cdot\text{cm}^{-1}$ when LSCM is sintered at 1450°C (Figure 8.5), due to its higher relative density. However, no further research has been done on this material, such as fuel cell fabrication, anode performance, stability, etc. In the future, all these analysis will be done.

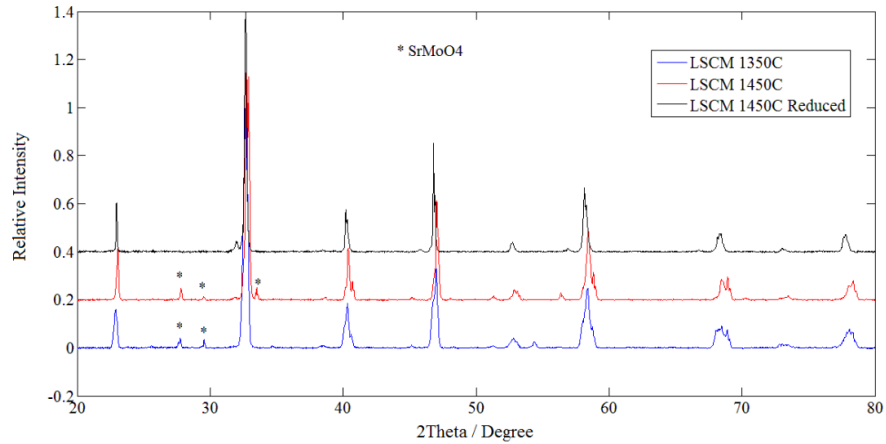


Figure 8.4 XRD patterns of LSCM before and after reduction. Before reduction there is SrMoO₄ impurity at all sintering temperatures, while it is gone after reduction.

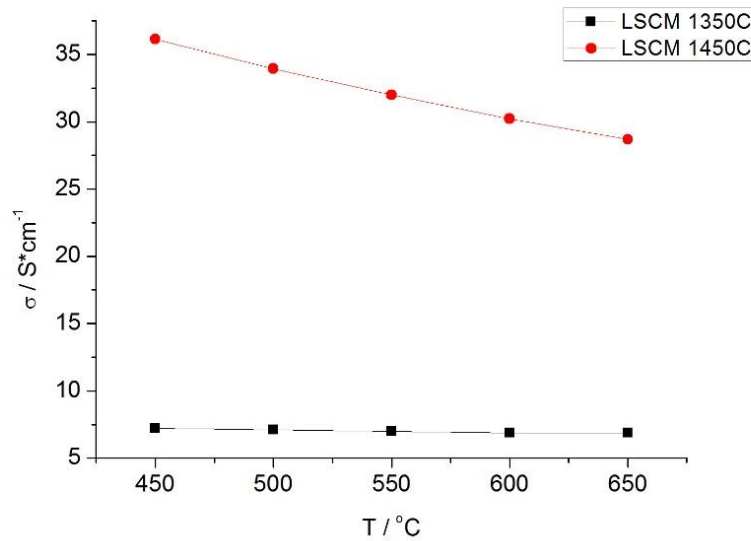


Figure 8.5 Conductivity of LSCM after sintering at 1350°C and 1450°C. Both samples were reduced at 650°C in 10% H₂ / 90% N₂.

At last, some other candidates such as doped BaSnO₃, Sr₂FeSbO₆ and Sr₂ZnMoO₆ were synthesized and the conductivity were measured, but either there is stability is an issue

or the conductivity is not high enough. In order to make anode with these materials, more effort should be taken in the future.

References

- 1 Hui, S. R. *et al.* A brief review of the ionic conductivity enhancement for selected oxide electrolytes. *Journal of Power Sources* **172**, 493-502 (2007).
- 2 Jacobson, A. J. Materials for solid oxide fuel cells†. *Chemistry of Materials* **22**, 660-674 (2009).
- 3 Bi, L., Fabbri, E. & Traversa, E. Effect of anode functional layer on the performance of proton-conducting solid oxide fuel cells (SOFCs). *Electrochemistry Communications* **16**, 37-40 (2012).
- 4 Ni Modellanoden, D.-I. H. S.
- 5 Koide, H., Someya, Y., Yoshida, T. & Maruyama, T. Properties of Ni/YSZ cermet as anode for SOFC. *Solid State Ionics* **132**, 253-260 (2000).
- 6 Müller, A. *Mehrschicht-Anode für die Hochtemperatur-Brennstoffzelle (SOFC)*, Karlsruhe, Univ., Diss., 2004, (2004).
- 7 Chen, K. *et al.* Performance of an anode-supported SOFC with anode functional layers. *Electrochimica Acta* **53**, 7825-7830 (2008).
- 8 Li, C.-X., Li, C.-J. & Guo, L.-J. Effect of composition of NiO/YSZ anode on the polarization characteristics of SOFC fabricated by atmospheric plasma spraying. *international journal of hydrogen energy* **35**, 2964-2969 (2010).
- 9 Mukhopadhyay, M., Mukhopadhyay, J., Sharma, A. D. & Basu, R. N. In-situ patterned intra-anode triple phase boundary in SOFC electroless anode: An enhancement of electrochemical performance. *international journal of hydrogen energy* **36**, 7677-7682 (2011).
- 10 Faes, A., Hessler-Wyser, A. & Zryd, A. A review of redox cycling of solid oxide fuel cells anode. *Membranes* **2**, 585-664 (2012).
- 11 Ringuede, A., Bronine, D. & Frade, J. Ni_{1-x}Co_x/YSZ cermet anodes for solid oxide fuel cells. *Electrochimica acta* **48**, 437-442 (2002).
- 12 Moon, H., Kim, S. D., Park, E. W., Hyun, S. H. & Kim, H. S. Characteristics of SOFC single cells with anode active layer via tape casting and co-firing. *International Journal of Hydrogen Energy* **33**, 2826-2833 (2008).
- 13 Virkar, A. V., Chen, J., Tanner, C. W. & Kim, J.-W. The role of electrode microstructure on activation and concentration polarizations in solid oxide fuel cells. *Solid State Ionics* **131**, 189-198 (2000).
- 14 Lee, K. T., Vito, N. J. & Wachsman, E. D. Comprehensive quantification of Ni-Gd_{0.1}Ce_{0.9}O_{1.95} anode functional layer microstructures by three-dimensional reconstruction using a FIB/SEM dual beam system. *Journal of Power Sources* **228**, 220-228 (2013).
- 15 Koh, J.-H., Yoo, Y.-S., Park, J.-W. & Lim, H. C. Carbon deposition and cell performance of Ni-YSZ anode support SOFC with methane fuel. *Solid State Ionics* **149**, 157-166 (2002).
- 16 Kim, T. *et al.* A study of carbon formation and prevention in hydrocarbon-fueled SOFC. *Journal of Power Sources* **155**, 231-238 (2006).
- 17 Maček, J., Novosel, B. & Marinšek, M. Ni-YSZ SOFC anodes—minimization of carbon deposition. *Journal of the European Ceramic Society* **27**, 487-491 (2007).

- 18 Alzate-Restrepo, V. & Hill, J. M. Carbon deposition on Ni/YSZ anodes exposed to CO/H₂ feeds. *Journal of Power Sources* **195**, 1344-1351 (2010).
- 19 Lorente, E., Millan, M. & Brandon, N. Use of gasification syngas in SOFC: Impact of real tar on anode materials. *international journal of hydrogen energy* **37**, 7271-7278 (2012).
- 20 Matsuzaki, Y. & Yasuda, I. The poisoning effect of sulfur-containing impurity gas on a SOFC anode: Part I. Dependence on temperature, time, and impurity concentration. *Solid State Ionics* **132**, 261-269 (2000).
- 21 Cheng, Z. & Liu, M. Characterization of sulfur poisoning of Ni-YSZ anodes for solid oxide fuel cells using in situ Raman microspectroscopy. *Solid State Ionics* **178**, 925-935 (2007).
- 22 Clark, J. O. E. *Physics Matters!*, Vol. 9 (Grolier Academic Reference, 2001).
- 23 Sunarso, J. *et al.* Mixed ionic-electronic conducting (MIEC) ceramic-based membranes for oxygen separation. *Journal of Membrane Science* **320**, 13-41 (2008).
- 24 Yamamoto, O., Takeda, Y., Kanno, R. & Noda, M. Perovskite-type oxides as oxygen electrodes for high temperature oxide fuel cells. *Solid State Ionics* **22**, 241-246 (1987).
- 25 Kenjo, T. & Nishiya, M. LaMnO₃ air cathodes containing ZrO₂ electrolyte for high temperature solid oxide fuel cells. *Solid State Ionics* **57**, 295-302 (1992).
- 26 Jiang, S. A comparison of O₂ reduction reactions on porous (La, Sr) MnO₃ and (La, Sr)(Co, Fe) O₃ electrodes. *Solid State Ionics* **146**, 1-22 (2002).
- 27 Teraoka, Y., Nobunaga, T., Okamoto, K., Miura, N. & Yamazoe, N. Influence of constituent metal cations in substituted LaCoO₃ on mixed conductivity and oxygen permeability. *Solid State Ionics* **48**, 207-212 (1991).
- 28 Tai, L.-W., Nasrallah, M., Anderson, H., Sparlin, D. & Sehlin, S. Structure and electrical properties of La_{1-x}Sr_xCo_{1-y}Fe_yO₃. Part 1. The system La_{0.8}Sr_{0.2}Co_{1-y}Fe_yO₃. *Solid State Ionics* **76**, 259-271 (1995).
- 29 Tai, L.-W., Nasrallah, M., Anderson, H., Sparlin, D. & Sehlin, S. Structure and electrical properties of La_{1-x}Sr_xCo_{1-y}Fe_yO₃. Part 2. The system La_{1-x}Sr_xCo_{0.2}Fe_{0.8}O₃. *Solid State Ionics* **76**, 273-283 (1995).
- 30 Petric, A., Huang, P. & Tietz, F. Evaluation of La-Sr-Co-Fe-O perovskites for solid oxide fuel cells and gas separation membranes. *Solid State Ionics* **135**, 719-725 (2000).
- 31 Piao, J. *et al.* Preparation and characterization of Pr_{1-x}Sr_xFeO₃ cathode material for intermediate temperature solid oxide fuel cells. *Journal of Power Sources* **172**, 633-640 (2007).
- 32 Katsura, T., Sato, K. & Ito, E. Electrical conductivity of silicate perovskite at lower-mantle conditions. *Nature* **395**, 493-495 (1998).
- 33 Patrakeevev, M. *et al.* Electron/hole and ion transport in La_{1-x}Sr_xFeO_{3-δ}. *Journal of solid state chemistry* **172**, 219-231 (2003).
- 34 Pyatiletova, E., Nemudry, A. & Lyakhov, N. Synthesis and properties of Sr_{1-x}M_xCo_{0.8-y}Al_yFe_{0.2O3-z} perovskite-like oxides. *Inorganic Materials* **43**, 1134-1141 (2007).

- 35 Ishihara, T., Fukui, S., Enoki, M. & Matsumoto, H. Oxide anode derived from Sr-doped LaMnO₃ perovskite oxide for SOFCs using LaGaO₃ electrolyte. *Journal of The Electrochemical Society* **153**, A2085-A2090 (2006).
- 36 Ding, X., Liu, Y., Gao, L. & Guo, L. Synthesis and characterization of doped LaCrO₃ perovskite prepared by EDTA–citrate complexing method. *Journal of Alloys and Compounds* **458**, 346-350 (2008).
- 37 Jiang, S. P. *et al.* Electrical conductivity and performance of doped LaCrO₃ perovskite oxides for solid oxide fuel cells. *Journal of Power Sources* **176**, 82-89 (2008).
- 38 Horita, T. in *Perovskite Oxide for Solid Oxide Fuel Cells* 285-296 (Springer, 2009).
- 39 Atkinson, A. *et al.* Advanced anodes for high-temperature fuel cells. *Nature materials* **3**, 17-27 (2004).
- 40 Fu, Q. & Tietz, F. Ceramic - Based Anode Materials for Improved Redox Cycling of Solid Oxide Fuel Cells. *Fuel Cells* **8**, 283-293 (2008).
- 41 Graves, C., Sudireddy, B. R. & Mogensen, M. Molybdate based ceramic negative-electrode materials for solid oxide cells. *ECS Transactions* **28**, 173-192 (2010).
- 42 Zhou, X., Yan, N., Chuang, K. T. & Luo, J. Progress in La-doped SrTiO₃ (LST)-based anode materials for solid oxide fuel cells. *Rsc Advances* **4**, 118-131 (2014).
- 43 Slater, P. R., Fagg, D. P. & Irvine, J. T. Synthesis and electrical characterisation of doped perovskite titanates as potential anode materials for solid oxide fuel cells. *Journal of Materials Chemistry* **7**, 2495-2498 (1997).
- 44 Hussain, A. M., Høgh, J. V., Jacobsen, T. & Bonanos, N. Nickel-ceria infiltrated Nb-doped SrTiO₃ for low temperature SOFC anodes and analysis on gas diffusion impedance. *international journal of hydrogen energy* **37**, 4309-4318 (2012).
- 45 Hussain, A. M., Høgh, J. V., Zhang, W. & Bonanos, N. Efficient ceramic anodes infiltrated with binary and ternary electrocatalysts for SOFCs operating at low temperatures. *Journal of Power Sources* **216**, 308-313 (2012).
- 46 Hussain, A. M. *et al.* Improved ceramic anodes for SOFCs with modified electrode/electrolyte interface. *Journal of Power Sources* **212**, 247-253 (2012).
- 47 Sonne, M., Van Nong, N., He, Z., Pryds, N. & Linderoth, S. in *8th European Conference on Thermoelectrics*. 175-178.
- 48 Shimonosono, T. *et al.* Electronic conductivity measurement of Sm-and La-doped ceria ceramics by Hebb–Wagner method. *Solid State Ionics* **174**, 27-33 (2004).
- 49 Kwon, T.-H., Lee, T. & Yoo, H.-I. Partial electronic conductivity and electrolytic domain of bilayer electrolyte Zr_{0.84}Y_{0.16}O_{1.92}/Ce_{0.9}Gd_{0.1}O_{1.95}. *Solid State Ionics* **195**, 25-35 (2011).
- 50 Wachsman, E., Jayaweera, P., Jiang, N., Lowe, D. & Pound, B. Stable high conductivity ceria/bismuth oxide bilayered electrolytes. *Journal of the Electrochemical Society* **144**, 233-236 (1997).

- 51 Wachsman, E. D. & Lee, K. T. Lowering the temperature of solid oxide fuel cells. *Science* **334**, 935-939 (2011).
- 52 Jiang, N. & Wachsman, E. D. Structural Stability and Conductivity of Phase - Stabilized Cubic Bismuth Oxides. *Journal of the American Ceramic Society* **82**, 3057-3064 (1999).
- 53 Wachsman, E. D., Boyapati, S. & Jiang, N. Effect of dopant polarizability on oxygen sublattice order in phase-stabilized cubic bismuth oxides. *Ionics* **7**, 1-6 (2001).
- 54 Park, J.-Y. & Wachsman, E. D. Stable and high conductivity ceria/bismuth oxide bilayer electrolytes for lower temperature solid oxide fuel cells. *Ionics* **12**, 15-20 (2006).
- 55 Jiang, N., Wachsman, E. D. & Jung, S.-H. A higher conductivity Bi₂O₃-based electrolyte. *Solid State Ionics* **150**, 347-353 (2002).
- 56 Wachsman, E. D., Jayaweera, P., Lowe, D. M. & Pound, B. G. (Google Patents, 1998).
- 57 Park, J. Y., Yoon, H. & Wachsman, E. D. Fabrication and Characterization of High - Conductivity Bilayer Electrolytes for Intermediate - Temperature Solid Oxide Fuel Cells. *Journal of the American Ceramic Society* **88**, 2402-2408 (2005).
- 58 Jung, D. W., Duncan, K. L. & Wachsman, E. D. Effect of total dopant concentration and dopant ratio on conductivity of (DyO_{1.5})_x-(WO₃)_y-(BiO_{1.5})_{1-x-y}. *Acta Materialia* **58**, 355-363 (2010).
- 59 Yaremchenko, A., Kharton, V., Naumovich, E. & Tonoyan, A. Stability of δ -Bi₂O₃-based solid electrolytes. *Materials research bulletin* **35**, 515-520 (2000).
- 60 Verkerk, M., Keizer, K. & Burggraaf, A. High oxygen ion conduction in sintered oxides of the Bi₂O₃-Er₂O₃ system. *Journal of applied electrochemistry* **10**, 81-90 (1980).
- 61 Verkerk, M. & Burggraaf, A. High oxygen ion conduction in sintered oxides of the Bi₂O₃---Ln₂O₃ system. *Solid State Ionics* **3**, 463-467 (1981).
- 62 Takahashi, T., Esaka, T. & Iwahara, H. Conduction in Bi₂O₃-based oxide ion conductors under low oxygen pressure. I. Current blackening of the Bi₂O₃-Y₂O₃ electrolyte. *Journal of Applied Electrochemistry* **7**, 299-302 (1977).
- 63 Hashimoto, S.-i. *et al.* Oxygen nonstoichiometry and thermo-chemical stability of La_{0.6}Sr_{0.4}Co_{1-y}Fe_yO_{3- δ} (y= 0.2, 0.4, 0.6, 0.8). *Solid State Ionics* **181**, 1713-1719 (2010).
- 64 Lein, H. L., Wiik, K. & Grande, T. Kinetic demixing and decomposition of oxygen permeable membranes. *Solid State Ionics* **177**, 1587-1590 (2006).
- 65 Yasuda, I. & Hishinuma, M. in *Proceedings of the 2nd International Symposium on Ionic and Mixed Conducting Oxide Ceramics, The Electrochemical Society, Pennington, NJ.* 209-221.
- 66 Hui, S. & Petric, A. in *Ionic and Mixed Conducting Ceramics: Proceedings of the... International Symposium.* 67 (The Electrochemical Society).
- 67 Ma, Q., Tietz, F., Sebold, D. & Stöver, D. Y-substituted SrTiO₃-YSZ composites as anode materials for solid oxide fuel cells: Interaction between SYT and YSZ. *Journal of Power Sources* **195**, 1920-1925 (2010).

- 68 Moos, R. & Härdtl, K. H. Electronic transport properties of Sr_{1-x}La_xTiO₃ ceramics. *Journal of applied physics* **80**, 393-400 (1996).
- 69 Hui, S. & Petric, A. Electrical properties of yttrium-doped strontium titanate under reducing conditions. *Journal of The Electrochemical Society* **149**, J1-J10 (2002).
- 70 Savaniu, C. & Irvine, J. La-doped SrTiO₃ as anode material for IT-SOFC. *Solid State Ionics* **192**, 491-493 (2011).
- 71 Park, B.-K. *et al.* La-doped SrTiO₃ interconnect materials for anode-supported flat-tubular solid oxide fuel cells. *international journal of hydrogen energy* **37**, 4319-4327 (2012).
- 72 Huang, Y.-H., Dass, R. I., Denyszyn, J. C. & Goodenough, J. B. Synthesis and characterization of Sr₂MgMoO_{6-δ} as an anode material for the solid oxide fuel cell. *Journal of The Electrochemical Society* **153**, A1266-A1272 (2006).
- 73 Huang, Y.-H., Dass, R. I., Xing, Z.-L. & Goodenough, J. B. Double perovskites as anode materials for solid-oxide fuel cells. *Science* **312**, 254-257 (2006).
- 74 Wei, T., Ji, Y., Meng, X. & Zhang, Y. Sr₂NiMoO_{6-δ} as anode material for LaGaO₃-based solid oxide fuel cell. *Electrochemistry Communications* **10**, 1369-1372 (2008).
- 75 Huang, Y.-H. *et al.* Double-perovskite anode materials Sr₂MMoO₆ (M= Co, Ni) for solid oxide fuel cells. *Chemistry of Materials* **21**, 2319-2326 (2009).
- 76 Markov, A. *et al.* Structural features, nonstoichiometry and high-temperature transport in SrFe_{1-x}Mo_xO_{3-δ}. *Journal of Solid State Chemistry* **182**, 799-806 (2009).
- 77 Zhang, L., Zhou, Q., He, Q. & He, T. Double-perovskites A₂FeMoO_{6-δ} (A= Ca, Sr, Ba) as anodes for solid oxide fuel cells. *Journal of Power Sources* **195**, 6356-6366 (2010).
- 78 Muñoz-García, A. B., Pavone, M. & Carter, E. A. Effect of antisite defects on the formation of oxygen vacancies in Sr₂FeMoO₆: Implications for ion and electron transport. *Chemistry of Materials* **23**, 4525-4536 (2011).
- 79 Zhang, P., Huang, Y.-H., Cheng, J.-G., Mao, Z.-Q. & Goodenough, J. B. Sr₂CoMoO₆ anode for solid oxide fuel cell running on H₂ and CH₄ fuels. *Journal of Power Sources* **196**, 1738-1743 (2011).
- 80 Martinez-Coronado, R., Alonso, J., Aguadero, A. & Fernández-Díaz, M. Optimized energy conversion efficiency in solid-oxide fuel cells implementing SrMo_{1-x}Fe_xO_{3-δ} perovskites as anodes. *Journal of Power Sources* **208**, 153-158 (2012).
- 81 Zhang, Q., Wei, T. & Huang, Y.-H. Electrochemical performance of double-perovskite Ba₂MMoO₆ (M= Fe, Co, Mn, Ni) anode materials for solid oxide fuel cells. *Journal of Power Sources* **198**, 59-65 (2012).
- 82 Cooper, M., Channa, K., De Silva, R. & Bayless, D. J. Comparison of LSV/YSZ and LSV/GDC SOFC anode performance in coal syngas containing H₂S. *Journal of the Electrochemical Society* **157**, B1713-B1718 (2010).
- 83 Vo, N. M. & Gross, M. D. The Effect of Vanadium Deficiency on the Stability of Pd and Pt Catalysts in Lanthanum Strontium Vanadate Solid

- Oxide Fuel Cell Anodes. *Journal of The Electrochemical Society* **159**, B641-B646 (2012).
- 84 刘张波, 刘蓓蓓 & 夏长荣. 镧掺杂的锡酸锶作为固体氧化物燃料电池阳极材料的初步研究. (2013).
- 85 Gil, V., Moure, C., Durán, P. & Tartaj, J. Low-temperature densification and grain growth of Bi₂O₃-doped-ceria gadolinia ceramics. *Solid State Ionics* **178**, 359-365 (2007).
- 86 Gil, V., Tartaj, J., Moure, C. & Duran, P. Effect of Bi₂O₃ addition on the sintering and microstructural development of gadolinia-doped ceria ceramics. *Journal of the European Ceramic Society* **27**, 801-805 (2007).
- 87 Fagg, D. P., Kharton, V. V. & Frade, J. R. P-type electronic transport in Ce_{0.8}Gd_{0.2}O_{2-δ}: the effect of transition metal oxide sintering aids. *Journal of electroceramics* **9**, 199-207 (2002).
- 88 Jud, E. & Gauckler, L. J. The effect of cobalt oxide addition on the conductivity of Ce_{0.9}Gd_{0.1}O_{1.95}. *Journal of electroceramics* **15**, 159-166 (2005).
- 89 Mori, M., Suda, E., Pacaud, B., Murai, K. & Moriga, T. Effect of components in electrodes on sintering characteristics of Ce_{0.9}Gd_{0.1}O_{1.95} electrolyte in intermediate-temperature solid oxide fuel cells during fabrication. *Journal of power sources* **157**, 688-694 (2006).
- 90 Dean, J. A. (McGraw-Hill).
- 91 Kolodiazhnyi, T. & Petric, A. The Applicability of Sr-deficient n-type SrTiO₃ for SOFC Anodes. *Journal of electroceramics* **15**, 5-11 (2005).
- 92 Dasgupta, R., Roy, S. & Tarafdar, S. Correlation between porosity, conductivity and permeability of sedimentary rocks—a ballistic deposition model. *Physica A: Statistical Mechanics and its Applications* **275**, 22-32 (2000).
- 93 Simwonis, D., Thülen, H., Dias, F., Naoumidis, A. & Stöver, D. Properties of Ni/YSZ porous cermets for SOFC anode substrates prepared by tape casting and coat-mix® process. *Journal of Materials Processing Technology* **92**, 107-111 (1999).
- 94 Pratihari, S. K., Dassharma, A. & Maiti, H. S. Processing microstructure property correlation of porous Ni-YSZ cermets anode for SOFC application. *Materials research bulletin* **40**, 1936-1944 (2005).
- 95 Mizusaki, J. *et al.* Simple mathematical model for the electrical conductivity of highly porous ceramics. *Journal of the American Ceramic Society* **79**, 109-113 (1996).
- 96 Childs, N. B. *Sr (2-X) VMoO (6-Y) double perovskites: A new generation of Solid Oxide Fuel Cell anodes.* (2013).
- 97 Oka, D., Hirose, Y., Nakao, S., Fukumura, T. & Hasegawa, T. Intrinsic high electrical conductivity of stoichiometric SrNbO₃ epitaxial thin films. *Physical Review B* **92**, 205102 (2015).
- 98 Moyer, J. A., Eaton, C. & Engel - Herbert, R. Highly conductive SrVO₃ as a bottom electrode for functional perovskite oxides. *Advanced Materials* **25**, 3578-3582 (2013).

- 99 Stein, K. *et al.* The Oxidation of Hydrocarbons on Simple Oxide Catalysts. *Journal of the Air Pollution Control Association* **10**, 275-281 (1960).
- 100 Pillai, U. R. & Sahle-Demessie, E. Vanadium phosphorus oxide as an efficient catalyst for hydrocarbon oxidations using hydrogen peroxide. *New Journal of chemistry* **27**, 525-528 (2003).
- 101 Adijanto, L., Küngas, R., Park, J., Vohs, J. M. & Gorte, R. J. SOFC anodes based on infiltration of tungsten bronzes. *International Journal of Hydrogen Energy* **36**, 15722-15730 (2011).
- 102 Tan, W. & Zhong, Q. in *5th European Fuel Cell Piero Lunghi Conference and Exhibition, EFC 2013; Rome; Italy*. 195-196.
- 103 Xie, Z. *et al.* Effects of Co doping on the electrochemical performance of double perovskite oxide Sr₂MgMoO_{6-δ} as an anode material for solid oxide fuel cells. *The Journal of Physical Chemistry C* **116**, 9734-9743 (2012).
- 104 Bi, Z. & Zhu, J. Effect of Current Collecting Materials on the Performance of the Double-Perovskite Sr₂MgMoO_{6-δ} Anode. *Journal of The Electrochemical Society* **158**, B605-B613 (2011).
- 105 Marrero-López, D., Peña-Martínez, J., Ruiz-Morales, J., Martín-Sedeño, M. & Nunez, P. High temperature phase transition in SOFC anodes based on Sr₂MgMoO_{6-δ}. *Journal of Solid State Chemistry* **182**, 1027-1034 (2009).
- 106 Xiao, G., Liu, Q., Nuansaeng, S. & Chen, F. F. Sr₂Fe_{1-x}Mo_{1-x}O_{6-δ} as Anode Materials for Solid Oxide Fuel Cells. *ECS Transactions* **45**, 355-362 (2012).
- 107 Falcon, H., Barbero, J., Alonso, J., Martinez-Lope, M. & Fierro, J. SrFeO_{3-δ} perovskite oxides: chemical features and performance for methane combustion. *Chemistry of materials* **14**, 2325-2333 (2002).
- 108 Viola, M. d. C. *et al.* Induction of colossal magnetoresistance in the double perovskite Sr₂CoMoO₆. *Chemistry of materials* **14**, 812-818 (2002).
- 109 Gagulin, V., Korchagina, S., Ivanova, V. & Shevchuk, Y. A. Synthesis and properties of Sr₂CoMoO₆ and Sr₂NiMoO₆. *Inorganic materials* **39**, 625-626 (2003).
- 110 Mineshige, A. *et al.* Introduction of A-site deficiency into La_{0.6}Sr_{0.4}Co_{0.2}Fe_{0.8}O_{3-δ} and its effect on structure and conductivity. *Solid State Ionics* **176**, 1145-1149 (2005).
- 111 Xiao, P. *et al.* H₂ and CH₄ oxidation on Gd_{0.2}Ce_{0.8}O_{1.9} infiltrated SrMoO₃-yttria-stabilized zirconia anode for solid oxide fuel cells. *international journal of hydrogen energy* **37**, 18349-18356 (2012).
- 112 Kawanishi, H., Hirano, A., Imanishi, N. & Takeda, Y. in *Meeting Abstracts*. 251-251 (The Electrochemical Society).
- 113 dos Santos-Gómez, L., Leon-Reina, L., Porras-Vazquez, J., Losilla, E. & Marrero-López, D. Chemical stability and compatibility of double perovskite anode materials for SOFCs. *Solid State Ionics* **239**, 1-7 (2013).
- 114 He, B. *et al.* Ti-doped molybdenum-based perovskites as anodes for solid oxide fuel cells. *Journal of Power Sources* **241**, 627-633 (2013).
- 115 Gore, C. M., Lee, K. T., Yoon, H. S. & Wachsman, E. D. Porous GDC Scaffold Anodes for Lower Temperature, Hydrocarbon-Fueled Solid Oxide Fuel Cells. *ECS Transactions* **50**, 53-62 (2013).

- 116 Shishkin, M. & Ziegler, T. Ab Initio Study of Activity and Coke-Tolerance of Ni/CeZrO₂ Anodes of SOFC as a Function of Zirconia Concentration. *ECS Transactions* **35**, 1611-1619 (2011).
- 117 Zheng, L. L., Wang, X., Zhang, L., Wang, J.-Y. & Jiang, S. P. Effect of Pd-impregnation on performance, sulfur poisoning and tolerance of Ni/GDC anode of solid oxide fuel cells. *international journal of hydrogen energy* **37**, 10299-10310 (2012).
- 118 Chan, S., Khor, K. & Xia, Z. A complete polarization model of a solid oxide fuel cell and its sensitivity to the change of cell component thickness. *Journal of Power Sources* **93**, 130-140 (2001).
- 119 Ni, M., Leung, M. K. & Leung, D. Y. Parametric study of solid oxide fuel cell performance. *Energy Conversion and Management* **48**, 1525-1535 (2007).
- 120 Adler, S. B. Chemical expansivity of electrochemical ceramics. *Journal of the American Ceramic Society* **84**, 2117-2119 (2001).
- 121 Hashimoto, S.-i. *et al.* Thermal and chemical lattice expansibility of La_{0.6}Sr_{0.4}Co_{1-y}Fe_yO_{3-δ} (y= 0.2, 0.4, 0.6 and 0.8). *Solid State Ionics* **186**, 37-43 (2011).
- 122 Mongkolkachit, C. & Wanakitti, S. Characterization of (La, Sr)(Co, Fe)O_{3-δ} Ferrite-Based Cathodes for Intermediate-Temperature SOFCs. *Journal of Metals, Materials and Minerals* **18**, 33-36 (2008).
- 123 Jung, H. *et al.* Effect of cathode current-collecting layer on unit-cell performance of anode-supported solid oxide fuel cells. *Journal of Power Sources* **155**, 145-151 (2006).
- 124 Corbel, G., Mestiri, S. & Lacorre, P. Physicochemical compatibility of CGO fluorite, LSM and LSCF perovskite electrode materials with La₂Mo₂O₉ fast oxide-ion conductor. *Solid state sciences* **7**, 1216-1224 (2005).
- 125 Zhao, F., Peng, R. & Xia, C. LSC-based electrode with high durability for IT-SOFCs. *Fuel Cells Bulletin* **2008**, 12-16 (2008).
- 126 Garbayo, I. *et al.* Porous La_{0.6}Sr_{0.4}CoO_{3-δ} thin film cathodes for large area micro solid oxide fuel cell power generators. *Journal of Power Sources* **248**, 1042-1049 (2014).
- 127 Liu, Z., Han, M.-F. & Miao, W.-T. Preparation and characterization of graded cathode La_{0.6}Sr_{0.4}Co_{0.2}Fe_{0.8}O_{3-δ}. *Journal of Power Sources* **173**, 837-841 (2007).
- 128 Zhao, F., Peng, R. & Xia, C. A La_{0.6}Sr_{0.4}CoO_{3-δ}-based electrode with high durability for intermediate temperature solid oxide fuel cells. *Materials Research Bulletin* **43**, 370-376 (2008).
- 129 Lü, S. *et al.* SmBaCoCuO_{5+x} as cathode material based on GDC electrolyte for intermediate-temperature solid oxide fuel cells. *Journal of Alloys and Compounds* **509**, 2824-2828 (2011).
- 130 Ahmed, B. *et al.* Development of Novel LSM/GDC Composite Cathode Material for Cathode-Supported Direct Carbon Fuel Cells. *ECS Transactions* **57**, 2075-2082 (2013).
- 131 Han, M.-F., Zhou, S., Liu, Z., Lei, Z. & Kang, Z.-C. Fabrication, sintering and electrical properties of cobalt oxide doped Gd_{0.1}Ce_{0.9}O_{2-δ}. *Solid State Ionics* **192**, 181-184 (2011).

- 132 Zhang, X. *et al.* A study on sintering aids for Sm_{0.2}Ce_{0.8}O_{1.9} electrolyte. *Journal of Power Sources* **162**, 480-485 (2006).
- 133 Wachsman, E. Functionally gradient bilayer oxide membranes and electrolytes. *Solid State Ionics* **152**, 657-662 (2002).
- 134 Ahn, J. S. *et al.* High-performance bilayered electrolyte intermediate temperature solid oxide fuel cells. *Electrochemistry Communications* **11**, 1504-1507 (2009).
- 135 Lee, K. T. *et al.* Gd_{0.1}Ce_{0.9}O_{1.95}/Er_{0.4}Bi_{1.6}O₃ bilayered electrolytes fabricated by a simple colloidal route using nano-sized Er_{0.4}Bi_{1.6}O₃ powders for high performance low temperature solid oxide fuel cells. *Journal of Power Sources* **205**, 122-128 (2012).
- 136 Trofimenko, N. & Ullmann, H. Co-doped LSGM: composition–structure–conductivity relations. *Solid State Ionics* **124**, 263-270 (1999).
- 137 Khorkounov, B., Näfe, H. & Aldinger, F. Relationship between the ionic and electronic partial conductivities of co-doped LSGM ceramics from oxygen partial pressure dependence of the total conductivity. *Journal of Solid State Electrochemistry* **10**, 479-487 (2006).
- 138 Boyapati, S., Wachsman, E. D. & Chakoumakos, B. C. Neutron diffraction study of occupancy and positional order of oxygen ions in phase stabilized cubic bismuth oxides. *Solid State Ionics* **138**, 293-304 (2001).
- 139 Jung, D. W., Duncan, K. & Wachsman, E. in *Meeting Abstracts*. 1049-1049 (The Electrochemical Society).
- 140 Wachsman, E. D. Effect of oxygen sublattice order on conductivity in highly defective fluorite oxides. *Journal of the European Ceramic Society* **24**, 1281-1285 (2004).
- 141 Wachsman, E. D. & Duncan, K. L. *Stable High Conductivity Bilayered Electrolytes for Low Temperature Solid Oxide Fuel Cells*. (University of Florida Department of Materials Science and Engineering, 2004).
- 142 Fagg, D. *et al.* The effect of cobalt oxide sintering aid on electronic transport in Ce_{0.80}Gd_{0.20}O_{2-δ} electrolyte. *Electrochimica Acta* **48**, 1023-1029 (2003).
- 143 Xia, C. & Liu, M. Microstructures, conductivities, and electrochemical properties of Ce_{0.9}Gd_{0.1}O₂ and GDC–Ni anodes for low-temperature SOFCs. *Solid State Ionics* **152**, 423-430 (2002).
- 144 Xia, C. & Liu, M. Novel cathodes for low-temperature solid oxide fuel cells. *Advanced Materials* **14**, 521 (2002).
- 145 Chang, C.-L., Hsu, C.-S., Huang, J.-B., Hsu, P.-H. & Hwang, B.-H. Preparation and characterization of SOFC cathodes made of SSC nanofibers. *Journal of Alloys and Compounds* **620**, 233-239 (2015).
- 146 Gao, Z., Liu, X., Bergman, B. & Zhao, Z. Investigation of oxygen reduction reaction kinetics on Sm_{0.5}Sr_{0.5}CoO_{3-δ} cathode supported on Ce_{0.85}Sm_{0.075}Nd_{0.075}O_{2-δ} electrolyte. *Journal of Power Sources* **196**, 9195-9203 (2011).
- 147 Yan, A., Maragou, V., Arico, A., Cheng, M. & Tsiakaras, P. Investigation of a Ba_{0.5}Sr_{0.5}Co_{0.8}Fe_{0.2}O_{3-δ} based cathode SOFC: II. The effect of

- CO₂ on the chemical stability. *Applied Catalysis B: Environmental* **76**, 320-327 (2007).
- 148 Arnold, M., Gesing, T. M., Martynczuk, J. & Feldhoff, A. Correlation of the formation and the decomposition process of the BSCF perovskite at intermediate temperatures. *Chemistry of Materials* **20**, 5851-5858 (2008).
- 149 Švarcová, S., Wiik, K., Tolchard, J., Bouwmeester, H. J. & Grande, T. Structural instability of cubic perovskite Ba_x Sr_{1-x} Co_{1-y} Fe_y O_{3-δ}. *Solid State Ionics* **178**, 1787-1791 (2008).
- 150 Sun, C., Hui, R. & Roller, J. Cathode materials for solid oxide fuel cells: a review. *J Solid State Electrochem* **14**, 1125-1144 (2009).
- 151 Jiang, S. P. Development of lanthanum strontium manganite perovskite cathode materials of solid oxide fuel cells: a review. *Journal of Materials Science* **43**, 6799-6833 (2008).
- 152 Adler, S. B. Factors governing oxygen reduction in solid oxide fuel cell cathodes. *Chemical reviews* **104**, 4791-4844 (2004).
- 153 Fleig, J. Solid oxide fuel cell cathodes: Polarization mechanisms and modeling of the electrochemical performance. *Annual Review of Materials Research* **33**, 361-382 (2003).
- 154 Richter, J., Holtappels, P., Graule, T., Nakamura, T. & Gauckler, L. J. Materials design for perovskite SOFC cathodes. *Monatshefte für Chemie-Chemical Monthly* **140**, 985-999 (2009).
- 155 Choi, Y., Mebane, D. S., Lin, M. & Liu, M. Oxygen reduction on LaMnO₃-based cathode materials in solid oxide fuel cells. *Chemistry of Materials* **19**, 1690-1699 (2007).
- 156 Liu, M., Lynch, M. E., Blinn, K., Alamgir, F. M. & Choi, Y. Rational SOFC material design: new advances and tools. *Materials today* **14**, 534-546 (2011).
- 157 Yamaguchi, T., Galloway, K. V., Yoon, J. & Sammes, N. M. Electrochemical characterizations of microtubular solid oxide fuel cells under a long-term testing at intermediate temperature operation. *Journal of Power Sources* **196**, 2627-2630 (2011).
- 158 Liu, M. *et al.* Enhanced performance of LSCF cathode through surface modification. *international journal of hydrogen energy* **37**, 8613-8620 (2012).
- 159 Charpentier, P., Fragnaud, P., Schleich, D. & Gehain, E. Preparation of thin film SOFCs working at reduced temperature. *Solid State Ionics* **135**, 373-380 (2000).
- 160 Jung, H. *et al.* Fabrication and performance evaluation of 3-cell SOFC stack based on planar 10cm× 10cm anode-supported cells. *Journal of power sources* **159**, 478-483 (2006).
- 161 Xia, C., Rauch, W., Chen, F. & Liu, M. Sm_{0.5} Sr_{0.5} CoO₃ cathodes for low-temperature SOFCs. *Solid State Ionics* **149**, 11-19 (2002).
- 162 Tao, Y., Shao, J., Wang, J. & Wang, W. G. Synthesis and properties of La_{0.6} Sr_{0.4} CoO_{3-δ} nanopowder. *Journal of Power Sources* **185**, 609-614 (2008).
- 163 Horita, T. *et al.* Oxygen reduction mechanism at porous La_{1-x} Sr_x CoO_{3-δ} cathodes/La_{0.8} Sr_{0.2} Ga_{0.8} Mg_{0.2} O_{2.8} electrolyte interface for solid oxide fuel cells. *Electrochimica Acta* **46**, 1837-1845 (2001).

- 164 Liu, Y., Zha, S. & Liu, M. Nanocomposite electrodes fabricated by a particle-solution spraying process for low-temperature SOFCs. *Chemistry of materials* **16**, 3502-3506 (2004).
- 165 Xia, C. & Liu, M. Low-temperature SOFCs based on Gd_{0.1}Ce_{0.9}O_{1.95} fabricated by dry pressing. *Solid State Ionics* **144**, 249-255 (2001).
- 166 Shao, Z. & Haile, S. M. A high-performance cathode for the next generation of solid-oxide fuel cells. *Nature* **431**, 170-173 (2004).
- 167 Zhou, W., Ran, R. & Shao, Z. Progress in understanding and development of Ba_{0.5}Sr_{0.5}Co_{0.8}Fe_{0.2}O_{3-δ}-based cathodes for intermediate-temperature solid-oxide fuel cells: a review. *Journal of Power Sources* **192**, 231-246 (2009).
- 168 Liu, Q., Khor, K. A. & Chan, S. High-performance low-temperature solid oxide fuel cell with novel BSCF cathode. *Journal of Power Sources* **161**, 123-128 (2006).
- 169 Zhao, Z. *et al.* Carbonates formed during BSCF preparation and their effects on performance of SOFCs with BSCF cathode. *international journal of hydrogen energy* **37**, 19036-19044 (2012).
- 170 Bucher, E., Egger, A., Caraman, G. & Sitte, W. Stability of the SOFC cathode material (Ba, Sr)(Co, Fe)O_{3-δ} in CO₂-containing atmospheres. *Journal of The Electrochemical Society* **155**, B1218-B1224 (2008).
- 171 Kuklja, M. M., Mastrikov, Y. A., Jansang, B. & Kotomin, E. A. The Intrinsic Defects, Disorder, and Structural Stability of Ba_xSr_{1-x}Co_yFe_{1-y}O_{3-δ} Perovskite Solid Solutions. *The Journal of Physical Chemistry C* **116**, 18605-18611 (2012).
- 172 Choi, S. *et al.* Highly efficient and robust cathode materials for low-temperature solid oxide fuel cells: PrBa_{0.5}Sr_{0.5}Co_{2-x}Fe_xO₅₊ [dgr]. *Scientific reports* **3** (2013).
- 173 Zhao, E. *et al.* Stability of nanorod-structured La_{0.8}Sr_{0.2}Co_{0.2}Fe_{0.8}O_{3-δ}-Gd_{0.2}Ce_{0.8}O_{1.9} composite cathodes for intermediate temperature solid oxide fuel cells. *Ceramics International* **40**, 14891-14898 (2014).
- 174 Choi, J., Kim, B. & Shin, D. Performance evaluation of Sm_{0.5}Sr_{0.5}CoO_{3-δ} fibers with embedded Sm_{0.2}Ce_{0.8}O_{1.9} particles as a solid oxide fuel cell composite cathode. *Journal of the European Ceramic Society* **33**, 2269-2273 (2013).
- 175 Lee, J. G., Park, J. H. & Shul, Y. G. Tailoring gadolinium-doped ceria-based solid oxide fuel cells to achieve 2 W cm⁻² at 550 C. *Nature communications* **5** (2014).
- 176 Wang, S., Lu, X. & Liu, M. Electrocatalytic properties of La_{0.9}Sr_{0.1}MnO₃-based electrodes for oxygen reduction. *Journal of Solid State Electrochemistry* **6**, 384-390 (2002).
- 177 Lee, K. T., Lidie, A. A., Yoon, H. S. & Wachsman, E. D. Rational Design of Lower - Temperature Solid Oxide Fuel Cell Cathodes via Nanotailoring of Co - Assembled Composite Structures. *Angewandte Chemie* **126**, 13681-13685 (2014).

- 178 Yan, R., Chu, F., Ma, Q., Liu, X. & Meng, G. Sintering kinetics of samarium doped ceria with addition of cobalt oxide. *Materials Letters* **60**, 3605-3609 (2006).
- 179 Shin, S., Huang, H., Ishigame, M. & Iwahara, H. Protonic conduction in the single crystals of SrZrO₃ and SrCeO₃ doped with Y₂O₃. *Solid State Ionics* **40**, 910-913 (1990).
- 180 Sata, N. *et al.* Fabrication of proton conducting thin films of SrZrO₃ and SrCeO₃ and their fundamental characterization. *Solid State Ionics* **97**, 437-441 (1997).
- 181 Katahira, K., Kohchi, Y., Shimura, T. & Iwahara, H. Protonic conduction in Zr-substituted BaCeO₃. *Solid State Ionics* **138**, 91-98 (2000).
- 182 Ranran, P., Yan, W., Lizhai, Y. & Zongqiang, M. Electrochemical properties of intermediate-temperature SOFCs based on proton conducting Sm-doped BaCeO₃ electrolyte thin film. *Solid State Ionics* **177**, 389-393 (2006).
- 183 Giannici, F. *et al.* Long-range and short-range structure of proton-conducting Y: BaZrO₃. *Chemistry of Materials* **23**, 2994-3002 (2011).
- 184 Kreuer, K. Proton-conducting oxides. *Annual Review of Materials Research* **33**, 333-359 (2003).
- 185 Bhide, S. V. & Virkar, A. V. Stability of BaCeO₃ - Based Proton Conductors in Water - Containing Atmospheres. *Journal of The Electrochemical Society* **146**, 2038-2044 (1999).
- 186 Tanner, C. W. & Virkar, A. V. Instability of BaCeO₃ in H₂O - Containing Atmospheres. *Journal of The Electrochemical Society* **143**, 1386-1389 (1996).
- 187 Park, J.-S., Lee, J.-H., Lee, H.-W. & Kim, B.-K. Low temperature sintering of BaZrO₃-based proton conductors for intermediate temperature solid oxide fuel cells. *Solid State Ionics* **181**, 163-167 (2010).
- 188 Tao, S. & Irvine, J. T. Conductivity studies of dense yttrium-doped BaZrO₃ sintered at 1325 C. *Journal of Solid State Chemistry* **180**, 3493-3503 (2007).
- 189 Wang, H., Peng, R., Wu, X., Hu, J. & Xia, C. Sintering Behavior and Conductivity Study of Yttrium - Doped BaCeO₃ - BaZrO₃ Solid Solutions Using ZnO Additives. *Journal of the American Ceramic Society* **92**, 2623-2629 (2009).
- 190 Azad, A.-M., Subramaniam, S. & Dung, T. W. On the development of high density barium metazirconate (BaZrO₃) ceramics. *Journal of alloys and compounds* **334**, 118-130 (2002).
- 191 Kreuer, K. On the complexity of proton conduction phenomena. *Solid state ionics* **136**, 149-160 (2000).
- 192 Matsushita, E. Tunneling mechanism on proton conduction in perovskite oxides. *Solid State Ionics* **145**, 445-450 (2001).
- 193 Song, S.-J., Wachsmann, E., Rhodes, J., Dorris, S. & Balachandran, U. Hydrogen permeability of SrCe_{1-x}M_xO_{3-δ} (x= 0.05, M= Eu, Sm). *Solid State Ionics* **167**, 99-105 (2004).
- 194 Li, J., Yoon, H., Oh, T.-K. & Wachsmann, E. D. High temperature SrCe_{0.9}Eu_{0.1}O_{3-δ} proton conducting membrane reactor for H₂ production using the water-gas shift reaction. *Applied Catalysis B: Environmental* **92**, 234-239 (2009).

- 195 Song, S.-J. *et al.* Hydrogen permeability and effect of microstructure on mixed protonic-electronic conducting Eu-doped strontium cerate. *Journal of materials science* **40**, 4061-4066 (2005).

Bibliography

Ke-Ji Pan was born in Jiangsu, China. He obtained his bachelor's degree in chemical engineering at Southeast University in 2008. At that time, he spent a lot of time on metal organic compound synthesis and tried to investigate the ferroelectric properties of the new materials. After his graduation, he came to United States. He got his master's degree in chemical engineering at Illinois Institute of Technology in 2010. His master's research was alkaline fuel cells. He found he was interested in the renewable energy technologies and planned to pursue a Ph.D degree in this field. During the same year, he joined University of Maryland at College Park to be a Ph.D student. He met Dr. Eric Wachsman, who is famous in fuel cells. Ke-Ji then became a student in Dr. Wachsman's group and devoted himself in ceramic anode development. Up to now, he has three first author articles and three patents published or to be published. He plans to graduate in May 2016 and then continue his work in this field.

Publications

Patents:

Ceramic Anode Materials for Solid Oxide Fuel Cells, Eric D. Wachsman*, Ke-Ji PAN, Colin GORE, Mohammed Hussain Abdul Jabbar, Hee Sung Yoon, US 20140302420 A1 (Published)

Alternative Anode for Solid Oxide Fuel Cells, Ke-Ji Pan, Mohammed Hussain Abdul Jabbar, Eric D. Wachsman*, Invention Disclosure No. PS-2016-016 (Submitted)

Solid Oxide Fuel Cells Cathode Functional layer, Ke-Ji Pan, Mohammed Hussain Abdul Jabbar, Eric D. Wachsman*, Invention Disclosure No. PS-2015-156 (Submitted)

Papers:

Investigation on $Sr_{0.2}Na_{0.8}Nb_{1-x}V_xO_3$ ($x=0.1, 0.2, 0.3$) as New Ceramic Anode Materials for Low-Temperature Solid Oxide Fuel Cells, Ke-Ji Pan, A. Mohammed Hussain, and Eric D. Wachsman* (Submitting)

High Performance Low-Temperature Solid Oxide Fuel Cells based on Ceramic Oxide as Anode Supports, Ke-Ji Pan, A. Mohammed Hussain and Eric D. Wachsman* (Submitting)

Increasing SOFC Performance by Reducing Cathode-Electrolyte Interfacial Resistance, Ke-Ji Pan, A. Mohammed Hussain, Yi-Lin Huang, Gil Cohn, Dong Ding, Yunhui Gong, and Eric D. Wachsman* (Submitting)

Stannate based ceramic oxide as anode materials for oxide-ion conducting low-temperature solid oxide fuel cells, A. Mohammed Hussain, Ke-Ji Pan, Ian Robinson, Tom Hays and Eric D.Wachsman* (Submitted)

Solid oxide fuel cells on hydrocarbon fuels at low-temperatures, Review article, A. Mohammed Hussain, Colin Gore, Ke-Ji Pan, Dong Ding, Bryan Blackburn and Eric D.Wachsman* (Submitting)

Investigation of calcium/copper-doped yttrium chromate as anode material for solid oxide fuel cells, A. Mohammed Hussain, Ke-Ji Pan, Ian Robinson and Eric D.Wachsman* (Submitting)

Conference:

Strontium and vanadium co-doped NaNbO_3 as Ceramic Anode Material for LT-SOFC, Ke-Ji Pan, A. Mohammed Hussain and Eric D.Wachsman*, 40th International Conference and Exposition on Advanced Ceramics and Composites (ICACC'16)